"HIGH TEMPERATURE SENSOR/MICROPHONE DEVELOPMENT FOR ACTIVE NOISE CONTROL"

NASA Research Contract #NA63-1225

Period: December 1, 1990–November 30, 1993

Final Technical Reports

Technical Contact:

Dr. Daniel Ng
Lewis Research Center
21000 Brookport Road
Cleveland, OH 44135

Submitted by:

Thomas R. Shrout
Materials Research Laboratory
The Pennsylvania State University
University Park, PA 16802

The Pennsylvania State University

The Graduate School

MATERIAL AND DESIGN ISSUES IN THE DEVELOPMENT OF HIGH TEMPERATURE PIEZOELECTRIC ACOUSTIC SENSORS AND MICROPHONES

A Thesis in

Materials

by

Ronald C. Turner

Submitted in Partial Fulfillment
of the Requirements
for the Degree of

Master of Science

May 1994

ABSTRACT

The industrial and scientific communities have shown genuine interest in electronic systems which can operate at high temperatures, among which are sensors to monitor noise, vibration, and acoustic emissions. Acoustic sensing can be accomplished by a wide variety of commercially available devices, including: simple piezoelectric sensors, accelerometers, strain gauges, proximity sensors, fiber optics. Of the several sensing mechanisms investigated, piezoelectrics were found to be the most prevalent, because of their simplicity of design and application and, because of their high sensitivity over broad ranges of frequencies and temperature.

Numerous piezoelectric materials are used in acoustic sensors today; but maximum use temperatures are imposed by their transition temperatures (T_c) and by their resistivity. Lithium niobate, in single crystal form, has the highest operating temperature of any commercially available material, 650°C; but that is not high enough for future requirements.

Only two piezoelectric materials show potential for use at 1000°C; AlN thin film reported to be piezoactive at 1150° C, and perovskite layer structure (PLS) materials, which possess among the highest T_c (>1500°C) reported for ferroelectrics. In this work, a ceramic PLS composition was chosen. The solid solution composition, 80% strontium niobate (SN) and 20% strontium tantalate (STa), with a $T_c \approx 1160$°C, was hot forged, a process which concurrently sinters and renders the plate-like grains into a highly oriented configuration to enhance piezo properties. Poled samples of this composition showed coupling (k_{33}) ~6 and piezoelectric strain constant (d_{33}) ~3. Piezoactivity was seen at 1125°C, the highest temperature measurement reported for a ferroelectric ceramic. The high temperature piezoelectric responses of this, and similar PLS materials, opens the possibility of their use in electronic devices operating at temperatures up to 1000°C.

Concurrent with the materials study was an effort to define issues involved in the development of a microphone capable of operation at temperatures up to 1000°C; important since microphones capable of operation above 260°C are not generally available. The distinguishing feature of a microphone is its diaphragm which receives sound from the atmosphere; whereas, most other acoustic sensors receive sound through the solid structure on which they are installed.

In order to gain an understanding of the potential problems involved in designing and testing a high temperature microphone, a prototype was constructed using a commercially available lithium niobate piezoelectric element in a stainless steel structure. The prototype showed excellent frequency response at room temperature, and responded to acoustic stimulation at 670°C, above which temperature the voltage output rapidly diminished because of decreased resistivity in the element.

Samples of the PLS material were also evaluated in a simulated microphone configuration, but their voltage output was found to be a few mV compared to the 10 V output of the prototype.

For future work, alternative high temperature microphone designs could be pursued, such as:

- The non-ferroelectric, AlN thin film, because high resistivity and high temperature piezoactivity, shows promise for use in microphones of unconventional designs.
- Electrostatic (condenser) microphones constructed of ceramic, (BeO, MgO, AlN) and refractory metal (Pt, Cr-Ni-Fe ... alloy) components.
- Piezoresistive microphones, using granules of high temperature conductive materials such as $LaCrO_3$, β-Al_2O_3, and C, are also a possibility.

TABLE OF CONTENTS

LIST OF FIGURES

LIST OF TABLES

ACKNOWLEDGMENTS

I also wish to thank my advisor Dr. Tom Shrout for his encouragement and guidance and to and Drs. Newnham and Dougherty for serving on my committee. Additional thanks are extended to Dr. Paul Fuierer for his help, to Dr. Jeri Tichy for allowing me to use the acoustic facilities at the Acoustics Research Laboratory, and to the staff at the IMRL for their technical assistance.

I wish to acknowledge the assistance of NASA Lewis for their suggestion of a research topic, and for their support for this project.

Last, but not least, I have a debt of gratitude to my wife, Mary Ann, for her love, patience and support, and to my son Clint for his assistance with electronic devices.

CHAPTER 1

INTRODUCTION

High temperature electronics is an area of research offering interesting materials and design challenges and one of significant industrial importance. A major impetus for the development of high temperature electronic materials, devices, circuits, and systems can be credited to the energy crisis of 1974, when a commitment was made to the development of national energy resources by geothermal exploration (McCormick 1981). At that time, geothermal and oil well logging industries voiced their need for sensors and electronic systems with higher operational temperatures for deep drilling in the earth's crust. The economic importance of world energy independence and reduced waste provided additional incentive for their development.

Other industries have expressed similar needs. The power electronics industry has pointed out that the radiators required to dissipate heat from electronic systems account for a major portion of the size of the system. In silicon devices, thermal energy at 150°C is sufficient to promote band-to-band electronic transitions and intrinsic conductivity begins to increase exponentially leading to failure. If active and passive power components could be made to operate efficiently at temperatures in excess of 200°C there would be a major shift in the power industry technology. Thus, considerable effort has been directed toward developing high temperature semiconducting materials such as single crystal SiC and thin film diamond (Davis 1989). A team of researchers at Penn State University has recently fabricated a high temperature, thin film diamond transistor operable at 300°C (Gildenblat *et al.* 1991).

The aerospace and aircraft industries have especially demanding high temperature requirements. With space and weight at a premium, engine designers and builders find it difficult to protect sensitive electronic systems in a cool, remote place. Electronic controls are to be placed directly inside jet engines because of reliability and noise requirements, so sensors need to be built that can withstand temperatures of 500°C to 1000°C while allowing mission lifetimes up to 100,000 hours.

In automotive electronics, the number of sensors and actuators continues to increase as higher fuel and tighter emissions standards are implemented (Sheppard 1992). Ceramic and semiconductor sensors designed to record temperature, oxygen partial-pressure, and preignition knock are used in conjunction with microprocessor based controls to improve the efficiency and reliability of internal combustion engines (Naito 1987). Further efficiency can be realized by operating combustion engines at higher temperatures. Research on the use of ceramic components in a diesel engine has led to higher operating temperatures, resulting in a potential increase in fuel efficiency up to 65%, along with a notable reduction in exhaust pollution (Kamo 1979). Higher operating temperatures do, however, place additional requirements on the sensors. Environments of 150°C with repeated temperature cycles are at present considered the automotive norm, and higher temperatures are expected in the future.

Sensors to monitor acoustic events are becoming increasing valuable tools in the optimization and control of many processes and systems. As these systems are pressed into higher temperature operations, acoustic devices must be available to fill the requirements.

It is the objective of this work to report on the current methods of conducting high temperature acoustic measurements (>150°C), then to present the results of efforts aimed at extending the limits imposed by existing devices and materials. In order to accomplish this objective, the subject matter has been divided into several topical discussions. The

first topic is a review of acoustic sensors commercially available and a discussion of the advantages and deficiencies with respect to high temperature performance. The second topic is a review of commercially available piezoelectric materials that exhibit useful high temperature properties. The third topic presents a high temperature piezoelectric material capable of continuous operation at temperatures up to 1000°, and shows promise of application in high temperature electronic devices. Along with the presentation of new materials is a discussion of a unique hot forging process use to texture layered structure materials in order to exploit their maximum piezoelectric potentials. The fourth topic treats issues relevant to the design and operation a high temperature microphone, including:

- Sensitivity appropriate for the application
- Structural components—including diaphragm
- Electrodes on the element
- Termination and interconnection
- Wiring—special shielded cable
- Long term effects at high temperature (aging)
- Thermal cycling effects

Included in this project are the design and construction of a prototype microphone using commercially available materials, capable of operation at 600-700°C, with the ultimate goal of sustained use at 1000°C in the hostile environment of a jet aircraft engine.

CHAPTER 2

ACOUSTIC MEASUREMENT TECHNIQUES AND APPLICATIONS

Critical parameters for acoustic and vibration sensors involve the measurement of dynamic pressure pulses, vibrations (relative and absolute), acoustic emissions, strains, and the dynamic proximity of machine components. An example of a dynamic pulse is the rapid increase in pressure upon ignition of the air-fuel mixture in the cylinders of an internal combustion engine. The timing and the shape of the pulse have a large effect upon engine efficiency. Transducers fitted into the cylinder head have been used for monitoring combustion pressure to optimize ignition timing (Kusakabe *et al.* 1992).

Dynamic monitoring is also employed in such machines as aircraft engines, gas turbines, and power generators, all of which have high speed rotors. Sensors strategically mounted on the machine detect destructive conditions of imbalance, or unequal loading of the rotor, enabling the implementation of corrective measures. The sensors convert the associated mechanical energy of the vibration to electrical energy which can then be amplified and monitored. Computer coupling, allows real time status reports of the condition of the machine while providing a comparison with an operating norm.

Non-destructive testing (NDT) is another widely used application of acoustic sensors that involves either passive sensing of "acoustic emissions", or active "ultrasonic testing" techniques. An application of the first method involves affixing a number of acoustic sensors in strategic locations on the wall of a vessel, such as a chemical storage tank, pressurizing the vessel to create strains, and examining the acoustic emissions that result from the Kaiser effect (Fowler 1988). Cracks and poor joints can then be detected and logged so that repairs can be made. This method has also been successfully applied in the inspection of the fuselage of large aircraft to detect cracks resulting from fatigue.

The ultrasonic method of NDT incorporates a transducer to generate an acoustic signal at ultrasonic frequencies that is transmitted through the test specimen. When the acoustic wave reaches an interface of the sample it is reflected back to the transmitter-sensor which, therefore, acts as a transceiver. If, however, the wave impinges upon a flaw, a portion of the wave is reflected and thus reaches the sensor ahead of the original wave. This, then, becomes a valuable tool for locating defects within a structure (Helmshaw 1991). Figure 2.1 is a simple illustration of the technique. Acoustic sensors also find use in the hostile environments of deep oil wells for seismic data logging, and in nuclear power plants to monitor the condition of heat exchange pumps and pipes (Managan 1981).

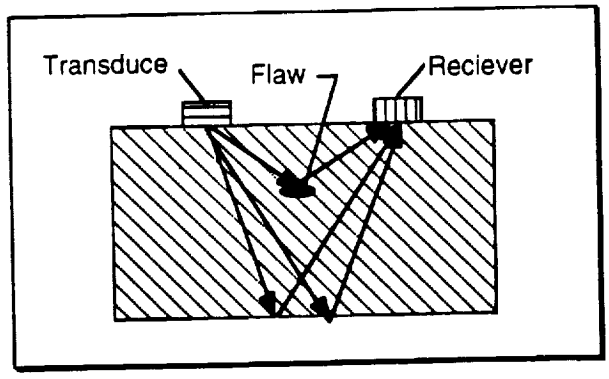

Figure 2.1 Detection of a flaw by ultrasonic testing (NDT).

An indirect way of sensing vibration is by measuring capacitive changes in an air gap. An air gap sensor placed in close proximity to a high speed rotor will detect dynamic changes in the spacing between the two which, in effect, is an indicator of an imbalance condition or some other malfunction. This type of sensor has found wide

acceptance in hydroelectric power plants (Bissonnette and. Cloutier 1989).

Examples of pressure, acoustic and vibration measurement techniques described above serve to illustrate the wide variety of possible applications. Additional applications are listed by industry in Table 2.1. These are routinely employed in the range of -55°C to 125°C; however, several devices are needed to operate in much harsher thermal conditions. Sensor designs and their respective temperature limitations are described in the next chapter.

Table 2.1

Acoustic and Vibration Measurement in Industrial Settings

Aerospace	Measure rotational speed of jet turbine rotors Space vehicle acceleration Trajectory monitor In-flight vibration monitor Nozzle pressure NDT test of air frames
Automotive	Knock sensor Suspension system monitors Fluid level sensor Crash test Vibration Control
Industrial	Dynamic pressure monitors Vibration detectors Flow detectors NDT testing Proximity detectors Noise "fingerprinting"
Medical	Diagnostic Imaging Impact sensors
Military	Hydrophones Range finders Noise detection in vehicles Security systems
Power Generation	Leak detector Liquid sodium coolant pump monitor Nuclear reactor monitor Air gap monitoring between stator and rotor Fuel rod monitor Coal feeder monitor NDT of pressure vessels
Commercial	Fish finders Phonograph pick-up Microphones Active noise control

CHAPTER 3

SENSOR DESIGNS

A variety of methods are used to detect noise and acoustic emissions; but at high temperatures (>150°C), fewer are options available. This chapter is the result of a careful literature search, and communication with major acoustic sensor manufactures in North America in an effort to catalog and describe important high temperature sensors. Devices include: piezoelectric discs or plates, accelerometers, strain gauges, proximity sensors, fiber optic sensors, and systems incorporating buffer rod extensions. Brief descriptions of these devices are given below:

3.1 Simple Disk

The most basic acoustic sensor incorporates a simple disc, plate, ring or other simple shape, of a piezoelectric ceramic, which is attached directly to the wall or frame of an engineering structure, embedded in a recess, or mounted in a replaceable fixture. Figure 3.1 is a schematic construction of a piezoelectric knock sensor using a bending mode resonance to detect vibrations. The piezoelectric element "generates" a voltage in response to stresses caused by the acoustic energy impinging upon it. The magnitude of the voltage generated is directly related to the product of the applied stress and the piezoelectric voltage or (*g*) constant of the material. The electrical signal is then amplified and fed to a microprocessor in the control system. This arrangement is capable of extremely high sensitivity on the order of pico (10^{-12}) strains. It is also self-generating, rugged, low-cost, and simple. The temperature limitations of these sensors arise from the loss of piezoelectric properties that occur as the material approaches its

transition (Curie) temperature (T_c), a topic which will be discussed later. For lead zirconate-titanate (commonly called PZT), the most widely used piezoelectric ceramic material, the maximum use temperature is ~200°C. Other temperature limitations result from the failure of the adhesives used to mount the disc, and the melting of the solder used to attach the leads.

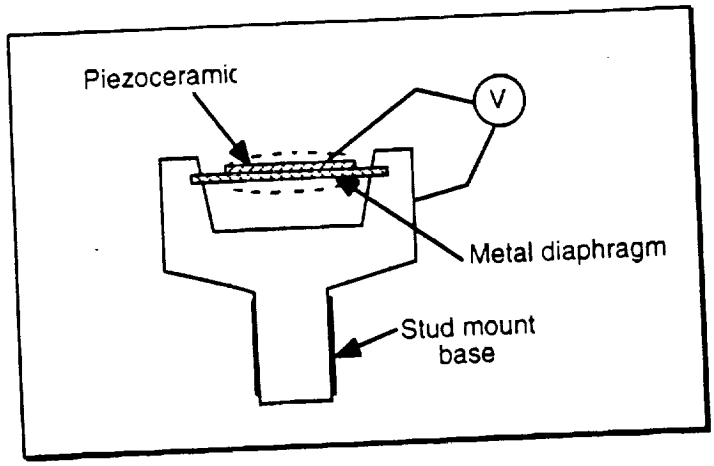

Figure 3.1 A method of mounting a piezobender used in automotive knock sensors (after Guess 1983).

3.2 Buffer Rod Extension

For many high temperature applications, buffer rod extensions are utilized to transmit and receive acoustic signals from very hot areas, effectively isolating temperature sensitive transducers from hostile environments. The rod serves as an acoustic wave guide to couple the hot test specimen with the sensitive piezoelectric transducer. The rods, often constructed of stainless steel, are cooled with water or air to prevent damage to the transducers. This arrangement permits the use of a conventional

piezoelectric material, which would otherwise lose its piezoelectric properties at high temperatures. This technique is widely used on NDT probes in the metals industry to detect cracks and other defects in hot steel blooms and pipes at temperatures in the neighborhood of 1100°C (Droney and Pfeiffer 1980). A related technique employs hollow "buffer pipes" to couple dynamic pressure sensors with jet and rocket engines. This method, however, adds to the size and complexity of the assembly and inevitably results in acoustic delay of the signal.

3.3 Accelerometers

Accelerometers most often use a *piezoelectric* material as the internal sensing element (Figure 3.2). The various designs exploit different mechanisms to translate mechanical energy to a measurable response, but all operate according to Newton's second law:

$$F = ma. \qquad \text{(eq. 3.1)}$$

The accelerometer differs from the simple disc piezoelectric sensor in that a seismic mass (m) is attached to the piezoelectric element and the assembly is hermetically sealed in a protective case. As a response to acceleration (a), the mass imparts a force (F) on the element, which in turn generates a voltage in proportion to the magnitude of the stress. Depending upon the sensitivity and temperature range required for the application, transducer manufacturers use several different piezoelectric materials. Commercial accelerometers using lithium niobate, $LiNbO_3$, single crystal elements are rated for continuous use up to 650°C (Endevco 1989, Vibrometer 1988).

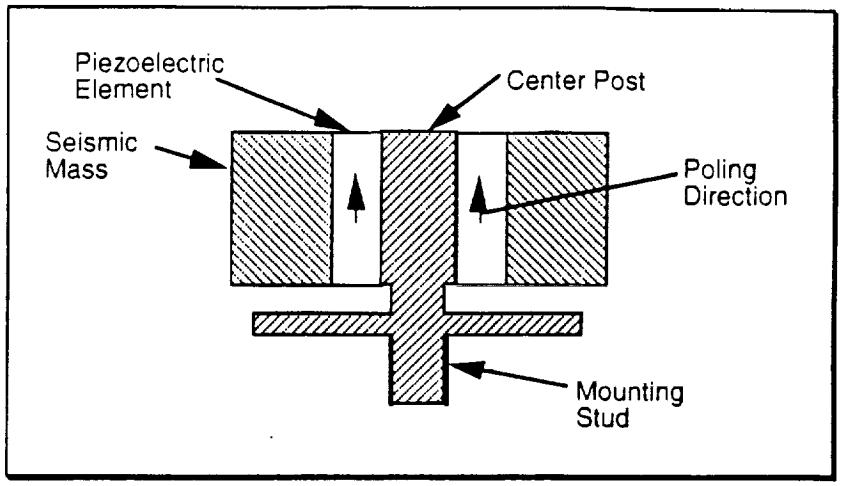

Figure 3.2 Schematic of an accelerometer using a ferroelectric, piezoelectric ceramic element.

Accelerometers based on magnetic induction, employ a permanent magnet as the seismic mass and a field coil for the active element. The mass is partially restrained by a spring; but when the mass is accelerated, it moves relative to the coil, thus inducing an electromotive force. As in the case of piezoelectric types, the resulting electric signal must be amplified and filtered before it is fed to the instrumentation. The upper temperature limit of this type of device is determined by the Curie temperature of the permanent magnet. Commercial units are rated for temperatures as high as 480°C (CEC 1991). This type of accelerometer is somewhat larger and heavier than piezoelectric types, factors which may exclude their use in some applications.

3.4 Strain Gauges

Resistive strain gauges involve a change in electrical resistance ΔR resulting from the mechanical strain $\Delta L/L$ of the sample to which the gauge is bonded. The sensitivity is determined by the gauge factor GF:

$$GF = \frac{\Delta R/R}{\Delta L/L} \qquad \text{(eq. 3.2)}$$

With a typical gauge factor of 2, and a nominal resistance R=100 ohm, these gauges require a highly sensitive ohmmeter to measure the ΔR accompanying a strain of 1×10^{-6}. A more accurate way of measuring small changes in resistance incorporates a Wheatstone bridge as shown in Figure 3.3. In order to compensate for the nonlinear character of the thermal coefficients of expansion of the alloys used, an unstrained reference gauge is installed in an adjacent bridge arm. This second gauge is subjected to the same temperature as the first, thereby effecting electrical cancellation of the apparent strain.

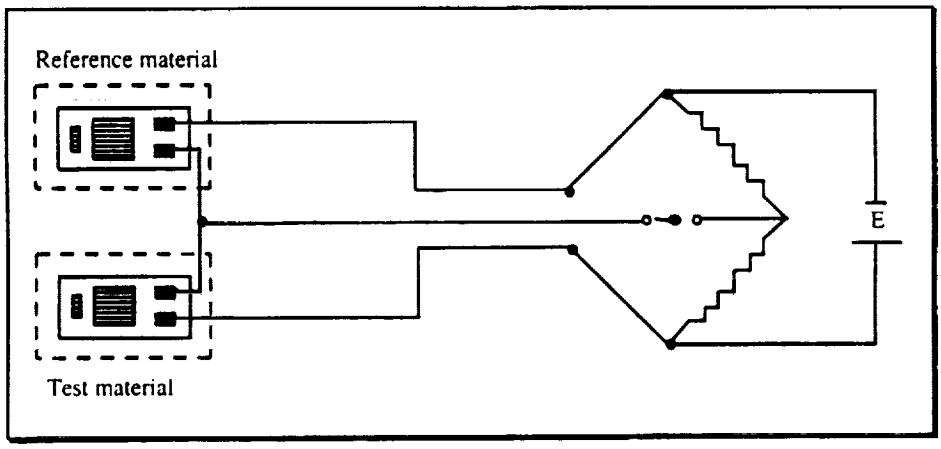

Figure 3.3 Bonded grid resistance gauges including the measurement and reference components and Wheatstone bridge circuit for measuring strain.

Commercial metal gauges are typically limited in temperature range to about 300°C; however, PtW wire gauges are available for use up to 850°C (Omega Eng. 1987), and other exotic metal alloys such as PdCr are being studied for use up to 1000°C (Lei, Mentor and Van Horn 1990).

Metal strain gauges are simple in design, low in cost and can detect static strains. Even when the Wheatstone bridge configuration is employed, strain sensitivity is low compared with piezoelectric transducers.

Piezoresistive (PR) strain gage elements are often made from silicon resistors attached to cantilever beams and electrically connected in a Wheatstone bridge to produce an electrical signal with vibratory motion (Endevco 1989). PR gages have greater strain sensitivity than metal wire gages (GF is 100 times that of the wire gage), but they are also very temperature sensitive and are limited to temperatures near 125°C. Another type of PR sensor can be made from conductive particles dispersed in an insulating polymer matrix (Carmona *et al.* 1986). Under compressive or flexural force, the conducting particles are brought into contact and the resistivity decreases abruptly with stress. The use of polymers as matrix materials severely restricts the operating temperature.

3.5 Proximity Sensors

Proximity sensors are often used to monitor the degree of rotation of the armatures of electric generators as well as the clearance between the armature and the stator. This serves as an indirect method of measuring vibration if an unbalanced condition exists. The two types of proximity sensors available commercially are: air gap capacitors and eddy current detectors. Both types require electronic conditioners to supply input signals and processors to analyze the signals modified by the sensors.

An example of an *air gap capacitor* is illustrated in Figure 3.4. In this application on an electric power generator, the armature serves as one plate of the capacitor while the other plate is an integral part of the sensor with air as the dielectric as shown in the equation,

$$\Delta C = \frac{K\varepsilon_0 A}{\Delta d} \qquad \text{(eq. 3.3)}$$

where (C) is the capacitance in farads (K) is the dielectric constant of air (1.00059), (ε_0) is the permittivity of free space (8.85×10^{-12} F/m), (A) is the area of the plate on the sensor, and (d) is the distance between the plates. The plates are maintained at a close proximity with one another so that a small change in spacing results in significant changes in capacitance, which detected by the control circuitry and acted upon accordingly. The detection of variations in air gap as small as one micro meter are possible in installations on hydroelectric power generators (Bissonnette and. Cloutier 1989). At present, commercial units are constructed of fiberglass composites for use at temperatures up to 150°C, but it seems reasonable that units could be constructed from more refractory materials for higher temperature applications.

The second kind of proximity sensor is the *eddy current* type. It determines the relative position of a rotating shaft by detecting changes in magnetic field between the sensor and the target shaft. The eddy current sensor operates in a manner similar to that of an electrical transformer. The sensing coil resembles the primary winding, and the small eddy current loops induced in the target by the variable magnetic field of the sensing coil act like the secondary windings. The small eddy currents cause a change in phase and amplitude of the sensing coil signal. The target material must therefore be metallic. The sensing coil is mounted near the rotating shaft or moving component of a

machine with lead cables attached to the exterior end. Commercial models are currently rated for use up to 450°C. The temperature limitation is primarily due to the temperature coefficient of resistance of the wire used to wind the probe coil (Car 1987).

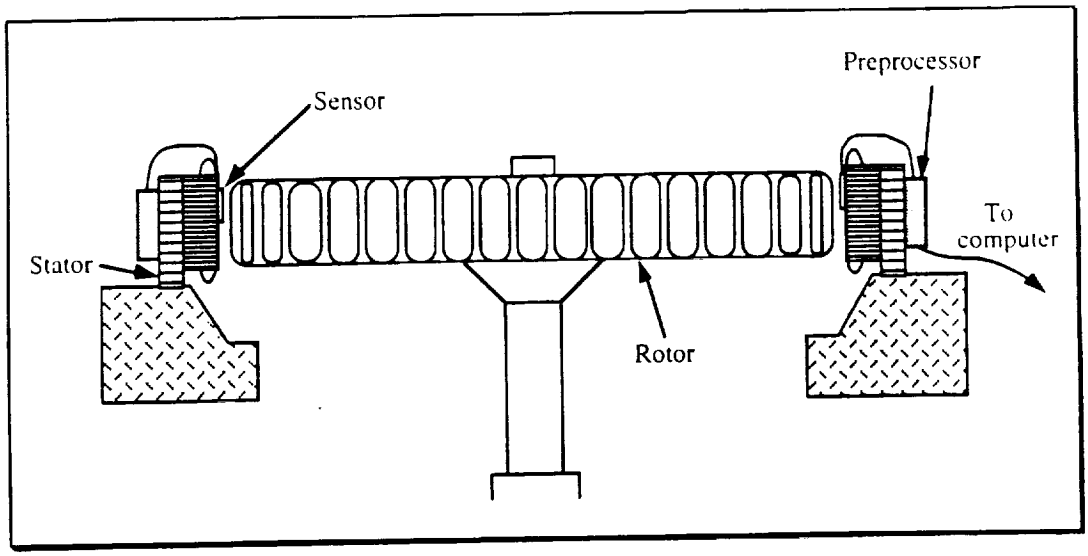

Figure 3.4 Air gap sensors mounted on an AC generator (Ménard and Bourgeois 1990).

3.6 Fiber Optic Sensor Interferometer

Fiber Optic Sensor (FOS) Interferometers or phase sensors are used to detect small strains (in the order of 10^{-7}) or vibrations in a sample without making physical contact. This capability allows measurements to be made inside a hostile environment, such as a furnace. A simplified schematic of a system is shown in Figure 3.5.

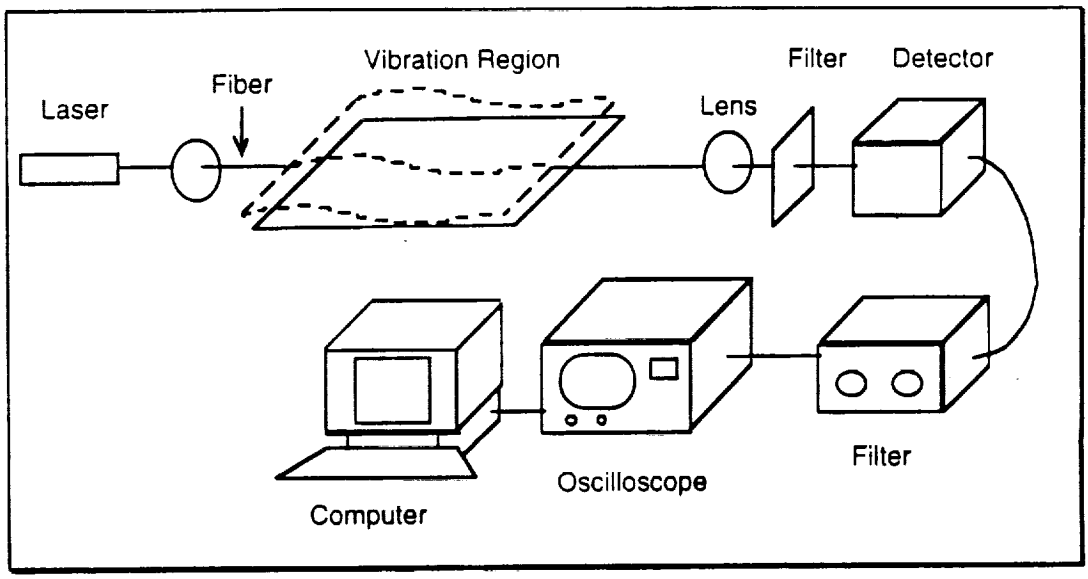

Figure 3.5 Fiber optic vibration sensor and associated electronics.

There are several different designs of interferometers, but all are based on measuring a phase change in the transmitted light signal resulting from a change in length of the optical fiber. Optical fibers are typically SiO_2 glass; however, fibers of more heat resistant materials such as sapphire (Al_2O_3) are commercially available. Along with the fiber, a large number of additional components, such as a laser source, phase demodulator, filters, and microprocessors, *etc.*, are needed for these systems. High cost, complexity, and sensitivity to variations in temperature are disadvantages of this approach.

3.7 Chapter Summary

With respect to the operational parameters listed in Table 3.1, piezoelectric transducers are most widely used because they offer many advantages over the other types of acoustic sensors. Specifically, their compliment of sensitivity, stability over a wide temperature range, and simple design offers the lowest cost per performance factor. Polycrystalline, ferroelectric ceramics are often the material of choice because they can be readily manufactured into a variety of configurations not available in single crystals. Therefore, the bulk of this work concentrates on high temperature piezoelectric materials, with a review of those currently available, and a discussion of future prospects.

TABLE 3.1

Comparison of Commercial Strain, Vibration, and Acoustic Sensors

Device	Piezoelectric Disc or Plate	Accelerometer		Strain Gage	Proximity Sensor		Buffer Rod	Fiber Optic Sensor
Operation Principle	Piezoelectric	Piezoelectric	Magnetic Induction	Resistive Metal	Capacitive	Eddy Current	Piezoelectric	Laser/Optic
Measured Parameter	Acoustic waves Vibration	Acceleration Absolute Dynamic	Vibration Pressure	Load, force Vibration Absolute	Relative air gap displacement	Vibration	Acoustic waves	Strain, vibration
Maximum Temperature	400°C	650°	480°C	850°C	150°C	450°C	1100°C	300°C
Temperature Stability	Good	Good	Good	Fair	Good	Fair	Good	Poor
Temperature Sensitivity	Good	Good	Good	Fair	Good	Fair	Good	Poor
Resolution/ Sensitivity	High	High	Fair	Low	Low	Low	Fair	High
Frequency Range	0.05-1 MHz	0.05- MHz	0.015-2kHz	DC-kHz	DC-kHz	DC-10kHz	50Hz-1 MHz	DC-10kHz
Power Consumption	Low	Low	Low	Medium	Medium	Medium	Low	High
Complexity	Low	Medium	Medium	Low	Low	High	High	High
Durability	Good	Good	Good	Fair	Good	Fair	Good	Poor

CHAPTER 4

PROPERTIES OF PIEZOELECTRIC MATERIALS

4.1 Piezoelectricity

Piezoelectricity is the phenomenon that occurs in certain materials which exhibit an electric field when subjected to an applied stress (sensor); or conversely, exhibit a mechanical deformation with the application of an electric field (actuator). Piezoelectric response was first reported in 1880 by Pierre and Jacques Curie. Since that time, a number of crystalline materials have been identified as being piezoelectric; but only a few are of practical concern. The common feature of all piezoelectric crystals is the absence of a center of symmetry along the piezoelectric axes. An example of piezoelectric material is found in lead titanate ($PbTiO_3$), whose perovskite structure is shown in Figure 4.1(*a*). The central Ti^{4+} ion, which does not quite fill the interstice in the octahedral site, is displaced off-center by a small distance, thus forming a dipole. The application of an electric field to the crystal will cause the off-centered ion to shift slightly to a position which is either "more off-centered" or "less off centered" depending upon the polarity of the field. This change in position results in distortions of the crystal lattice (*i.e.*, strain) and a subsequent shifting of the relative position of the lead ion to oxygen ion. In addition to being piezoelectric, $PbTiO_3$ is ferroelectric; wherein the application of a field of sufficient magnitude will induce the ion to assume a new state of equilibrium favoring the polarity of the field. This reversal of the polarization is referred to as ferroelectric hysteresis, as seen in Figure 4.2. It is generally held that ferroelectric materials exhibit the highest degree of piezoactivity (Jaffe *et al.* 1971).

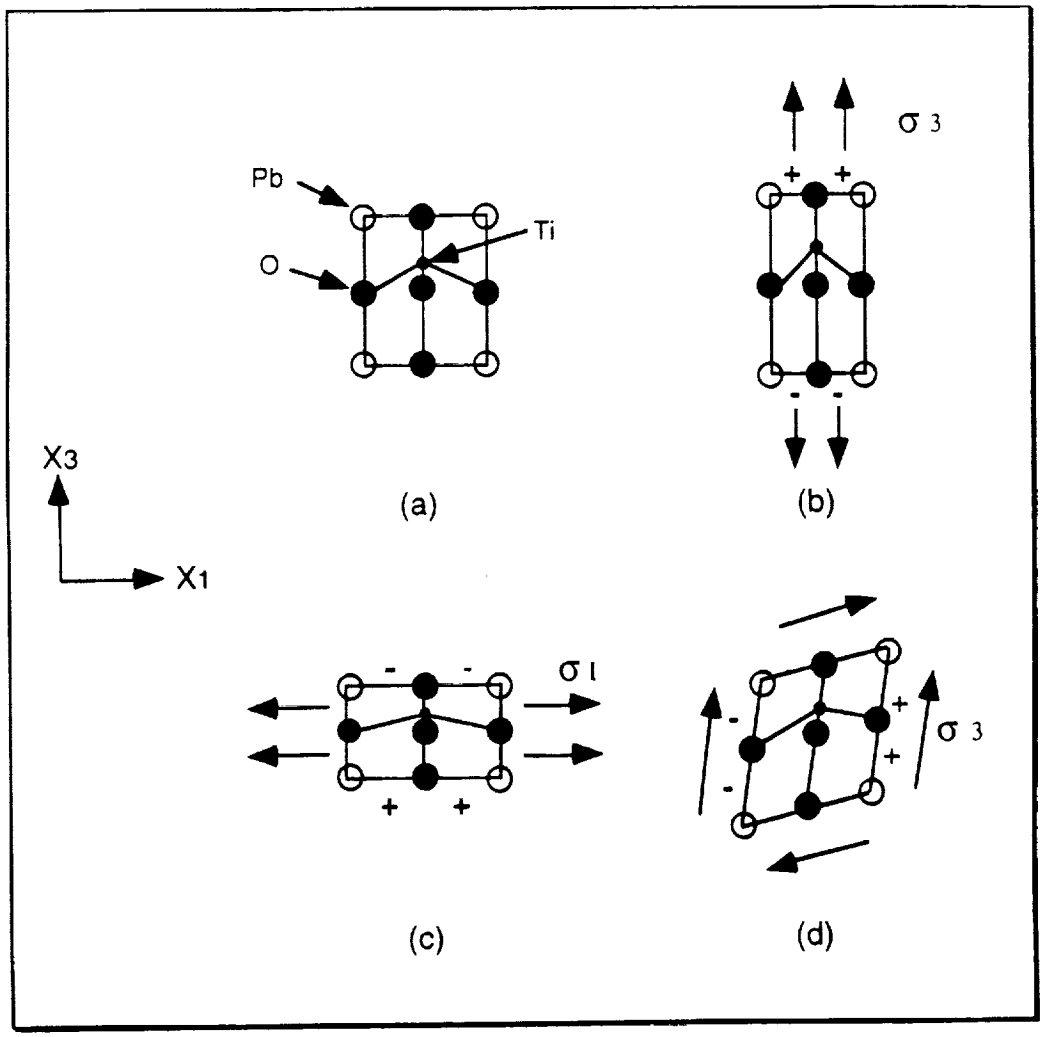

Figure 4.1 (a) A two-dimensional representation of the tetragonal $PbTiO_3$ perovskite structure with the titanium ion displaced from the center of the unit cell. (b) If a tensile stress is applied along X_3, the Ti^{4+} ion is shifted further off-center, yielding a positive polarization in this direction. (c) If the stress is applied along X_1, the dipole moment is decreased and a negative polarization results. (d) A shear stress around X_2 produces a polarization in the X_1 direction (after Newnham and Huebner 1989).

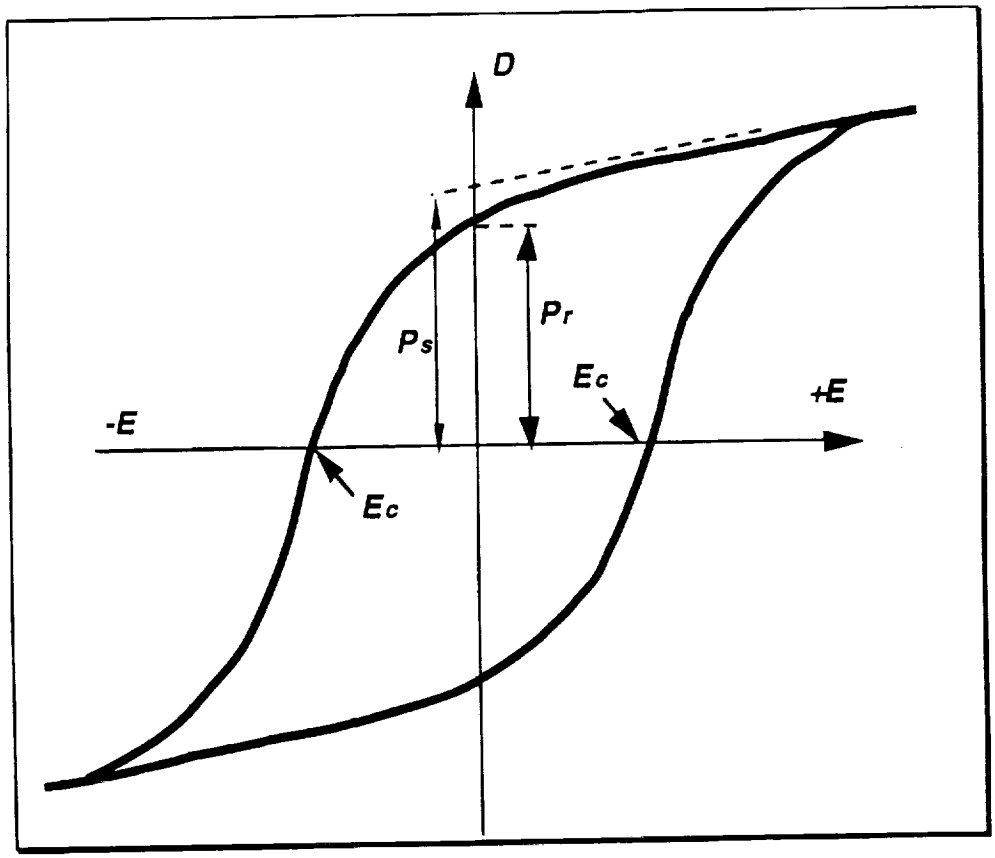

Figure 4.2 The dielectric displacement (D) *vs.* applied electric field (E) hysteresis loop characteristic of ferroelectric behavior, showing coercive field (E_c), saturation polarization (P_s) and remnant polarization (P_r).

Single crystals of a given ferroelectric material generally exhibit a greater degree of polarizability; however, large crystals of many of the ferroelectric materials such as lead titanate are difficult and expensive to fabricate. Most commercial ferroelectric materials are in the form of polycrystalline ceramics, which makes possible wide ranges of compositions, with numerous combinations of dielectric constants, electromechanical coupling coefficients and other properties.

Polycrystalline ceramics are formed from pre-reacted powders, compacted into shapes and sintered to achieve the required density. The obvious advantage of this process is its low cost and versatility. Occasionally the compacting and sintering operations are performed simultaneously by *hot pressing*. Individual dipoles in the ceramic assume a random orientation; thus, their net dipole effect is zero. If a large electric field is applied (often at an elevated temperature) in a process called poling, a significant number of the dipoles are realigned so that the net dipole moment is parallel to the field. With a sufficient degree of alignment, the ceramic is rendered piezoelectric. Further information on piezoelectricity is found in other sources (Cady 1946, Jaffe *et al.* 1971, Swartz 1990).

4.2 Electromechanical Properties;

Poling induces anisotropy in the ceramic body, giving rise to certain allowable piezoelectric coefficients. Three basic piezoelectric modes of a ceramic element can be exploited (Figure 4.3). The subscript (33) refers to a thickness or length longitudinal mode, (31) represents a transverse mode and (15) signifies a shear motion. Single crystals or grain-oriented ceramics with lower symmetry will have additional modes of vibration than those of higher symmetry. The first number in the subscript refers to the direction of electric field and the second refers to the type of mechanical stress.

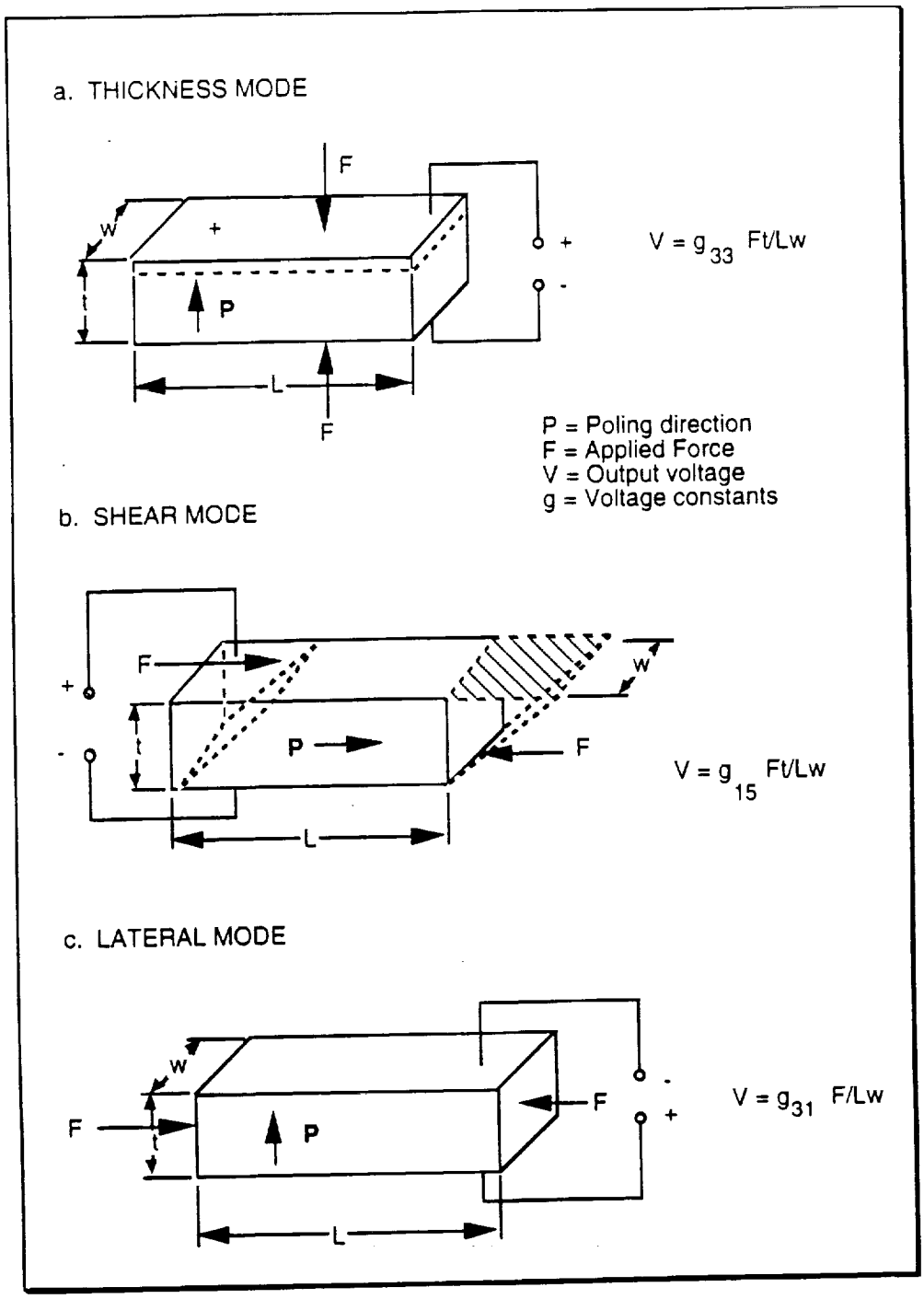

Figure 4.3 (*a*) Thickness (*b*) shear (*c*) and lateral mode piezoelectric sensors. (*P*) indicates the poling direction. The output voltage (*V*) is proportional to the applied force (*F*) and piezoelectric voltage coefficient (g_{ij}) of the material.

By convention, X_3 is the poling axis, and X_1 and X_2 are the other two orthogonal axes. Subscripts 1, 2, and 3 represent longitudinal tensile stresses along the X_1, X_2, and X_3 axes, respectively. Shearing stresses about X_1, X_2, and X_3 are indicated by the subscripts 4, 5 and 6.

4.2.1 Coupling Coefficients

The coupling coefficient (k_{ij}) is possibly the best single measurement of the strength of the piezoelectric effect. It is a convenient, though not strictly correct, expression of the efficiency in which the material converts electrical energy to mechanical energy, and vice versa and may be expressed according to the following relationship (Jaffe *et al.* 1971):

$$k^2 = \frac{\text{electrical energy converted to mechanical energy}}{\text{input electrical energy}} \qquad \text{(eq. 4.1)}$$

or

$$k^2 = \frac{\text{mechanical energy converted to electrical energ}}{\text{input mechanical energy}} \qquad \text{(eq. 4.2)}$$

For single crystals, the electromechanical coupling factors are material constants, but for ceramics, they depend on the degree of poling. Most piezoelectric materials have several k factors, each associated with a particular resonant frequency along the various possible geometric dimensions. The coupling factors can be calculated as a function of the piezoelectric d constants, the elastic compliance s, and the permittivity ε A representative equation for k_{ij} is for k_{33}:

$$k_{33} = \frac{d_{33}}{\sqrt{s_{33}^{E}\varepsilon_{3}^{T}}} \qquad \text{(eq. 4.3)}$$

It is not always convenient to measure elastic compliance or d constants other

than d_{33}, so other expressions for coupling factors have been derived which involve only the resonant and antiresonant frequencies associated with the particular mode. For most commercial materials, a generally accepted method of calculating k_{33} is one presented in a publication by the American Standards Association (ASA 1961):

$$k_{33}^2 = \frac{\pi f_s}{2 f_p} \tan \frac{\pi \Delta f}{2 f_p} \qquad \text{(eq. 4.4)}$$

The frequencies (f_s) and (f_p) are the series and parallel frequencies respectively. For piezoelectric ceramics with low electromechanical losses, (f_s) and (f_p) are often replaced by (f_m) and (f_n) — frequencies at minimum and maximum impedance. This substitution is possible because, in many cases, two frequency sets are nearly identical and the latter are often much easier to measure. For resonators with small coupling factors and high losses, the differences between the frequency sets may become greater, thus precise calculations of the coupling factors become more complex.

A simplified method for calculating an "effective coupling" factor for (k_{ij}) was presented by Onoe and Jumonji (1967), and was used by Fuierer (1991) in his work, and was used to calculate the data given later in this work.

$$\frac{1}{k^2} = a \frac{f_m}{f_n - f_m} + b \qquad \text{(eq. 4.5)}$$

The coefficients (a and b) are dependent on the direction of applied field in relation to the direction of elastic-wave motion. The values for the coefficients are, a = 0.404 and b = 0.81 for the k_{33} and k_{24} modes, and a = 0.395 and b = 0.574 for the planar (k_p) mode.

4.2.2 Piezoelectric Strain and Voltage Coefficients

From the coupling coefficient k_{ij}, the resonant frequency f_r, and the dielectric permittivity ε_{ii}, one can calculate the other electromechanical parameters including the elastic compliance (s_{ijkl}) (m^2/N),

$$s_{ij}^E = \frac{1}{(2lf_m)^2 \rho} \qquad \text{(eq. 4.6)}$$

the piezoelectric strain coefficient d_{ij} (C/N)

$$d_{ij} = k_{ij} \sqrt{\varepsilon_{ii}^X s_{ij}^E} \qquad \text{(eq. 4.7)}$$

and the piezoelectric voltage coefficient g_{ij} (Vm/N). While d indicates "short circuit" sensitivity and g indicates "open circuit" sensitivity, the short and open circuit coefficients are related by the following equation:

$$g = \frac{d}{K\varepsilon_o} \qquad \text{(eq. 4.8)}$$

The piezo strain (d_{31}) constant gives the ratio of the strain developed in the specimen in the X_1 direction to the electric field applied at the electrodes which are perpendicular to the poling direction X_3, and conversely, gives the ratio of short circuit charge, per electrode area, to the applied stress. The stress can be applied to the body in different modes as illustrated in Figure 4.3. The piezoelectric voltage coefficient, g_{33}, denotes the ratio of field developed in the X_3 direction to stress applied in the same direction, when all other external stresses are zero, and conversely, the ratio of strain to the voltage applied between the electroded areas. If used as a basis for selecting a piezoelectric material for use at high temperatures, g tends to be a more meaningful

coefficient than d.

The sensitivity of an acoustic sensor directly relates to d and g of the piezoelectric material used. For a given stress applied to the device, the output voltage generated by the piezoelectric "generator" should be sufficiently high to be detected above background noise. The most sensitive devices produce the greatest output per unit of stress. Increased permittivity, resulting from increased temperature, can effectively reduce g. Every piezoelectric material reaches some temperature at which g and resistivity (ρ) are diminished to the point where the output becomes undetectable. In practice, the relatively small output signals generated by high temperature accelerometers necessitate the use of electronic charge amplifiers for enhancement, but there is a practical limit as to how small a signal that can be detected accurately.

4.2.3 Other Important Coefficients

The *frequency constant* (N) expresses the resonance frequency of a mode in terms of the controlling dimension (l) of that mode. It is a necessary coefficient for the designer to determine the critical dimension of a transducer to achieve a desired resonant frequency. N is given by the expression:

$$N = f_m l \text{ (Hz-meter)} \qquad \text{(eq. 4.9)}$$

Generally speaking, the product of N and twice the resonant frequency fr (in Hz) gives an approximation of the speed of sound through the piezoelectric material.

The *dielectric loss* (*tan* δ) of a material is usually reported with the dielectric constant K and is an important indicator of the "quality" of the dielectric. Stated simply:

$$\tan \delta = \frac{\text{energy dissipated per cycle}}{\text{average energy stored}} \qquad \text{(eq. 4.10)}$$

or

$$tan\ \delta = \frac{I_C}{I_R} \qquad \text{(eq. 4.11)}$$

where, for the current (I), I_C is the vector component representing a "Wattless" capacitive current proportional to the charge stored in the capacitor, and I_R is the vector component of and AC conduction current in phase with the applied voltage. The quality factor (Q), the reciprocal of *tan* δ, is also used (Buchanan 1986).

4.3 Requirements for High Temperature Piezoelectric Materials

In addition to the electrical and electromechanical properties discussed earlier, other properties which must be considered when considering a piezoelectric material for high temperature applications, including T_c and resistivity, are presented below.

4.3.1 Ferroelectric Curie Temperature

Most of the piezoelectric materials described in this thesis are ferroelectric and capable of being polarized, with the polarization resulting from the asymmetry of its crystal structure. When the crystal is heated, its internal kinetic energy increases. At a certain temperature, called the Curie temperature (T_c), the crystal changes to a structure of a higher symmetry, and in most ferroelectrics, the alignment of the dipoles is lost, with a resulting loss of piezoelectric activity. Upon cooling, the dipoles do not realign unless they are subjected to a strong electric field. Other consequences of increasing temperature are changes in the values of electromechanical coefficients, which become more pronounced as the T_c is neared. This can be particularly important in applications

in which the electrical properties of the sensor are closely matched to the instrumentation. In addition, dipoles that were aligned by poling, have a tendency to revert to a more nearly random orientation, thus, degrading the piezoelectric effect in a process known as "thermally activated aging" or "depoling". A "rule of thumb" for the operational temperature limit of piezoelectric materials is ~one-half T_c, above which the material depoles (Haertling 1986); although it will be shown later that some piezoelectric materials that can operate well above this generalized limit.

4.3.2 Resistivity and the RC Time Constant

High electrical resistivity (ρ) is necessary so that a large field can be applied to the sample during poling without breakdown or excessive charge leakage. High insulation resistance R is also required during operation of the device. The transducer must not only develop a charge for an applied stress or strain, but must also maintain the charge for a time long enough to be detected by the electronic system. The length of time the charge is maintained is proportional to the RC time constant (resistance x capacitance). The minimum useful frequency of a sensor, known as the lower limiting frequency (f_{LL}), is inversely proportional to the time constant:

$$f_{LL} = \frac{1}{2\pi RC} \qquad \text{(eq. 4.12)}$$

where C is the device capacitance.

Below f_{LL}, the charge will drain off before it is detected because of conduction in the sensor. With low f_{LL} the dynamic bandwidth can be extended into audio frequencies; thus, a large RC constant is desirable for many applications.

CHAPTER 5

COMMERCIAL PIEZOELECTRIC CERAMICS

There are only a few piezoelectric materials found to have application in commercial acoustic sensors, and fewer still which can be used at elevated temperatures. This chapter gives a brief description of the these "high temperature" materials along with some of their important electrical properties.

Table 5.1 lists typical piezoelectric ceramic materials found in commercial accelerometers and vibration sensors, along with reported room temperature properties; and Table 5.2 lists some of the high temperature dielectric and piezoelectric properties or representative samples obtained from commercial sources. Table 5.2 also includes properties of a new high temperature piezoelectric perovskite layer structure (PLS) material, which will be discussed later in this work material.

The resistivity of each material was also measured over a wide range of temperatures as shown in Figure 5.1. Measured values show good agreement with those reported in the literature. The resistivities of AlN and PLS material are also included.

5.1 Quartz (SiO_2)

Quartz is one of the earliest piezoelectric materials used in electronic devices. It differs from the commercial piezoelectric ceramics in that it is a non-polar, non-ferroelectric single crystal. Originally natural quartz crystals were used, but now have been widely replaced by hydrothermally-grown synthetic quartz. Because of its low mechanical loss, narrow bandwidth, and highly temperature-stable resonant frequency, quartz is the material of choice for frequency standards and monolithic filters in

TABLE 5.1

Reported Room Temperature Electrical Properties of Several Commercial High Temperature Piezoelectric Materials

Material	Structure	Transition Temp T_C °C	Dielectric Constant K	Piezoelectric Strain Const. d_{33} d_{15} 10^{-12} C/N	Piezoelectric Voltage Const. g_{33} g_{15} 10^{-3} Vm/N	Electromech. Coupling k_{33} k_{15}	Resistivity 20°C ρ $10^{12}\Omega$-cm	Reference
$Pb(Zr,Ti)O_3$(Soft PZT)–DOD II	Perovskite	330	1800	417 710	25 41	0.73 0.77	100	Token N-21
$(BaPb)Nb_2O_6$ (BPN)	Tungsten Bronze	400	300	85 100	32 46	0.30	1	Keramos K-81
$PbTiO_3$ (PT)	Perovskite	470	190	56 68	33 32	0.45	10	Matsushita LTT-3
$Na_{0.5}Bi_{4.5}Ti_4O_{15}$ (NBT)	Bismuth Layer	600	140	18	15	0.15	1000	Keramos K-15
$LiNbO_3$ (LN)	Corundum	1150	25	6 69	23 91	0.23 0.60	1	Crystal Tech..
SiO_2	α-quartz	573	4.5	$2(d_{11})$	50	$0.1(k_{11})$	1000	Herbert (1982)

TABLE 5.2

Selected High Temperature Properties of Several Piezoelectric Materials

(PZT and BPN were evaluated at approximate maximum use temperatures, the others at 400°C.
Room temperature values (RT) also shown for the voltage constant (g)

Material	Transition temp Tc (°C)	Vibration Mode (ij)	Voltage const. g (RT) ($x10^{-3}$Vm/N)	Resistivity ρ (Ω-cm)	Dielectric constant K (@10 kHz)	Dissipation tan δ (10 kHz)	Time const RC (sec.)	Reference
PZT (DOD II) (200°C)	360°	[33]	15 (25)	10^{12}	3000	0.025	250	Token (N-21)
$(BaPb)Nb_2O_6$ (300°C)	400°	[33]	24 (30)	10^7	530	0.036	0.0005	Keramos (K-81)
$PbTiO_3$ (400°C)	450°	[15]	21 (29)	$2x10^5$	1000	0.35	0.00002	Matsushita (LTT-3)
$Na_{0.5}Bi_{4.5}Ti_4O_{15}$ (400°C)	600°	[33]	10 (18)	$3x10^8$	262	0.10	0.007	Keramos (K-15)
$LiNbO_3$ (400°C)	1150°	[15]	93 (99)	$3x10^7$	100	0.001	0.0003	Crystal Technology
$Sr_2(Nb_{.5}Ta_{.5})_2O_7$ (400°C)	823°	[24]	5 (6)	$4x10^9$	40	0.10	0.01	Fuierer (1991)

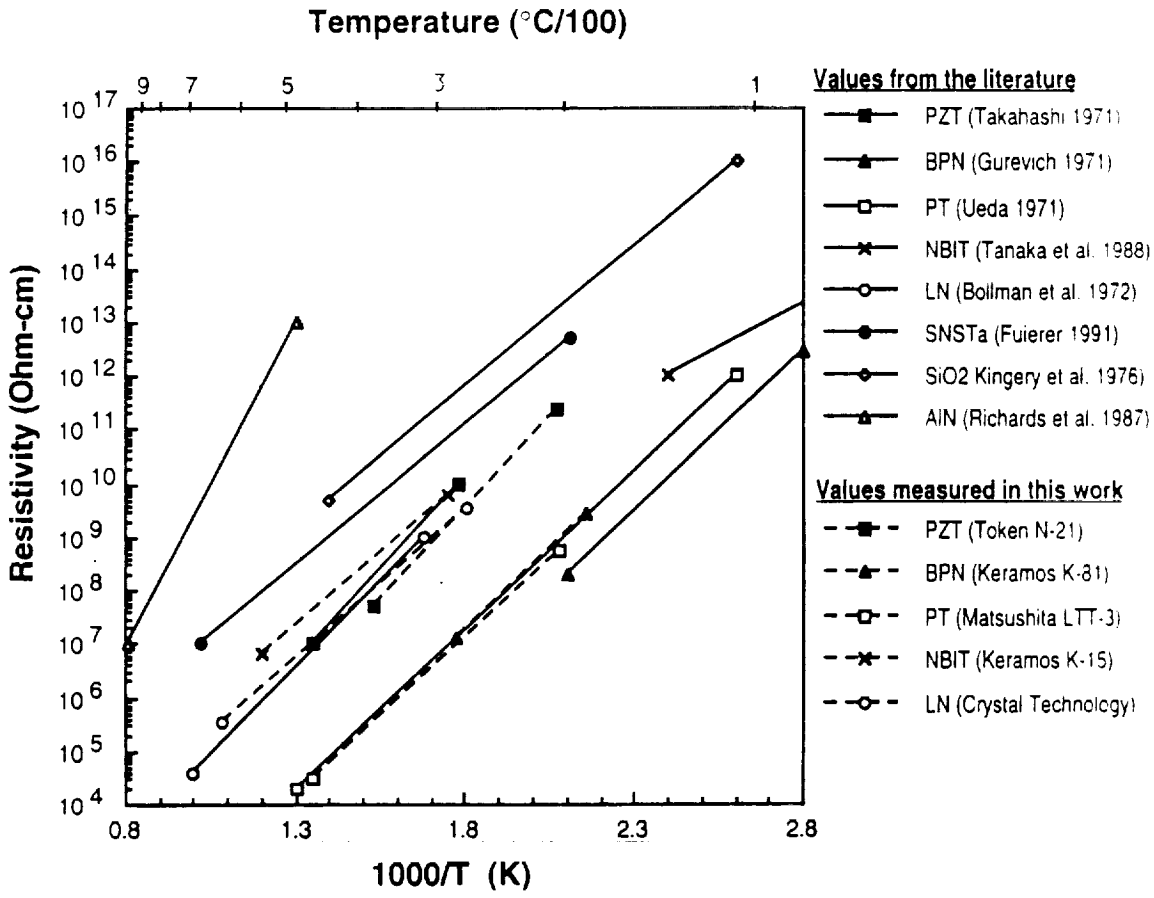

Figure 5.1 Temperature dependence of resistivity for piezoelectric ceramics: "soft" lead zirconate titanate (PZT), barium doped lead metaniobate (BPN), sodium bismuth titanate (NBIT), lead titanate (PT), lithium niobate (LN), and perovskite layer structure strontium niobate tantalate (SNSTa). Solid lines represent data taken from literature, while dashed lines represent data measured from commercial materials for this work. All are polycrystalline ceramics except LN and SiO_2, single crystals and thin film AlN.

communication equipment. However, as seen in Table 5.1, the piezo *d* coefficient is relatively small; thus, the amount of electric charge that can be generated is low. Although piezoelectric α-quartz has a transition temperature of 573°C, its use temperature is normally limited to 350°C. Above that temperature the crystal structure is subject to *twinning*, destroying its piezoelectric properties (Kistler 1989).

5.2 Lead Zirconate Titanate [$Pb(ZrTi)O_3$]

Lead zirconate titanate (PZT) has the perovskite structure and is a solid solution of tetragonal $PbTiO_3$ [PT] and orthorhombic $PbZrO_3$ [PZ]. Because of the large number of polarization directions available, compositions near the morphotropic phase boundary at approximately 53:47 PZ to PT are easily poled to high remanent polarization and exhibit extremely high values of electromechanical coupling coefficients and electrical permittivity (Jaffe *et al.* 1971). Because of its superior piezoelectric properties and higher operating temperature, PZT has largely replaced barium titanate (BT) – T_c ~130°C, the first widely used ferroelectric, in all but the lowest cost commercial products. Useful variations in properties of PZT can be obtained by compositional additives. Niobium doped PZT (DOD Type II) is used extensively in accelerometers, hydrophones (underwater microphones), and acoustic emission instruments (Herbert 1982). Although its electrical resistivity and *RC* time constant remain quite high up to a T_c of 360°C (Table 5.2 and Figure 5.1), its use is kept well under 200°C because of its tendency to age very rapidly at higher temperatures.

5.3 Lead Titanate ($PbTiO_3$)

Lead titanate (PT), with the general formula ABO_3, is the solid solution end member of PZT family, and exhibits the highest T_c of the group (~490°C). As in the case of PZT, numerous modifications have been developed to optimize specific electrical and mechanical characteristics. Many commercial compositions of PT are doped with samarium or calcium for use in hydrophones (Xue *et al.* 1985); but this has the effect of lowering the T_c to around 240°C. Compositions, doped with other elements, have T_c values near 490°C and have found applications in knock sensors for automobile engines (Kusakabe 1992). The higher operating temperature of PT allows it to be mounted closer to the combustion chamber, thus giving a faster response time as compared to PZT. The data presented in Tables 5.1 and 5.2 and Figure 5.1 reflects the latter composition. Evaluation at 400°C has shown it to have a resistivity of only about 10^5 ohm-cm.

5.4 Lead Metaniobate ($PbNb_2O_6$)

Lead Metaniobate (PN) belongs to the tungsten bronze (K_xWO_3) family. Because of its low Q_m (wide bandwidth) and relatively high d_{33} to d_{31} ratio (directionality), PN finds its greatest use in transducers in NDT and medical diagnostic imaging. Commercial PN compositions are modified to enhance specific electrical characteristics but at the expense of the T_c. A commonly used composition contains about 10% Ba (BPN) and has a T_c of about 400°C. Although BPN is reported to resist depoling up to its T_c, limitations are imposed by its high conductivity above 300°C (Gurevich and Rez 1960). Figure 5.1 reveals that BPN exhibits the lowest resistivity of the materials tested. Other problems associated with this material are its 6-10% open porosity and relatively low mechanical strength (Herbert 1982).

5.5 Bismuth Titanate ($Bi_4Ti_3O_{12}$)

Bismuth titanate (BIT) is the titular compound of bismuth layer structure ferroelectrics (BLSF). Modification by one or more of a large number of other elements, to enhance dielectric and piezoelectric properties, is also possible (Ikegami and Ueda 1974). A member of the family, reported to have favorable piezoelectric properties, high resistivity and high T_c (>600°C), is $Na_{0.5}Bi_{4.5}Ti_4O_{15}$ (NBT). Commercially available (Keramos 1991), it is used in accelerometers operated at temperatures up to 400°C (Angleton and Hayer 1967). The strongest mode of vibration in NBT is the [33] mode but d_{33} and g_{33} are somewhat lower than many of the perovskite ferroelectrics previously discussed (Table 5.1); nevertheless, the high T_c and high resistivity make NBT an attractive, moderately high temperature piezoelectric.

Although not commercially available, other complex variations of BLSF compounds have been reported to have Curie temperatures of over 800°C. Representative of this group is Bi_3TiNbO_9 for which room temperature values of d_{33}, and g_{33} were reported to be near those of NBT (Korzunova 1992). To date, little else has been reported about other properties, particularly at high temperature.

BLSF materials can be made with grains having a plate-like morphology. In ceramic formed and fired by conventional processes, these grains orient in a more or less random fashion, leaving only a limited number of crystallographic orientation directions available for polarization due to the low symmetry of the structure. The achievement of an optimum degree of remnant polarization in polycrystalline ceramics necessitates the use of some mechanism to provide grain orientation. By employing hot forging techniques, Takenaka and Sakata (1988) prepared samples of several BLSF family members which display a high degree of texturing. These samples exhibited a twofold increase in the coefficients k_{33} and d_{33} over samples sintered by conventional methods.

5.6 Lithium Niobate ($LiNbO_3$)

Lithium Niobate (LN) has the corundum structure and a reported Curie point near 1150°C. Single crystals are grown from a melt using the *Czochralski* technique. Single crystals are preferred because of the higher piezoactivity, as well as the avoidance of difficulties encountered in conventional sintering of the polycrystalline form of the material. As with polycrystalline ferroelectrics, single crystals of $LiNbO_3$ exhibit a multi-domain structure and must be poled. This is accomplished by applying a relatively small electric field (≈1 V/cm DC) at a temperature just below the T_c and cooling to about 800°C with the field in place. In the poling process the structure is converted to a single domain. The crystal is then sliced along the desired axis indicated for the application; the faces are polished and electrodes applied (Fraser 1989). For accelerometers, electrodes are usually applied parallel to the poling axis to take advantage of the greater value of the d_{15} piezoelectric constant and to eliminate pyroelectric effects. The voltage output of LN ($g_{15} = 91 \times 10^{-3}$ Vm/N) is significantly larger than those of the other piezoelectric materials listed in Table 5.1 due to the inherently low dielectric constant. Sensitivity remains high at 400°C (Table 5.2), but resistivity is the limiting factor for use above 650°C (Figure 5.1).

The tantalum analog, $LiTaO_3$, exhibits many of the same characteristics of $LiNbO_3$; however, the T_c (720°C) and piezoelectric constants are somewhat lower, thus offers no apparent advantage for high temperature acoustic sensors.

5.7 Chapter Summary and Conclusions

If an operating temperature of 400°C or greater is required, the number of available sensor materials is clearly limited. If an operating temperature a 700°C is chosen, there is no commercial material available. It is reasonable to assume that there now exists a need for vibration sensors that can function at 700°C, or even at 1000°C, and that the need will be even more pressing in the future. The design of such sensors presents a great challenge and will require the development of new materials and novel processing techniques.

CHAPTER 6

NEW HIGH TEMPERATURE PIEZOELECTRIC MATERIALS

The ferroelectric ceramics discussed in the previous chapter are limited to temperatures of approximately one-half T_c with none capable of operation above 700°C. For applications requiring higher temperatures, the choice is limited to only the few experimental materials which are discussed in this chapter. At present, the only two materials which show promise of useful piezoelectric activity up to 1000°C are AlN thin films and PLS materials. In Figure 6.1, the anticipated maximum use temperatures of these two new materials are graphically compared with the commercial piezoelectric materials discussed in Chapter 5.

6.1 AlN Thin Films

In recent years, numerous studies have been made of the piezoelectric properties of thin films of several materials, including some of the ferroelectrics previously discussed (Francombe and Krishnaswamy 1990). Thin films of non-ferroelectric materials, including aluminum nitride (AlN), are also of great interest. Because of its exceptionally high thermal conductivity and dielectric breakdown strength, polycrystalline AlN is an important ceramic material used in substrates for hybrid microelectronics, but in the bulk form shows no piezoelectric activity. However, when properly oriented on a compatible substrate, AlN thin films exhibit piezoelectric properties which have been studied for their potential use as transducers, speakers, and SAW devices (Mujasaka *et al.* 1987).

Of most interest for this report are the high temperature piezoelectric properties of AlN thin films. A recent paper by Patel and Nicholson (1990) reported that a surface

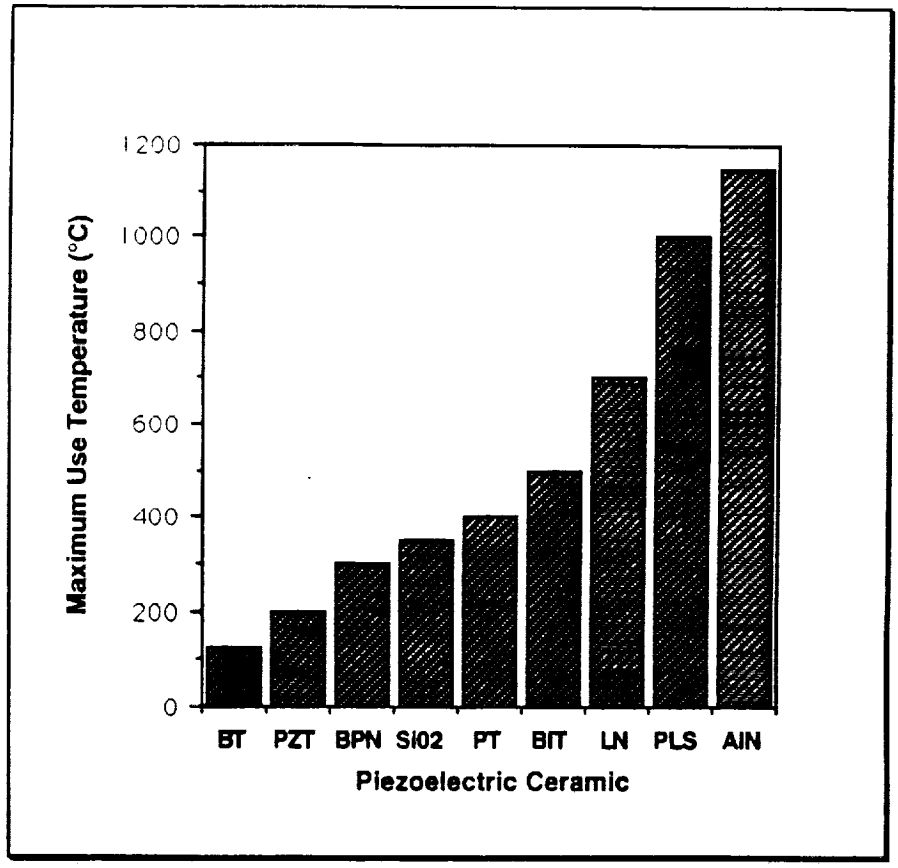

Figure 6.1 Approximate maximum temperature of operation for piezoelectric ceramics. Most are estimated by combined consideration of the ferroelectric Curie temperature, sensitivity, and measured electrical resistivity. Others are known with a higher degree of certainty such as barium titanate (BT) limited by its *Tc* of 125°C, lead zirconate titanate (PZT) known to experience accelerated depoling at 200°C and quartz (SiO_2) with a maximum use temperature of 350°C.

acoustic wave (SAW) device, using an AlN thin film deposited on a fused silica substrate, operating at 60-100 MHz, exhibited piezoelectric responses at temperatures up to 1150°C. Other reports on chemical vapor deposited (MOCVD) AlN thin films have shown room temperature d_{33} values of 5.5 x 10^{-12} Vm/N (about the same as $LiNbO_3$) and a dielectric constant K_{33} of 12 (Shiosaki *et al.* 1982). Tsubouchi and Mikoshiba (1983) reported room temperature resistivity values of 10^{16} ohm-cm, a value higher than any other piezoelectric material discussed in this paper. With this combination of very high temperature operation, high resistivity, and reasonable piezoelectric coefficients, it seems that AlN thin films warrant further investigation in the future. At this time, however, it was felt that designing and testing (at high temperature) high frequency, AlN thin film SAW devices would be beyond the scope of this work. Consequently, efforts were concentrated on, a study of lower frequency devices using PLS ceramic.

6.2 Perovskite Layer Structure PLS Ceramics

The PLS family of compound possess the general formula, $A_2B_2O_7$, the same as the naturally occurring mineral pyrochlore, CaNaNb2O6F. Pyrochlore has a face centered cubic structure; whereas, PLS compounds have been described as having a "distorted pyrochlore structure" (Jaffe *et al.* 1971). Depending on the exact composition, there are a number of polymorphs possible that can form from the high temperature prototype having the space group symmetry, *Cmcm*. The polymorphs are characterized by stacked perovskite-like slabs containing twelve-coordinated "*A*" cations and four thicknesses of corner-shared BO_6 octahedra linked by '*A*' cations positioned at their boundaries (Ishizawa 1981). The crystal structure of the PLS compound, $Sr_2Nb_2O_7$, as viewed along the *c*-axis is illustrated in Figure 6.2.

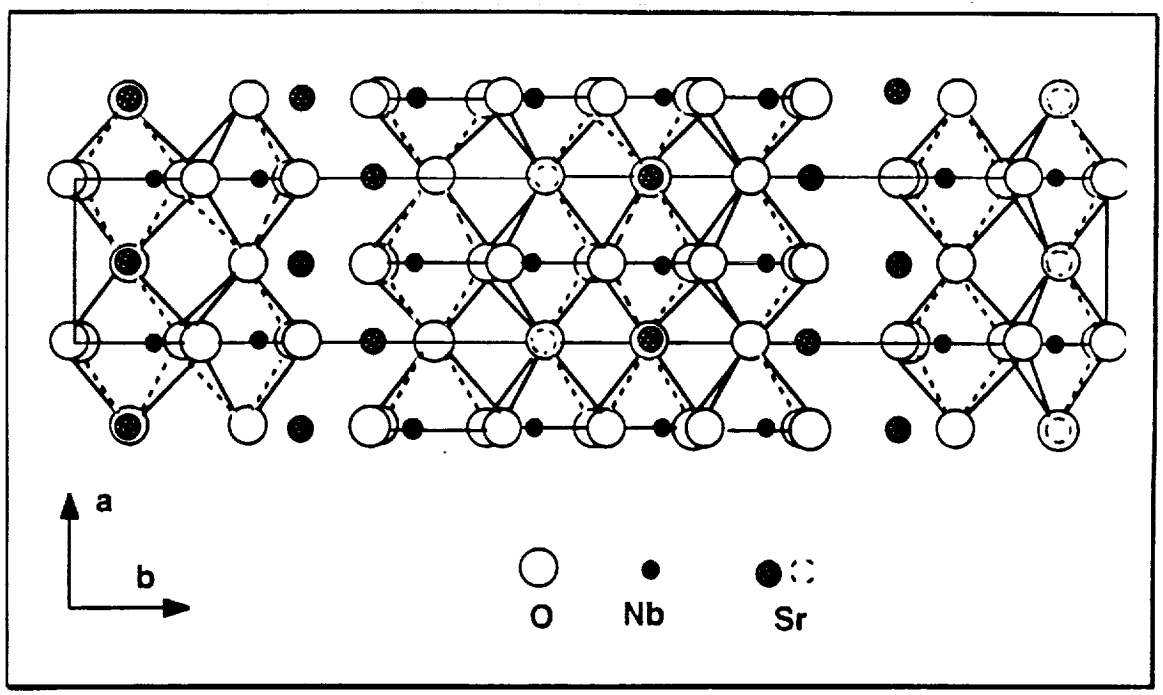

Figure 6.2 The crystal structure of the PLS compound, $Sr_2Nb_2O_7$, as viewed along the *c*-axis (after Ishizawa *et al.* 1975)

In SN and STa crystals, a transition occurs at T_c when the structure passes from the high temperature *Cmcm* paraelectric phase to the ferroelectric normal phase $Cmc2_1$. At that point there occurs a slight deformation of the oxygen atom framework in the perovskite-like slab. This change is illustrated in Figure 6.3. The distortion effects a slight rotation of the BO_6 octahedra around axes parallel to the *a* axis resulting in a spontaneous polarization. The transition is also accompanied by the characteristic rapid rise in dielectric constant that occurs as the T_c is approached (see Figure 6.1).

In SNSTa solid solution systems, an additional phase transition has been reported (Yamamoto 1980) to occur in the range of 170°C, for STa, to 215°C for SN (Figure 6.4). Although, when passing through this transition temperature, the structure transforms to a different symmetry (lower upon cooling, and higher upon heating), there appears to be no significant loss of piezoelectric effect in poled samples.

6.2.1 SNSTa Solid Solutions for High Temperature Sensors

Two PLS compositions, $Sr_2Nb_2O_7$ and $La_2Ti_2O_7$, reported by Nanamatsu *et al.* (1971, 1974), exhibit T_c values of 1342°C and 1500°C respectively, which are among the highest for any ferroelectric. In those works, both materials were prepared in the form of single crystals using techniques which required processing temperatures in excess of 2000°C. For those materials to be commercially viable, conventional mixed powder processing techniques would be necessary. Fuierer (1991) investigated both materials prepared by bulk powder techniques in the form of several variant compositions. In a manner similar to that used for BLSF compounds mentioned earlier, hot-forging was used to synthesize PLS compounds. The resulting samples were found to exhibit near theoretical density, a high degree of orientation, and polarizability (Fuierer and Newnham 1991, Fuierer1991).

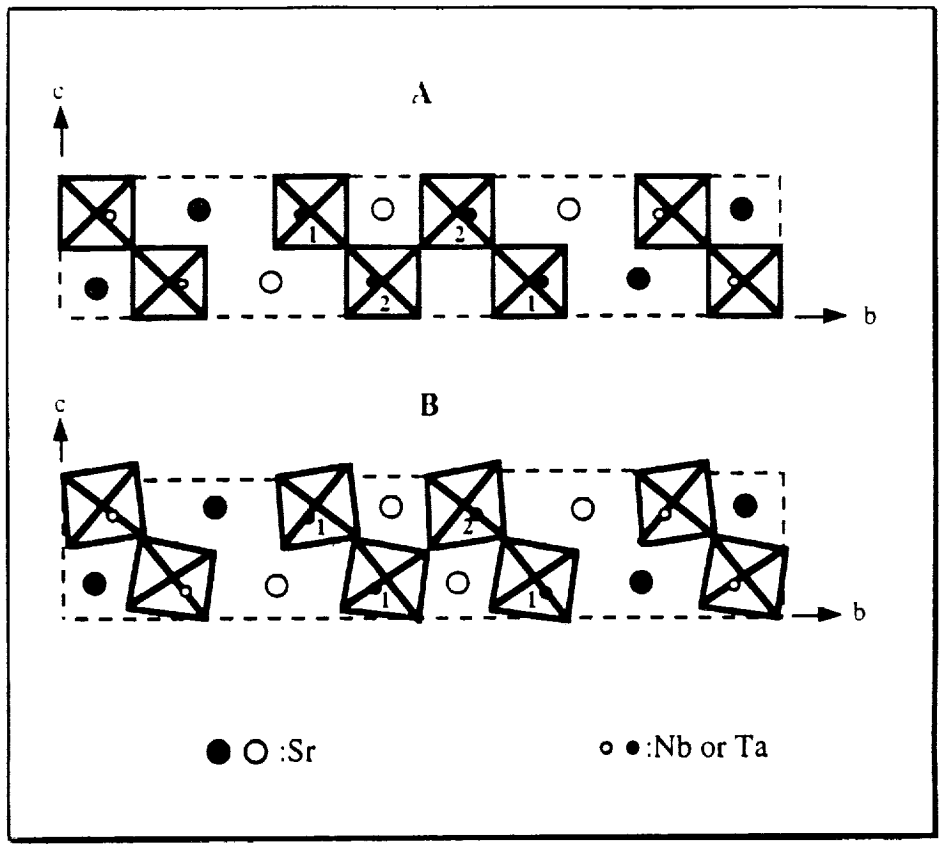

Figure 6.3 A schematic of crystal structure of $Sr_2(Nb,Ta)_2O_7$ as viewed along the *a*-axis. (A) is the high temperature paraelectric phase *mmm*, and (B) is the ferroelectric phase *mm*2. Numbers 1 and 2 and the dark and light circles represent two different sites (after Akishige *et al.* 1982).

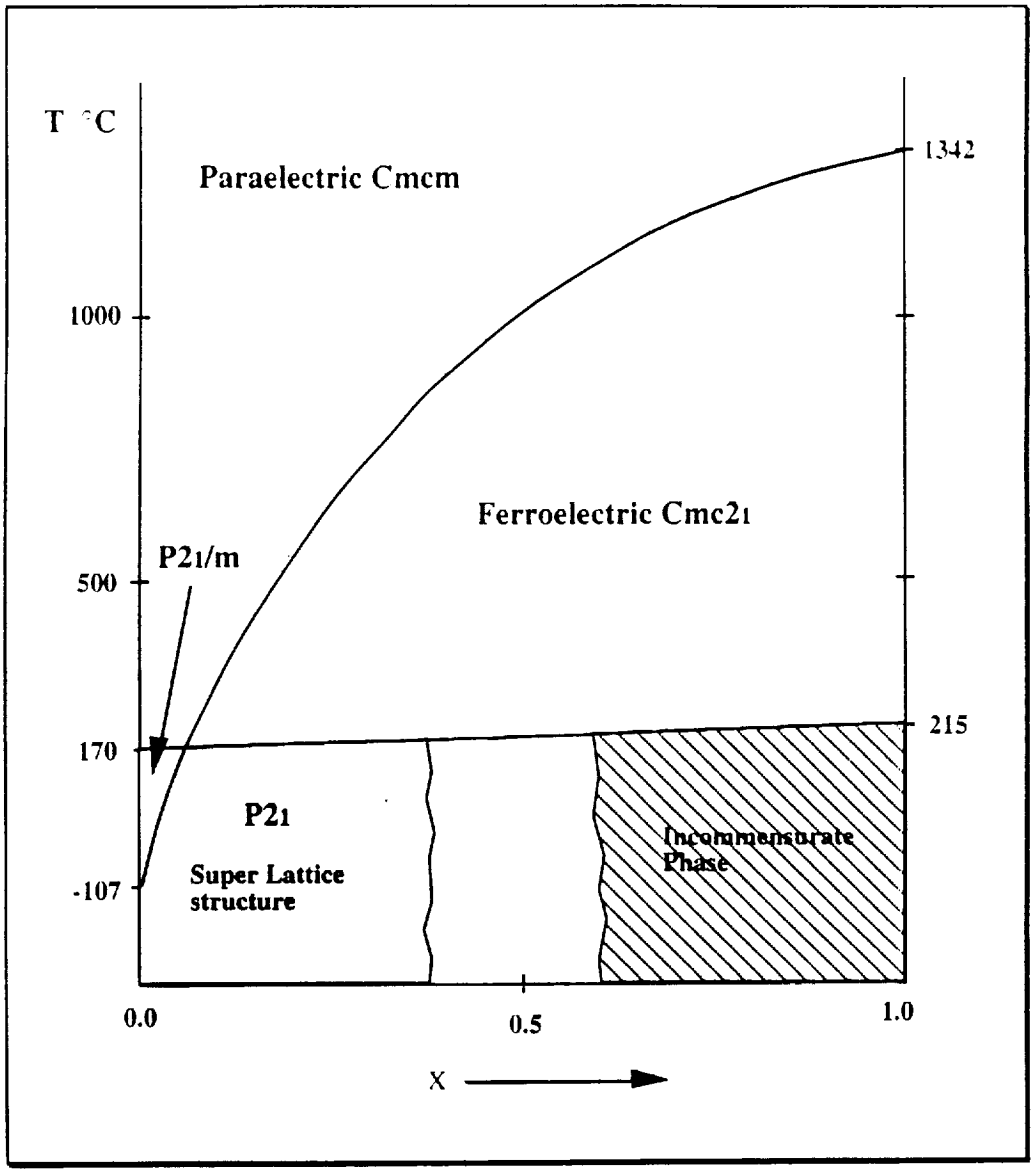

Figure 6.4 Phase diagram on the $Sr_2(Nb_xTa_{1-x})_2O_7$ system (after Yamamoto 1980).

Samples of $La_2Ti_2O_7$ compounds, however, were difficult to densify and isovalent substitutions, to effectively decrease the T_c to make sintering easier, could not be found. Hot forged samples were difficult to pole and exhibited very small piezoelectric coefficients (<1 pC/N).

Neto (1978) investigated $Sr_2Nb_2O_7$ (SN), prepared by conventional bulk powder and sintering techiques, but was unsuccessful in making dense samples which could be poled. SN can, however, be modified with $Sr_2Ta_2O_7$ to form a continuum of T_c values ranging from -107°C for pure $Sr_2Ta_2O_7$ to 1342°C for pure $Sr_2Nb_2O_7$ (Nanamatsu 1975), as shown in Figure 6.5, thus, providing a variety of options. Fuierer prepared solid solutions in the range of 25 mol% SN—75 mol% STa (25SN75STa) to 60 mol% SN—40 mol% STa (6SN4STa), along with SN, with an emphasis placed on 5SN5STa.

An important recommendation for the SNSTa family members is their excellent high temperature resistivity. As discussed in Chapter 4, high resistivity is of paramount importance when operating a piezoelectric device at high temperatures; therefore, it is beneficial to obtain the highest possible resistivity. Resistivity can sometimes be increased by the substitution of appropriate ions of a different valence for a few of the ions of the host material. The intent is to compensate for charge carriers originating from defects in the host structure. Often, these defects, which originate from physical imperfections in the structure or from the presence of impurities, are the largest contributors to conductivity in ceramic materials.

Unfortunately, little information about the defect chemistry of SN-STa system could be found in the available literature. Fuierer (1991) did, however, investigate the effect on resistivity of SN by the donor substitution of La^{3+} for Sr^{2+} in the A site, and acceptor substitution of Ti^{4+} for Nb^{5+} in the B site. He found that the Ti^{4+} acceptor addition decreased the resistivity; whereas, the donor substitution of La^{3+} increased resistivity slightly, with the maximum resistivity occurring at a level of 0.5 mol%.

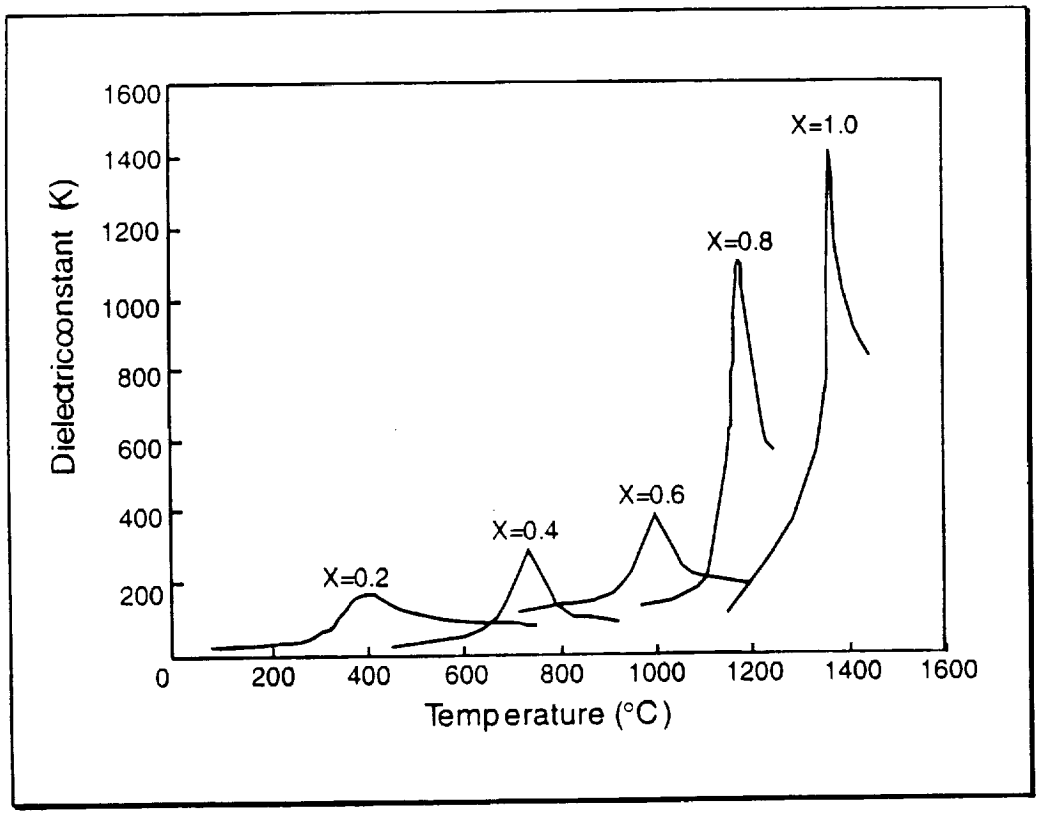

Figure 6.5 Dielectric constants of solid solution $Sr_2(Ta_{1-x}Nb_x)_2O_7$ at 1 MHz as a function of temperature (after Nanamatsu 1975).

Fuierer reasoned that the increased resistivity was due, in the most part, to the compensating effect of the donor for possible acceptors resulting from impurities in the raw materials used in the formulation, and from contamination picked up during milling. As their levels are increased, donor ions become the dominant source for increased conductivity.

6.2.2 Selection of the SNSTa Composition for this Work

Of the possible SNSTa compounds, Fuierer (1991) worked primarily on the composition 5SN5STa; but for the present work the T_c of 823°C for that composition is too low. With a target operating temperature of 1000°C, a high T_c is requisite. Using Figure 6.5 as a guide, the composition 8SN2STa, having a T_c of 1160°C, was selected.

The rationale for the selection of the 8SN2STa composition is further supported by Fuierer's data for the electrical properties of compositions having the same end members but different ratios (Table 6.1).

Table 6.1

Electrical properties of various SN_xSTa_{1-x} compositions (Fuierer 1991).

Comp.	T_c °C	K_3	k_{33} %	k_{24} %	$d_{33} \times 10^{-12}$ C/N	$d_{24} \times 10^{-3}$ Vm/N
25SN75Sta	473	85	nil	2.1	nil	1.3
5SN5STa	823	60	3.2	3.0	1.6	2.6
6SN4Sta	933	61	4.4	3.6	2.2	2.9
SN	1342	60	2.5	1.2	1.3	1.0

This chart shows a trend of increased values of the piezoelectric properties with increased SN content and suggests that even higher values may be possible. The lower values for "pure" SN indicate that the maximum values must occur at some SN/STa composition ratio between 0.6 and 1.0; with this in mind, it seemed that the 8SN2STa would be a reasonable choice.

6.3 Conclusion

This chapter has discussed two options for very high temperature piezoelectric materials: the first was non-ferroelectric AlN thin film with a reported operating temperature of 1150°C, and the second was the family of PLS ferroelectrics, with the highest known T_c (some greater than 1500°C). For this work, the PLS ceramic 8SN2STa was selected for further studies because of its reported T_c of 1160°C, and because of its potential of having piezoelectric properties large enough to be of practical interest. The ceramic also avoids the difficulties associated with the fabrication of AlN thin films and the potential difficulties posed by the high frequencies required in evaluating SAW devices at high temperature.

CHAPTER 7

EXPERIMENTAL PROCEDURE

Samples of 8SN2STa ceramics were prepared by conventional mixed oxide preparation methods. A few of the samples were sintered by ordinary firing (OF) methods; but the main focus was on hot forging techniques to attain grain orientation of the layer structure material. A variant method of hot forging, using a die to control the direction of material flow was also examined.

Experiments in poling were performed at temperatures ranging from 200°C to 1340°C, in an effort to optimize piezoelectric properties.

Samples of HF and OF ceramics were evaluated for their room temperature and high temperature electrical properties. This section discusses the tests performed and the equipment and fixtures used.

7.1 Powder Preparation

The raw materials used in the preparation of the samples were reagent grade oxides with a purity of at least 99.8%. Each composition variant was calculated and batched individually. In an effort to improve the resistivity of the 8SN2STa system, the effect of donor substitution in the *B* site was investigated. The cation W^{6+} was chosen for the study since its ionic radius (r =74 pm) is very near that of Nb^{5+} and Ta^{5+} (r =78 pm) (Shannon 1976) and the 6+ valence state is usually stable.

For the initial resistance studies, compositions containing no dopant, 0.001, 0.002, and 0.005 mol% W^{6+} were mixed in 25 gm batches. After the final formulation had been determined, 100 gm batches were made. Batches were milled in ethanol in

polypropylene jars filled to 60% capacity with 9.5 x 9.5 mm calcium stabilized zirconia cylinders*. Milling times were 4 hours for pre-calcine, and 16 hours post calcine. All batches were calcined in covered alumina crucibles at 1250°C for 2 hours.

Each batch of powder was then admixed with a polyvinyl alcohol-polyethylene glycol-water solution, calculated to give a final binder content of about 1.5 weight %. The mixtures were granulated through a 50 mesh sieve then dried. Individual parts were uniaxially dry pressed at 100 mPa in three sizes: 12.5 mm OD *x* 1 mm and 12.5 mm OD x 19 mm cylinders; and 6 *x* 8 *x* 25 mm bars. The first group (ordinary fired [OF]) was sintered at in air 1425°C for 2 hours. The other groups were used in hot forging experiments.

7.2 Hot Forging

The piezoelectric properties of ferroelectric materials are usually manifested at their maximum values when the dipoles of each domain have the same orientation as occurs in single crystals. However, in the case of layered structure ceramics, such as PLS and BLSF materials, the piezoelectric activity is curtailed due to two-dimensional restrictions on the permissible rotations of the spontaneous polarization, in contrast to the three-dimensionally permitted rotations found in perovskites. Thus, the layered structure ferroelectric ceramics whose crystallites have lower symmetry will not exhibit a satisfactorily large remanent polarization by conventional poling methods.

In order to overcome this problem, unconventional fabrication processes of piezoelectric ceramics have been devised to provide texturing of the microstructure to give preferred grain orientations. One process is a topotaxial reaction based on the shape

---

* Norton Co.

of the platelet-like characteristics of particles within the of the raw material powder. Layered structured materials possess such platelets, thus lend themselves to orientation by such techniques as extrusion and tape casting (Swartz *et al.* 1981). Another texturing method involves hot working which makes use of the motion of dislocations in grains and of the slip in the grain boundaries at high temperatures. Takanaka and Sakata (1980, 1988), in their work with BLSF materials, suggested that *hot forging* (HF) might be the most successful texturing technique for layered structure materials. More recently, Fuierer (1991) used hot forging with PLS ceramics. These references reported that hot forged samples were superior, in terms of density, and piezoelectric properties, to those produced by ordinary firing techniques.

7.2.1 Hot Forging by the Free Flow (conventional) Technique

In concept, hot forging is rather simple. The sample is heated to its "yield point", pressure is applied to opposite surfaces, and the material is allowed to flow laterally. Unlike hot pressing, where the hot ceramic is contained in a die and subjected to relatively high pressures for a short period of time, hot forging takes place more slowly, at lower pressures and at a controlled rate. Since the sample is free to flow horizontally in all directions, the rams of the forge must be parallel and have good alignment, otherwise, the forged sample will be wedge shaped and have irregular platelet alignment.

The heart of the process is the hot forging apparatus. The one used for this work, illustrated in Figure 7.1, was designed for high temperature creep studies (Dayton 1980) and was modified by Fuierer (1991) for his research. Further modifications were made to the apparatus for the present work.

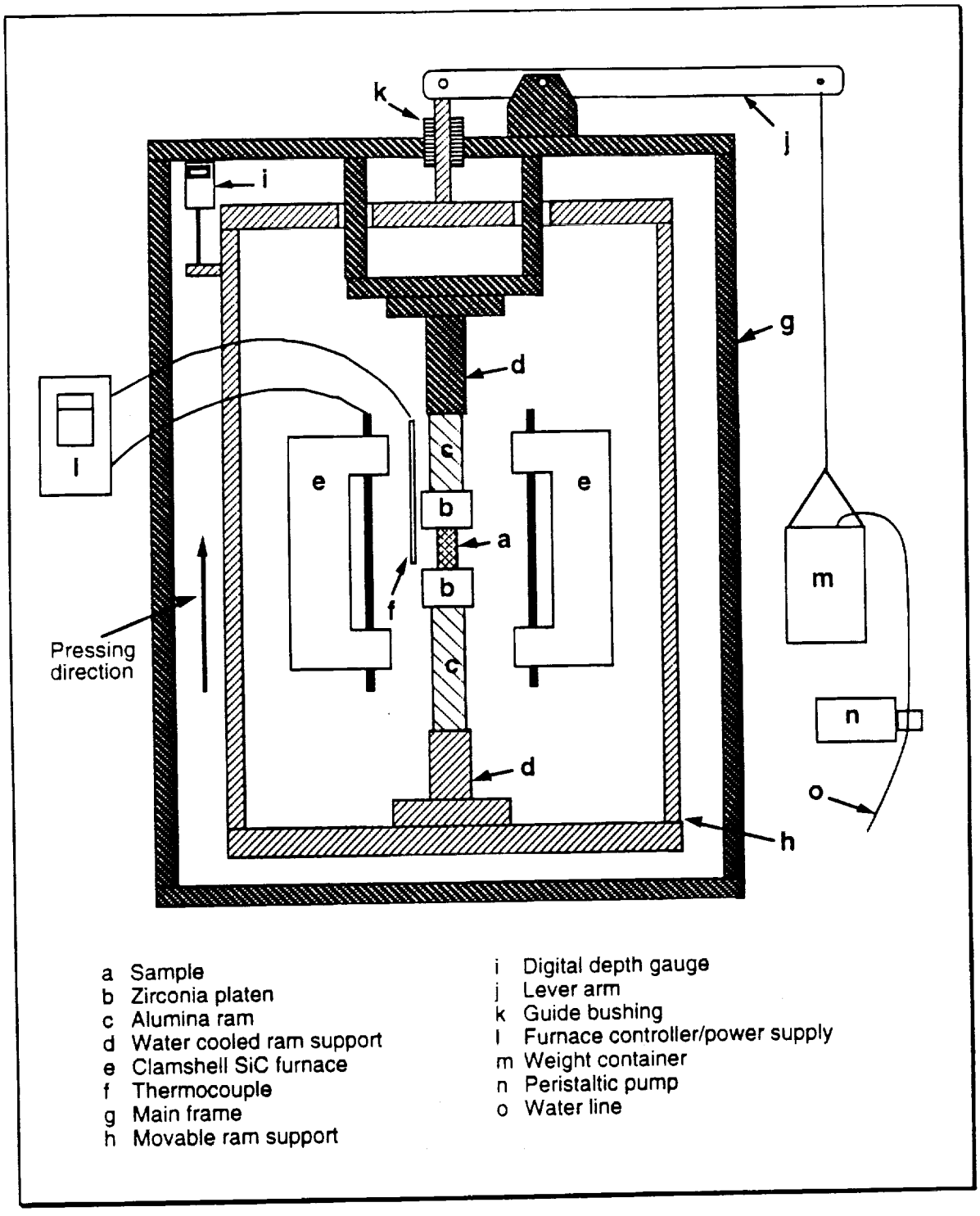

Figure 7.1 Apparatus used for hot forging experiments.

The sample [a] is positioned between the two calcium-stabilized zirconia platens* [b] which in turn, are in contact with the upper and lower rams [c]. Furnace [e] is a clamshell arrangement which surrounds the sample. After the furnace reaches the desired temperature, water is added to container [m] at a precisely controlled rate by means of a peristaltic pump [n]. The added weight of the water in the container, through the lever arm [j], raises the movable ram support [h] to apply force on the sample. The change in thickness of the sample is monitored by the digital depth gauge [i].

The green strength of the samples used was high enough to make it unnecessary to pre-sinter them before installing them in the hot forge apparatus. During the heat up, there was sufficient air flow in the furnace to allow complete binder burnout.

After considerable experimentation, the firing and weight loading cycles, shown in Figure 7.2, were found to have given the most satisfactory results for the 8SN2STa material. After the furnace had reached the forging temperature, water was added to the weight containers at a rate so as to maintain a rate of the sample compression of approximately 0.1 mm/minute. As the sample compressed, its diameter and density increased, thus, requiring a periodic increase in the rate at which the was water added. The final load of 33 kg of water (a pressure on the sample of about 24 mPa) was maintained for 30 minutes, then removed gradually over a 20 minute time span. The sample was annealed for 30 minutes, at the peak temperature, then cooled to 25°C over a 16 hour period. At end of the cycle, the sample had decreased in thickness from 19 mm to approximately 4 mm and had increased in diameter from 12.5 mm to approximately 20 mm. The final shape of a typical HF disc was that of a lozenge having a rather rounded edge. The color was a light tan, and thin slices are translucent, indicating its high density. The surfaces were smooth and showed no indication of reaction with the zirconia platens.

---

* Zircoa Corp.

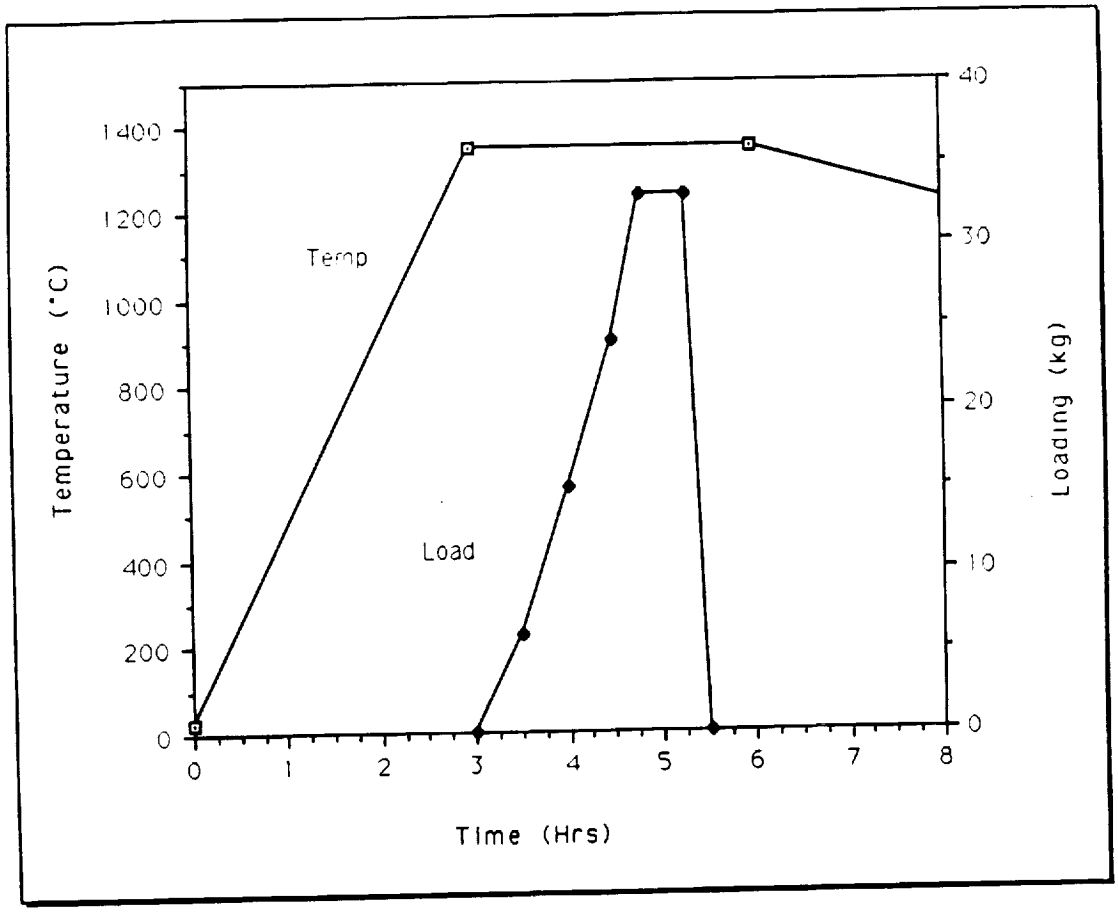

Figure 7.2 Temperature and loading as a function of time used for hot forging 8SN2STa composition.

7.2.2 Die Assisted Hot Forging Technique

The die assisted hot forging technique is similar to that outlined earlier and uses the same apparatus, but differs in that the sample, contained in a rectangular die during forging, is forced to flow along one horizontal axis of the die, while flow is constrained along the other axis. The sample, a rectangular, dry pressed bar (6 mm *x* 8 mm *x* 25 mm long), is installed in a rectangular shaped die with the internal dimensions of 7 mm *x* 28 mm *x* 45 mm deep, so that it is located in the center of the die with the long axis lying in the direction of punch movement. Figure 7.3 illustrates this concept. When the sample is heated to the forging temperature and pressure is applied to the punches, the flow of material is directed along a single axis. A few of the anticipated advantages of this method over the other method were as follows:

- More efficient use of sample material by forming the sample into a rectangular bar rather than a round disc.
- Better control of material flow because flow occurs only in a single dimension. Modification of the process could also be used to direct the flow in a single direction.
- Sample alignment in the furnace becomes less critical. The die assembly performs some of the alignment functions.
- This technique presents an opportunity to install electrodes in the die wall, allowing the application of an electric field across the sample, normal to the forging axis, in an attempt to influence dipole alignment while the material is flowing.

The die set used for these experiments is shown in Figure 7.4. The dense, 99.5% alumina cavity was constructed in two pieces to facilitate sample loading and removal. In order to hold the cavity segments tightly together while under load, they were installed in a dense alumina cylinder with the gap space filled with 60-mesh fused zirconia grain. The punches were made of alumina with zirconia inserts making contact with the sample.

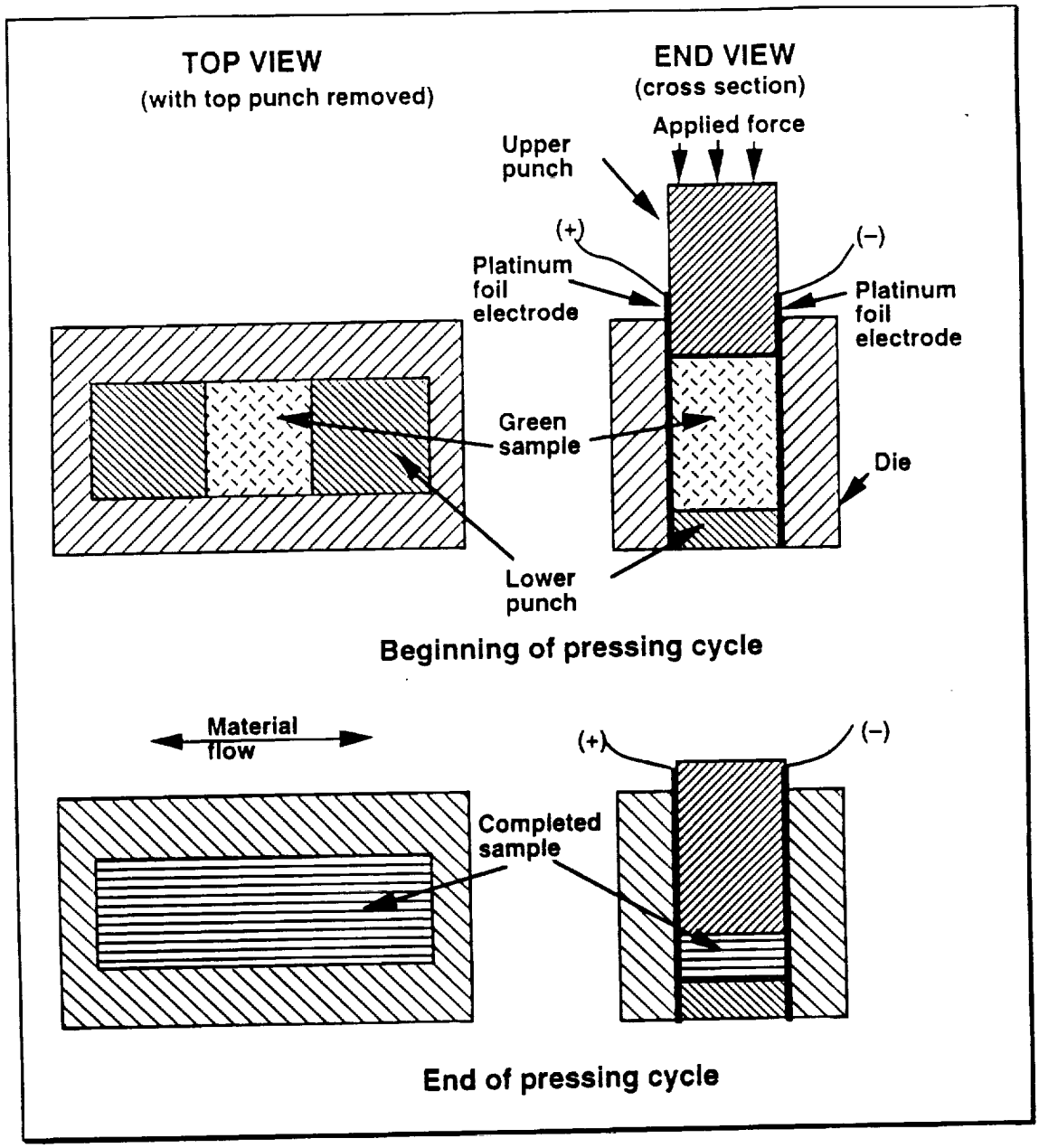

Figure 7.3 A schematic of die assisted hot forging.

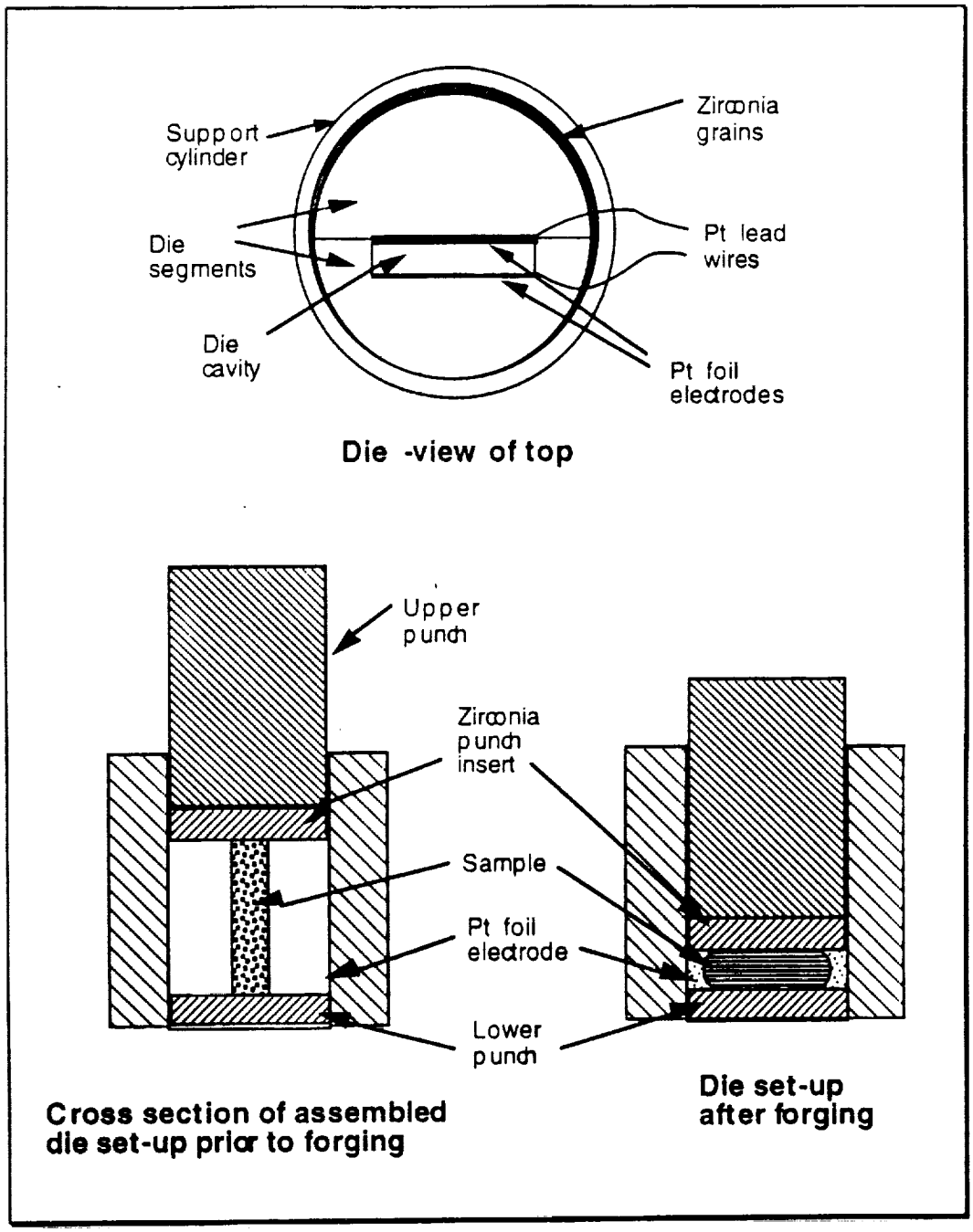

Figure 7.4 Illustration of hot forging die and set-up.

The die was assembled with the sample in place and was installed in the hot forge apparatus between the rams. The temperature and loading cycles procedures were similar to those described earlier. During the initial part of the hot forging cycle, the material flowed outward against the die wall and making intimate contact with the platinum electrodes, permitting the application of an electric field across the sample.

7.3 Test Sample Preparation

The ordinary fired "OF" discs were 10.8 mm in diameter and 1.0 mm thick. The hot forged, "HF", samples were bars which were sliced with a diamond saw* from discs approximately 25 mm *x* 4 mm thick (the fabrication of which was described earlier in this chapter). The bars were limited in size because of numerous cracks in the parent discs; however, it was possible to produce several bars, averaging 7 mm *x* 1.8 mm *x* 3.5 mm with the 1.8 mm dimension parallel to the forging axis.

Electrodes were applied to all samples used in electrical measurements. For initial low temperature evaluations sputtered gold electrodes were used. For samples used in high temperature tests, platinum paste was painted on and fired at 1000°C. All electroded surfaces were sanded and polished prior to electrode application.

7.4 Physical Characterization

Samples were measured with a micrometer and electronic thickness indicator, and weighed on an analytical balance in order to calculate densities. Scanning electron microscopy was used to determine grain morphology and alignment. X-ray diffraction

---

* Motion Dynamics, Inc.

was used to confirm grain alignment. Hot forged samples were soaked in a dye penetrant and examined under a 10-40X optical microscope to inspect for cracking.

7.5 Poling

The SNSTa samples required poling in order to render them piezoelectric. This required the application of fields up to 50 kV/cm at a temperature of 225°C, a temperature above the intermediate phase transition, and cooling them to 150°C, below the transition, while still under the high field. Attempts to pole above the high temperature transition, 1160°C, were also made, but without success.

7.5.1 Low Temperature Poling

As mentioned in the last chapter, spontaneous polarization occurs in SNSTa crystal when there is slight rotation of the BO_6 octahedra around axes parallel to the *a*-axis (see Figure 6.2). In the case of hot forged ceramic, polarization occurs along the axis perpendicular to the hot forging axis, the direction along which all samples were poled. Fuierer (1991) had reported that of all the possible modes, those exhibiting the strongest piezoelectric activity were the thickness (33) mode and shear (24) mode (Table 6.1); therefore, these modes became the focus of this study.

In an effort to optimize piezoelectric and coupling coefficients, it was necessary to determine the maximum electric field which the sample could sustain before dielectric breakdown occurred. For the 1.0 mm thick OF discs, a field of 50 kV/cm* could be safely applied; whereas, 33 kV /cm was the maximum safe voltage that could be applied

---

* Hipotronics model 875-13 high voltage power supply

to the 3.5 mm thick HF bars. This relationship of increasing field requirements with decreasing thickness is consistent with that found in other piezoelectric ceramics (Jaffe *et al.* 1971).

All samples were poled in silicone oil for 30 minutes either at 200°C or at 225°C. Those poled at 200°C showed no piezoactivity, but those poled at 225°C did. The higher temperature requirement can be attributed to the intermediate ferroelectric to ferroelectric phase transition which occurs at about 215°C (see Figure 6.3). To help facilitate the dipole alignment, the electric field was maintained above the transition temperature for 30 minutes, and then, while cooling to about 150°C. Such T_c crossing poling techniques are commonly employed while poling other ferroelectrics, such as, lithium niobate (Fraser 1989) and barium titanate (Jaffe *et al.* 1971).

Longer poling times (up to 90 minutes) were difficult to achieve and seemed to offer no particular advantage. The rate cooling was imposed by the oil bath** (about 4° per minute), so no study was made of its effect.

The HF samples were poled thorough the 3.5 mm dimension (33 mode), the axis perpendicular to the forging axis. Shear (24) mode samples were fabricated by removing the electrodes from poled (33) mode pieces and then applying new electrodes on the two major surfaces (perpendicular to the forging axis). The replacement electrodes were of platinum thick film paste fired at 1000°C. Owing to the high (reported) T_c 1160°C of the material, the piezoelectric properties of the samples degraded only slightly by the electrode firing cycle. This was verified by including control (33) mode samples in the firing.

** Exacal-Ex-250-HT, Neslab Instruments, Inc.

7.5.2 High Temperature Poling

It would be advantageous to polarize the SNSTa material simultaneously with the hot forging operation. An electric field applied at a temperature T_c, then held while cooling from the paraelectric phase to the ferroelectric phase, while using only a small electric field, could maximize dipole alignment, resulting in enhanced piezoelectric. Poling through the T_c is common practice with lithium niobate single crystals (Fraser 1989), and has been demonstrate to be effective for improving the coupling coefficient in polycrystalline PZTs (Shrout *et al.* 1983).

In the die assisted hot forging, it was a simple matter to apply an electric field to the sample through platinum foil electrodes installed on the die walls. At the forging temperature, the resistivity of the material was so low that only about 3 volts (~2 V/cm) could be applied before the 40 mA limit of the DC power supply* was exceeded. Unfortunately, because of the lack of uniform alignment of the grains, and excessive cracking resulting from die assisted hot forging, high temperature polarization of SNSTa materials could not be established. Attempts to "heal" cracked samples by refiring them with a modest pressure applied, were unsuccessful.

An effort was made to pole a grain-oriented bar, cut from a disc that had been previously hot forged by the free flow method. The bar was placed in the die positioned so as to maintain the original forging orientation, and making contact with the platinum electrodes installed in the die wall. After heating to 1340°C, sufficient pressure was applied to the punches to insure that the material flowed only enough to provide intimate contact with the electrodes. An electric field of ~2 V/cm was applied with a current flow of 40 mA. The sample was cooled while maintaining the field. As the resistivity of the

---

* Kepco model BOP 1000

sample decreased, the power supply increased the voltage to its limit of 1000V (~1500 V/cm field) as the current flow decreased below the 40 mA limit of the power supply.

It was noted that samples, to which the electric field had been applied, showed resistance value (calculated by Ohms Law, $E=IR$) several kΩ lower than was expected previous resistance measurements. At room temperature, the region thought to be the primary path of electron conduction through the sample, as outlined by a network of cracks, was nearly black in color, as opposed to the light tan color of the surrounding material. It is believed that the dark color and decreased resistivity result from the reduction of a portion of the metal cations (Nb^{5+} and/or Ta^{5+}) to some lower valence state by the flow of electrons through the structure. Current induced reduction has been observed in titanium and other multi-valence ions (Jaffe et al. 1971). Darkened samples, subsequently reheated to 1340°C without an applied field, returned to their normal light color, suggesting re-oxidation had taken place.

A lesser degree of darkening was also observed in samples poled by the low temperature method described earlier. After heating to 1000°C the samples returned to their normal color. Fuierer (1991) had also observed the same effect in his poled samples, and suggested that the coloration is caused by field induced "color centers" the structure.

Efforts were made to pole a OF sample at 1220°C, about 60 C above the expected high temperature T_c. The disc, 10 mm in diameter and 2.0 mm thick, with fired-on platinum electrodes, was placed in the hot forging furnace in the between platinum foil electrodes. At 1220°C a field of ~2.5 V/cm was applied with the current limited to ~2 mA, in an attempt to minimize possible cation reduction resulting from a greater current flow. As the sample cooled, the voltage was increased to maintain the current at ~2 mA until the 1000 V limit of the power supply was reached (~650°C). At this point the dielectric strength of the sample broke down and the broke into pieces, one of which was

expelled from the fixture. After cooling, the sample pieces were tested in the impedance analyzer, but they exhibited no piezoelectric activity. Visual inspection of the sample showed no darkening except at the site of dielectric breakdown.

7.6 Electrical Measurement Procedures

Electrical measurements were made at room temperature and at ranges of temperatures as high as 1375°C. Measurements, performed at room temperature, were made using simple spring loaded fixtures mounted on the test instruments. High temperature measurements were more difficult, however, and required devising a fixture made using Pt wire and foil, and using weights to maintain electrical contact. Despite its simple design, the fixture functioned adequately.

7.6.1 Resistance Measurements

The electroded samples were mounted between spring loaded platinum contacts (1.0 mm diameter) in a simple fixture. The fixture was then installed in a vertical tube furnace (51 mm inside diameter and 450 mm long). The leads were connected to a Keithly model 617 electrometer coupled with a Hewlett Packard 16055A test fixture. In order to avoid the difficulties often encountered in making resistance measurements in the TΩ range, readings began at 250°C, and were taken at 50°C intervals, both with increasing and decreasing temperatures. At each interval, the temperature was held until both the resistance and temperature reached a reasonable degree of stability. At the time of the actual reading, the furnace controller was switched off to eliminate electromagnetic radiation interference originating at the triac circuitry in the controller. Using this technique, repeated runs showed good repeatability.

7.6.2 Capacitance Measurements

Capacitance measurements were made at 1 MHz and 0.5V, using a Hewlett Packard 4194A Impedance Analyzer. For room temperature measurements, the samples were mounted in a simple, two wire holder connected to the instrument (Figure 7.5a). For high temperature measurements, the samples were heated in the furnace used for hot forging, described earlier in this chapter. The samples were held between two strips of platinum foil welded to 20 gauge platinum wires. The lead wires were passed out of the furnace through a length of 7 mm diameter alumina insulator (Figure 7.5b).

7.6.3 Piezoelectric Measurements

Resonance, impedance and phase angle measurements were made on a Hewlett Packard 4194A Impedance Analyzer using the capacitance fixture described earlier. High temperature measurements were made in a specially modified fiber lined furnace with a built in high temperature sample holder (similar to that shown in Figure 7.5a).

The piezoelectric constant d_{33} was measured on poled samples using a Berlincourt d_{33} meter at room temperature. The d_{33} value was obtained by first, mounting the sample in the fixture in the positive orientation, observing the reading, then repeating the procedure in the negative orientation. In both orientations the readout shifted approximately 1 pC/N in the appropriate polarity. In order to determine if the shift were the result of forces other than piezoelectric activity, the test was repeated using unpoled samples no shifts were observed.

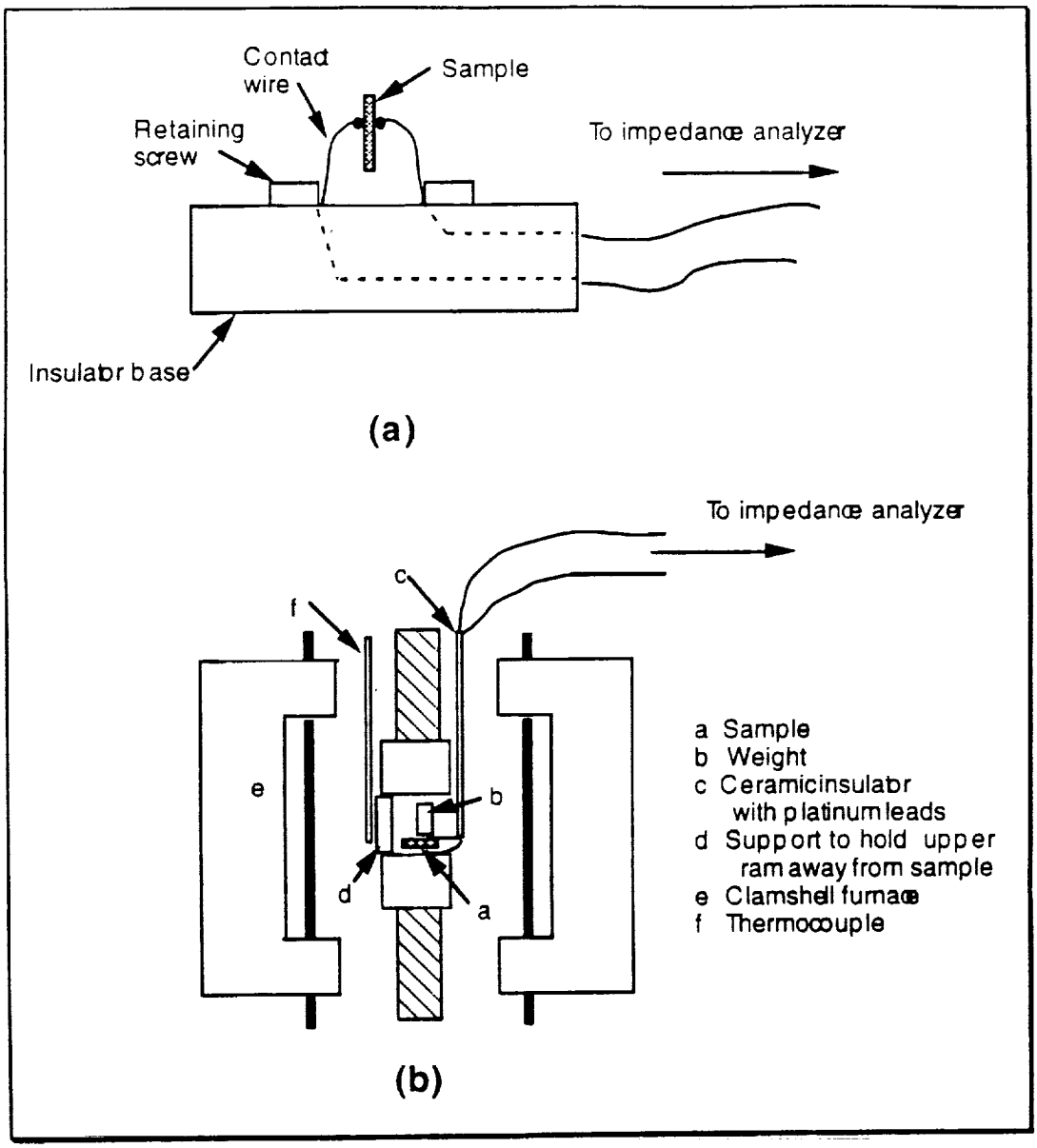

Figure 7.5 Sample holders used during (a) capacitance and resonant frequency measurements at room temperature (b) arrangement for high temperature capacitance using the hot forge furnace (See Figure 7.2 for details of the furnace).

CHAPTER 8

EXPERIMENTAL RESULTS

Samples of the 8SN2STa material were evaluated as hot forged HF bars and as ordinary fired discs. Density was calculated and the morphology was determined by means of scanning electron microscopy. The resistivity of the compositional variants was determined over a wide range of temperatures. Dielectric and electromechanical measurements were made at room temperature and at high temperatures.

8.1 Physical Properties

Table 8.1 shows the densities of the 8SN2STa composition, determined for both ordinary fired (OF) and hot forged (HF) samples. Results were compared with theoretical density data calculated from unit cell dimensions from X-ray diffraction data.

Table 8.1

Densities of 8SN2STa HF and OF ceramics

	Theo.	OF	HF
Density ρ (g/cm^3)	5.58	5.39	5.53
% of Theoretical	100	96.5	99.2

The high relative density of the HF samples is consistent with that obtained from other pressure sintering methods (Kingery, *et al.* 1976). Figure 8.1*a*, a (SEM)

photomicrograph of the microstructure of an HF sample, shows tightly packed, highly oriented grains with little porosity between them, further confirming the high density of the sample.

The 8SN2STa specimens, used in the SEM studies, were obtained from slices cut from the center portions of the hot forged discs, parallel and perpendicular to the HF axis and from the rounded outer perimeter. Samples were also sliced from the of the OF discs. The surfaces were then polished, and thermally etched at 1410°C for 2 hours.

Figure 8.1*a* is a view of a surface parallel to the forging axis of a slice taken from the interior portion of a disc forged by the "free flow" hot forging method. The microstructure is relatively pore free. The plate-like grains show a high degree of preferred orientation in the directions perpendicular to the forging axis, giving a "brick wall" appearance. In the outer perimeter of the same disc (not shown), the plates are fairly well ordered, but tend align themselves in directions following the curvature of the edge. The estimated average size (from SEM observations) of the plate-like grains is 4.5 μm in length by 1 μm in thickness.

Figure 8.1*b* shows the microstructure of a sample hot forged by the die assisted method. The grains, although mostly parallel with one another, are skewed at some angle away from a plane parallel to the punch faces. The angle of orientation differs depending upon its location within the sample, giving the appearance that the material had moved by plug flow; this in part, is the result of its adherence to the die wall. It is unlikely that this hot forging method could be used to make samples with well-oriented microstructures.

The platelet-like grains within the samples sintered by ordinary firing indicate no orientation and higher porosity than the hot forged samples (Figure 8.2).

Figure 8.1 SEM photomicrographs of the microstructure of hot forged 8SN2STa material. [*a*] The conventional free flow method shows a high degree of grain alignment. [*b*] The die assisted method shows regional alignment (note the direction of the grains in the lower part of the photo compared with that in the upper indicating a possible "turbulent" flow). Both views are from slices taken from the center sections of the samples with the surfaces parallel to the hot forging axis. The samples were polished and thermally etched for 2 hours at 1410°C.

Further evidence of significant grain orientation of the hot forged material is provided by X-ray diffraction, indexed to the orthorhombic $Pbn2_1$ modification suggested, first by Scheunemann and Muller-Buschbaum (1975) and later by Fuierer (1991). The surface perpendicular to the forging axis (Figure 8.3a) shows the domination of $0k0$ intensities, whereas these intensities are greatly diminished in the surface parallel to the forging axis (Figure 8.3b). The latter surface indicates increased $h00$ and $00l$ intensities not found in the former. X-ray patterns taken of perpendicular surfaces of ordinary fired, unoriented samples would be nearly identical and would include many of the intensities found in the two patterns of the oriented specimen.

8.2 Fracturing in Hot Forged Material

Fracturing was a serious problem encountered in hot forged samples in this work, and was also reported by Fuierer (1991). The most plausible cause of cracking is a consequence of the anisotropy of the SNSTa plate-like grains. Fuierer reported the average thermal expansion coefficients for SN and 5SN5STa compositions (parallel and perpendicular to the forging axis) over the range of 100-950°C as shown in Table 8.2.

Table 8.2

Thermal expansion coefficients over the range of 100-950°C in the composition 5SN5STa along the axes parallel and perpendicular to the hot forging axis (Fuierer 1991)

Orientation	α x 10^{-6}
∥ FA	16.5
⊥ FA	11.5

Figure 8.2 A photomicrograph of the microstructure of ordinary fired 8SN2STa composition showing an absence of platelet morphology.

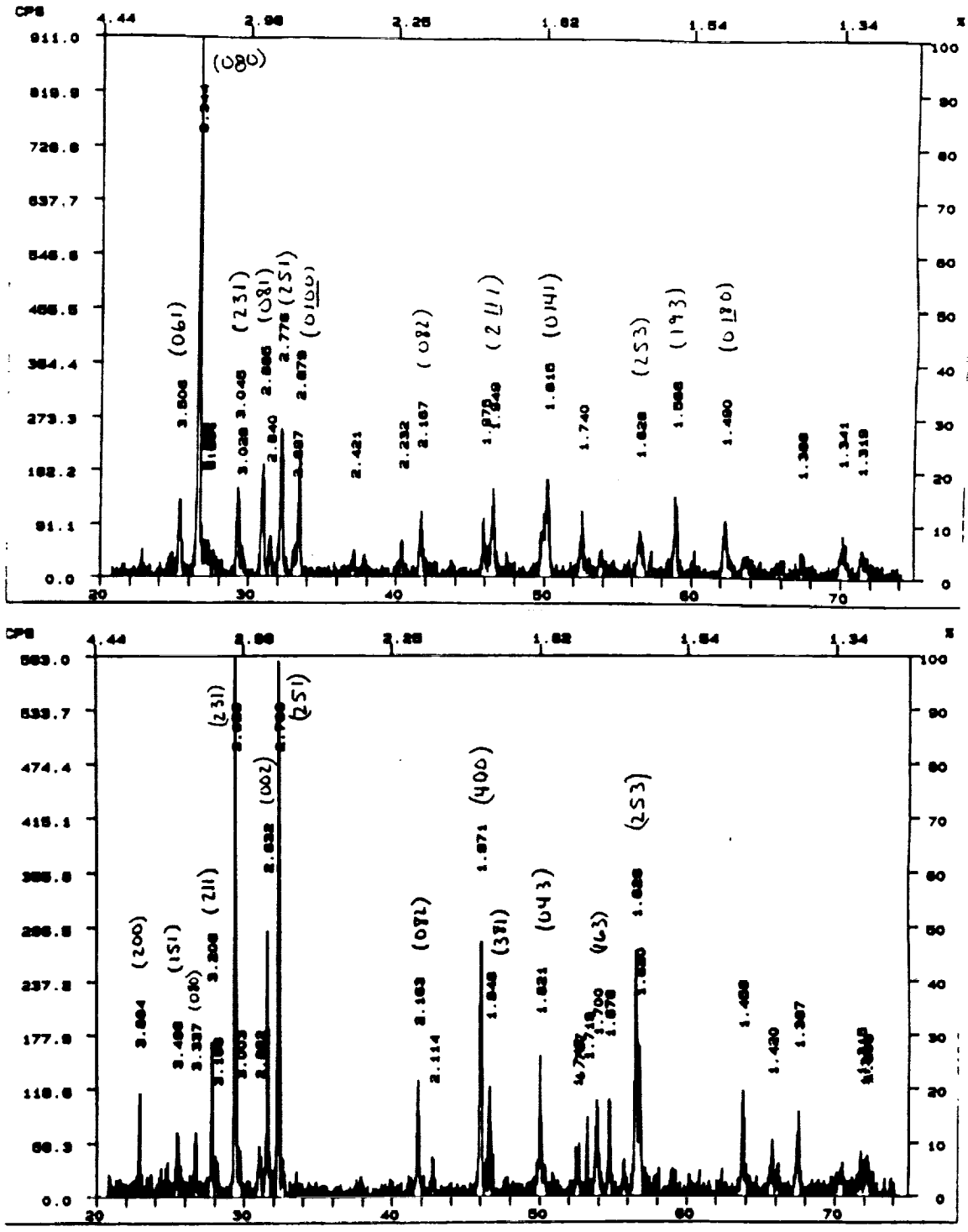

Figure 8.3 X-ray patterns of hot forged 8SN2STa for the surfaces (top) perpendicular and (bottom) parallel to the hot forging axis.

With the differences in magnitude of the two expansion coefficients, it is not difficult to see that as the sample cools after hot forging, high tensile stresses can develop between adjacent regions whose plate-shaped grains are oriented in different directions. Figure 8.4 provides a schematic model of (*a*) ideal orientation, and (*b*) of what is believed to have occurred within the hot forged discs. The entire margin between the outer perimeter of the discs and the center 16 mm diameter portion cracked. Some discs split cleanly through the middle creating two discs, nearly the same thickness; whereas, others shattered. Localized cracking also occurred in various locations throughout the disc.

Except for the large longitudinal fracture, nearly all of the cracks in the HF disc were closed cracks and most were difficult to see without magnification. Some cracks seem to have developed only after the piece was sliced, indicating the pre-existence of tensile stresses. The samples also seemed to fracture more easily along the planes of the oriented grains.

The die assisted HF samples were more prone to cracking due to tensile stresses generated at the sites between adjacent regions with somewhat different platelet alignment, localized (see Figure 8.2*b*). Every specimen forged in the die method showed similar patterns of dome shaped cracks which appeared to have traced the path followed by the flow of the initial bar configuration as it spread outward. Numerous other cracks were also present throughout the sample. Attempts to "heal" the cracks by subsequent refiring samples, with applied pressure, were unsuccessful.

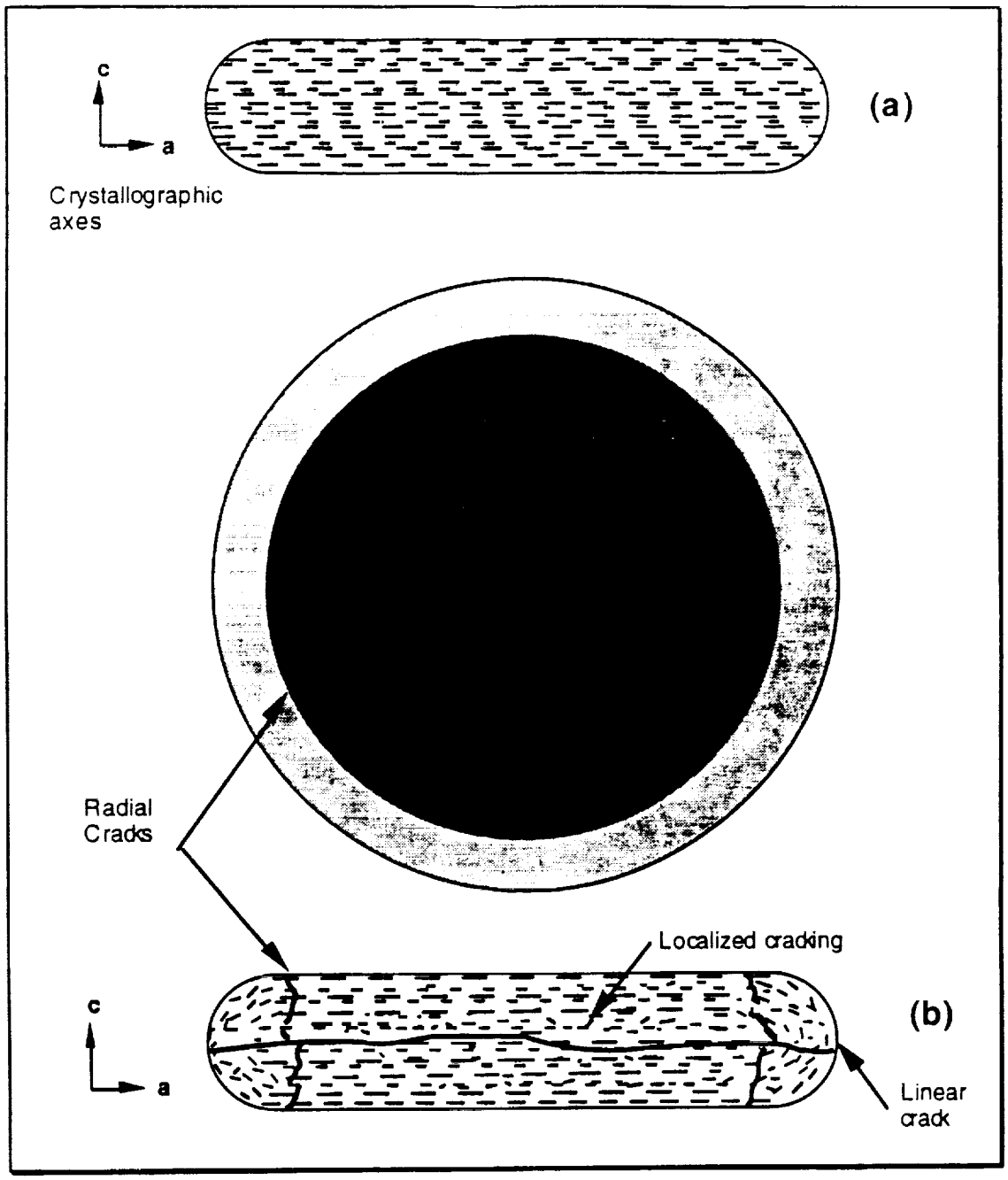

Figure 8.4 Schematic model of grain alignment in a hot forged disc, mostly perpendicular to the forging axis in: (a) an ideal alignment (b) a more likely alignment with some grains not in common alignment with the bulk leading to internal tensile stresses and fractures.

8.3 Electrical Properties

Electrical properties of both hot forged and ordinary fired samples were evaluated at room temperature and at high temperatures. The following section includes the results of these measurements for resistivity, dielectric, and electromechanical properties.

8.3.1 Resistivity

Figure 8.5 shows the effect of different donor levels of W^{6+} on the resistivity of the 8SN2STa composition. There was only a slight increase in resistivity at low donor levels (0.001 mol%); most likely the result of compensating effects for impurities in the body. At the highest (0.005 mol%) level, the resistivity exhibited a marked decrease. Because it showed the highest resistivity, the composition $Sr_2(Nb_{0.8}Ta_{0.2})_{1.999}W_{0.001}O_7$ was chosen for the hot forging and piezoelectric properties studies.

In the course of this work, no high temperature resistivity measurements were made on hot forged samples along the different axes. However, for the 5SN5STa composition, Fuierer (1991) reported that, over the range of 100°C to 750°C, the resistivity measured along the axis parallel to the hot forging axis was approximately one magnitude higher than that measured along the axis perpendicular to the forging axis. The differences in resistivities along the different orientations is further evidence of the anisotropic nature of the material. Ordinary fired samples showed the resistivity to be about midway between that exhibited for the two orientations, and to be very near the value for 8SN2STa measured in this work.

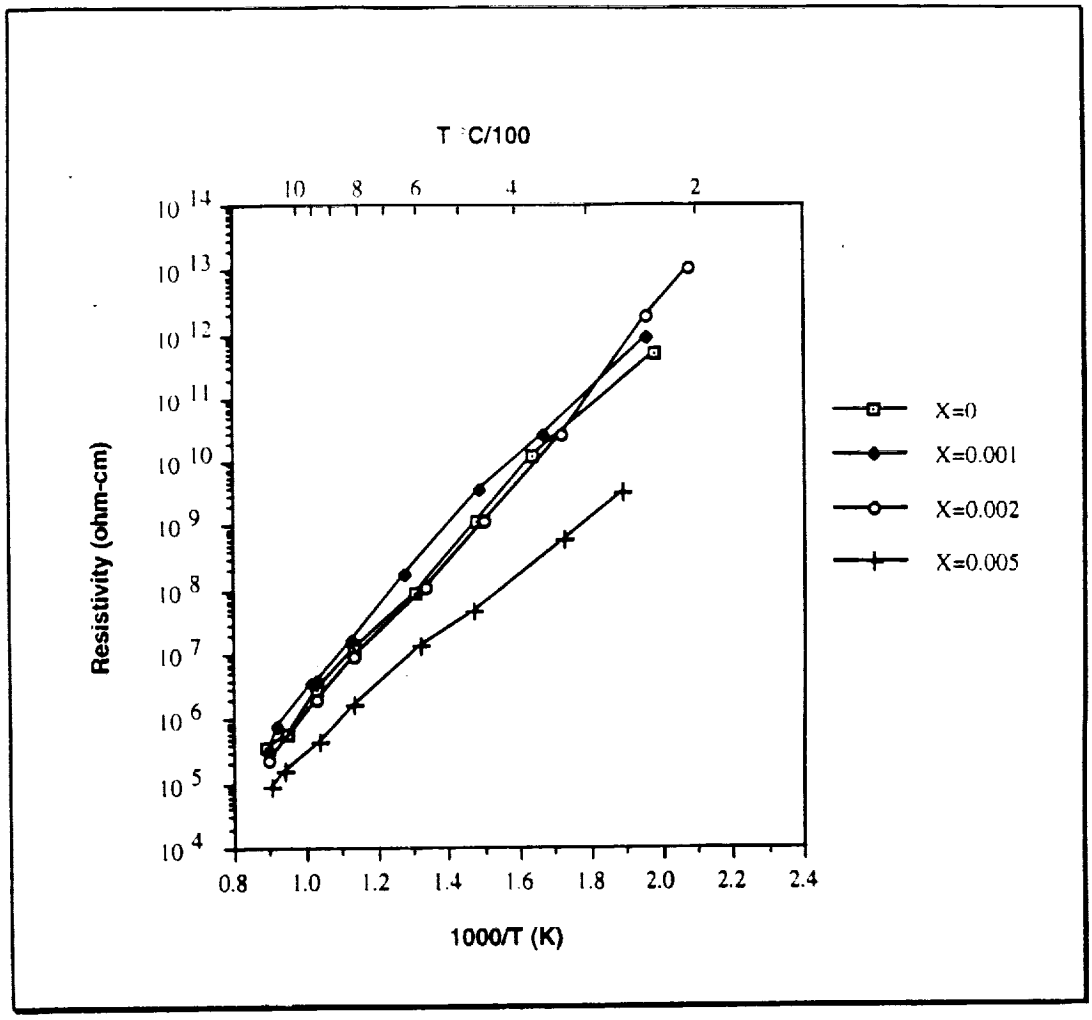

Figure 8.5 Temperature dependence of resistivity for the donor doped compositions of $Sr_2([Nb_{.8}Ta_{.2}]_{1-x}W_x)_2O_7$.

8.3.2 Dielectric Constant

The room temperature dielectric constants of each donor variant group of ordinary fired ceramics were found to be nearly identical. Hot forged samples were also measured parallel and perpendicular to the forging axis which lies parallel to the crystallographic c axis. Values for K along with the dissipation factor, *tan* δ, are shown in Table 8.3. The calculations were made for several samples, but are subject to some error owing to the small capacitance readings (1.5-7.5 pf) of the test samples. The difference in K between the parallel and perpendicular samples, does, however, suggest anisotropy in the material.

High temperature capacitance measurements, to determine the T_c, were also performed (Figure 8.6). As was expected, the (apparent) capacitance increased sharply as the temperature approached the anticipated T_c of 1160°C (Figure 6.1), but did not exhibit the expected decline beyond that point. The upward trend in capacitance continued to 1370°C at which temperature, measurements were discontinued.

Table 8.3

Room temperature dielectric properties for ordinary fired and hot forged 8SN2STa ceramics at 0.5 V and 100 kHz (the averages of several samples)

Sample	K	tan δ
OF	54	0.003
HF ∥ FA	49	0.001
HF ⊥ FA	60	0.003

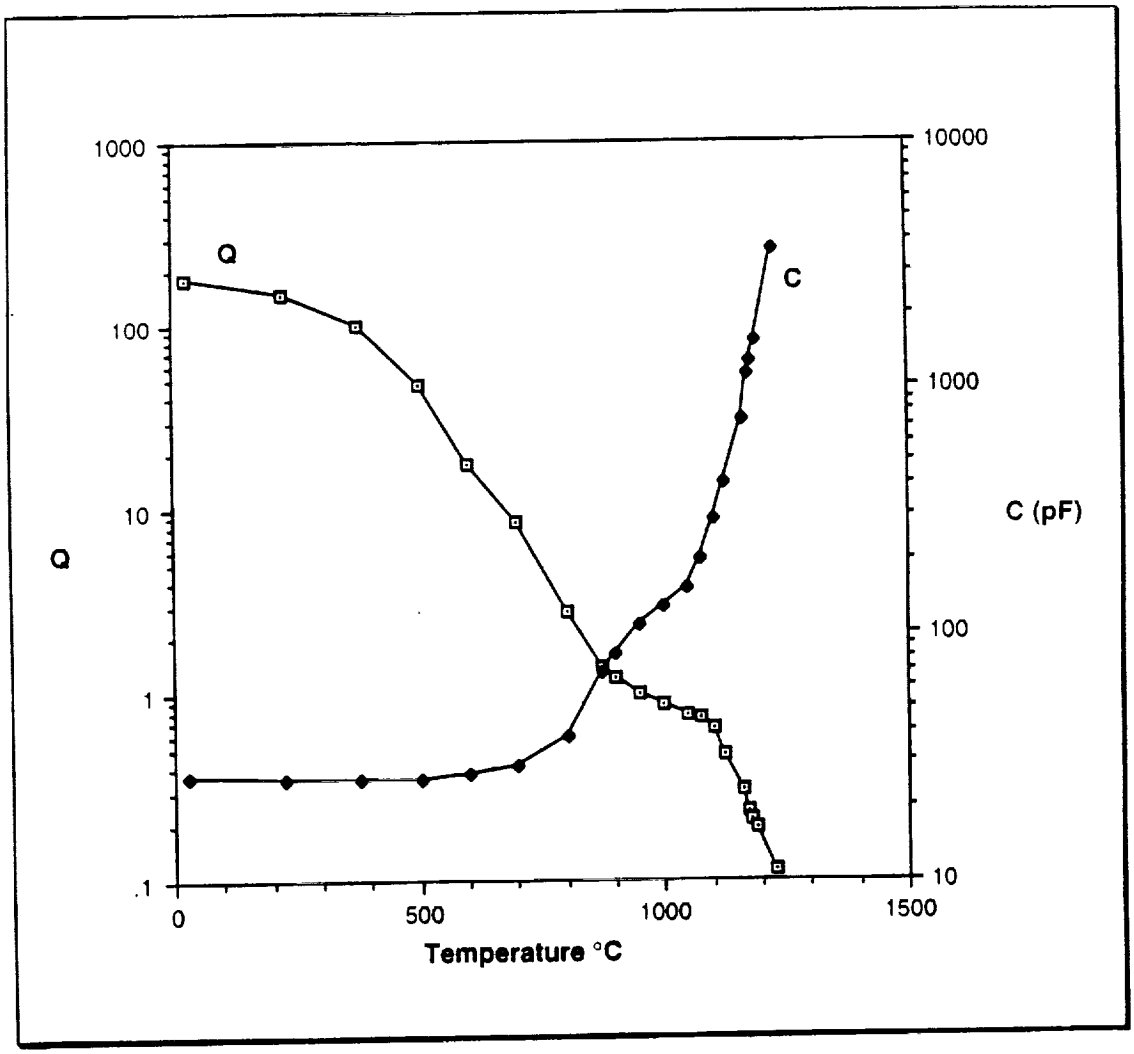

Figure 8.6 Apparent capacitance C and electrical quality factor *Q* (1/*tan δ)* of 8SN2STa ceramic as a function of temperature, measured at 0.5V and 1 mHz.

This result does not indicate the absence of a phase transition at the expected temperature, but rather, the effect of other mechanisms such as conduction and ionization coming into play. Dramatic increases in capacitance with increased temperature are found in many non-ferroelectric ceramics which indicates the presence of important mechanisms other than ferroelectric dipole action (Buchanan 1986). Ultimately these other mechanisms mask the location of the T_c of the sample. Nevertheless, Nanamatsu *et al.* (1974) had reported a T_c of 1160°C for this composition from samples made from a melt at 2000°C. Attempts to determine the T_c by differential thermal analysis (DTA) also failed to show an anomaly indicating a phase transition.

8.4 Piezoelectric Properties

Resonant and antiresonant frequencies of both HF and OF samples were measured with an impedance analyzer. Using this frequency data, and data given previously, important piezoelectric properties were evaluated. The piezoelectric properties of hot forged samples were also evaluated at temperatures up to 1125°C.

8.4.1 Room Temperature Results

Resonant and antiresonant frequencies were measured and evaluated for the three groups of samples. In the HF samples, the (24), (15) and the (33) modes were strongest. The (31), (32), and several overtones, were also observed, but they were too weak to be of interest. Figure 8.7 shows an impedance analyzer trace of the frequency- impedance peaks of [*a*] the (33) mode plus the weaker (31) mode, and [*b*] the shear modes, (24) (15). In the case of the ordinary fired disc-shaped samples, both the (33) and planar mode could be observed, but only the planar mode was strong enough to be considered.

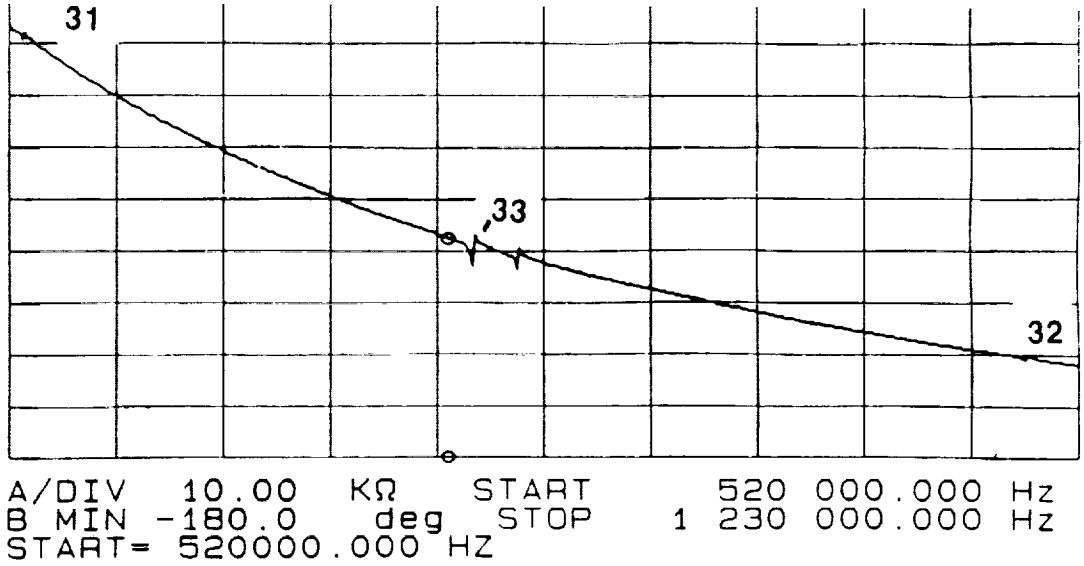

a

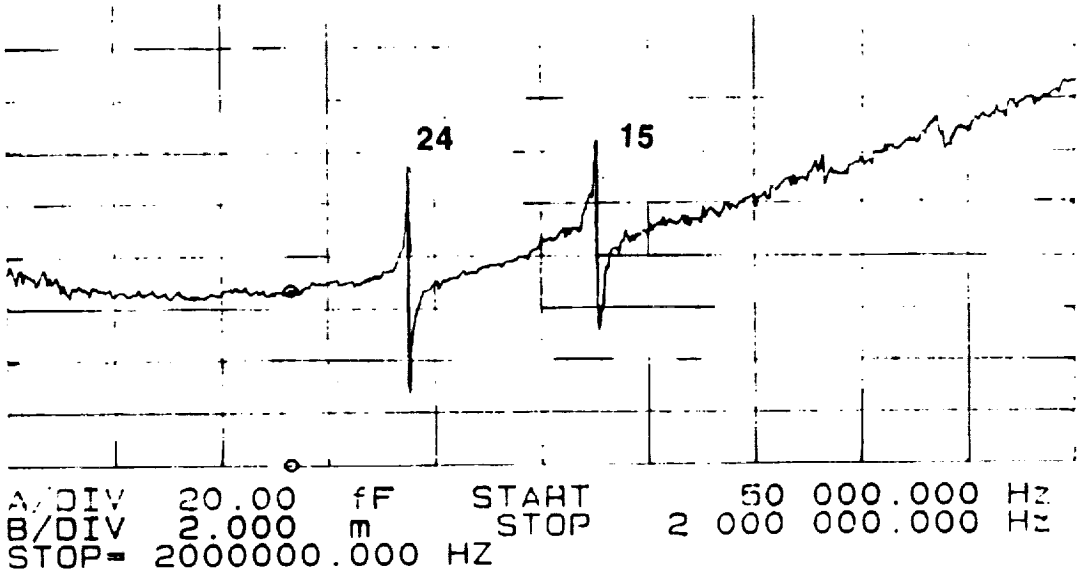

b

Figure 8.7 Impedance analyzer traces showing the frequency (ordinant) vs. impedance (abscissa)peaks of (*a*) the (33) and the weaker (31) modes, and (*b*) the (24) and (15) modes.

Using the equations 4.5 through 4.10, the piezoelectric and frequency constants and elastic compliance were calculated for the HF and OF samples. The results are tabulated in Table 8.4.

Table 8.4

Electromechanical constants of 8SN2STa ceramic at room temperature.

MODE	ρ (kg-m^{-3})	K	N_{ij} (Hz-m)	tan δ	s_{ii} (x 10^{-12} m^2/N)	k_{ij} (%)	d_{ij} (x 10^{-12} C/N)	g_{ij} (x 10^{-3} Vm/N)
33 (HF)	5530	60	3008	0.001	5.0 (s_{33})	5.8	2.9	5.6
24 (HF)	5530	49	1429	0.003	22.1 (s_{44})	7.7	8.4	15.8
planar	5390	54	3550	0.001	3.7 (s_{11})	2.8	–	–

The coupling of the (24) mode was about 50% larger than the (33) and (15) mode and substantially larger than the planar (k_p) mode. On the basis of on its higher coupling factor, its lower frequency constant and its non-pyroelectric nature, the (24) mode appeared to be the best choice for sensor applications. Another advantage was that thin (24) mode samples seemed to have considerably higher flexural strength than equivalent sized (33) mode plates; probably as a result of the laminar texture of the hot forged material.

Because of their smaller coupling coefficients. the OF planar mode samples were not given further investigation.

8.4.2 High Temperature Piezoelectric Measurements

Upon heating the shear (24) mode sample, resonance and antiresonance peaks—and consequently the coupling coefficient—steadily decreased in strength until, at approximately 600°C, they became indiscernible. Figure 8.8*a* shows in the impedance analyzer traces of the frequency *vs* impedance and phase angle for the (24) mode sample at room temperature and at 600°C (8.8*b*).

Continued heating up to 800°C produced no reappearance of the peaks. The peaks, however, returned as the temperature was reduced and disappeared again upon re-heating indicating that this reaction is reversible. When cooled to room temperature, the sample showed no appreciable reduction in electromechanical properties from depoling. The (15) mode responded in a similar fashion to that of the (24) mode.

Figure 8.9 shows the high temperature frequency constant and coupling of the (33) mode. From room temperature to about 300°C, N_{33} increased slightly while the k_{33} decreased; but at ~300° these slopes changed in response to the low temperature phase transition. A similar change in slope was seen with the (24) mode. Above ~300°C, N_{33} decreased and the k_{33} increased steadily to about 1060°C, at which temperature they reached their respective nadir and apex. Above ~1080°C, both slopes changed directions sharply indicating the onset of depoling as the temperature approached the T_c. Piezoactivity was still present after 30 minutes at 1125°C, after which time, the sample holder failed, making further measurements impossible. Figure 8.10 shows the frequency *vs.* impedance trace at.1125°C.

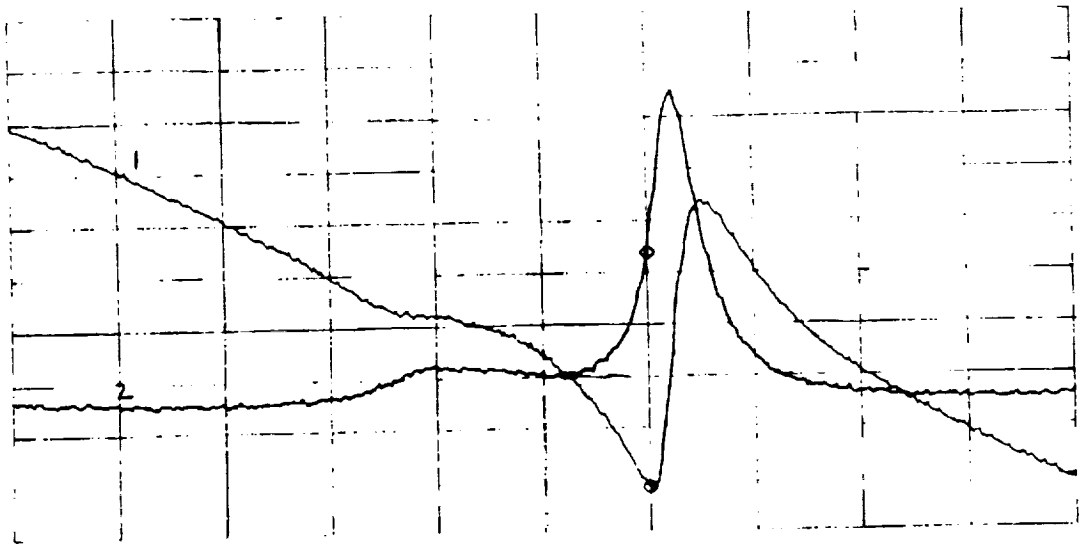

a

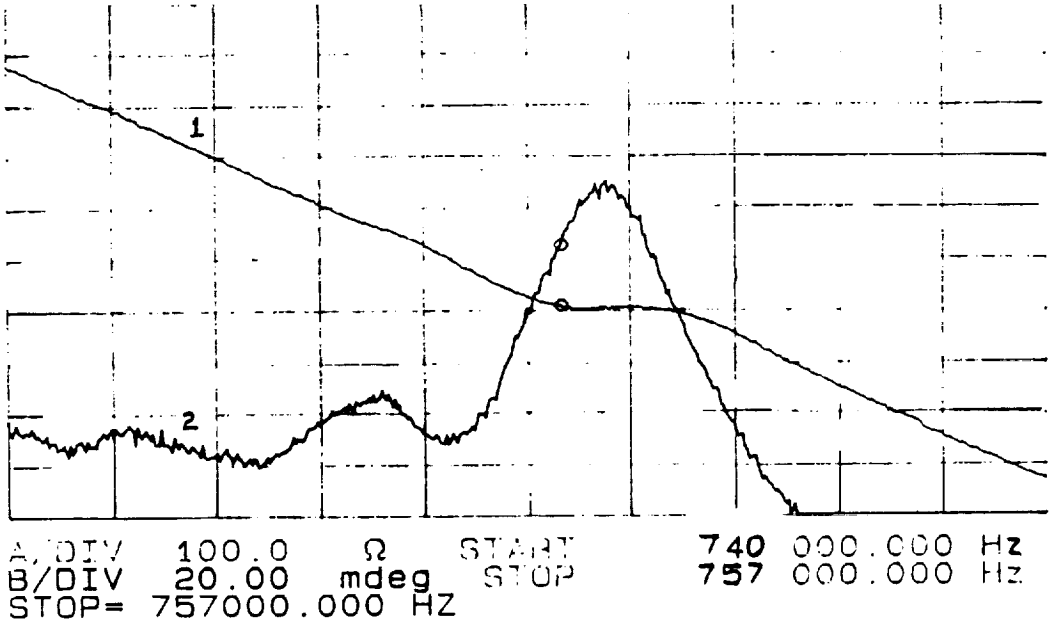

b

Figure 8.8 Resonance Impedance for the (24) mode at (*a*) 25°C and at (*b*) 600°C. Curve (1) in the impedance and (2) is the phase angle. The abscissa represents frequency (kHz); the ordinant represents impedance (kΩ) and phase angle (θ).

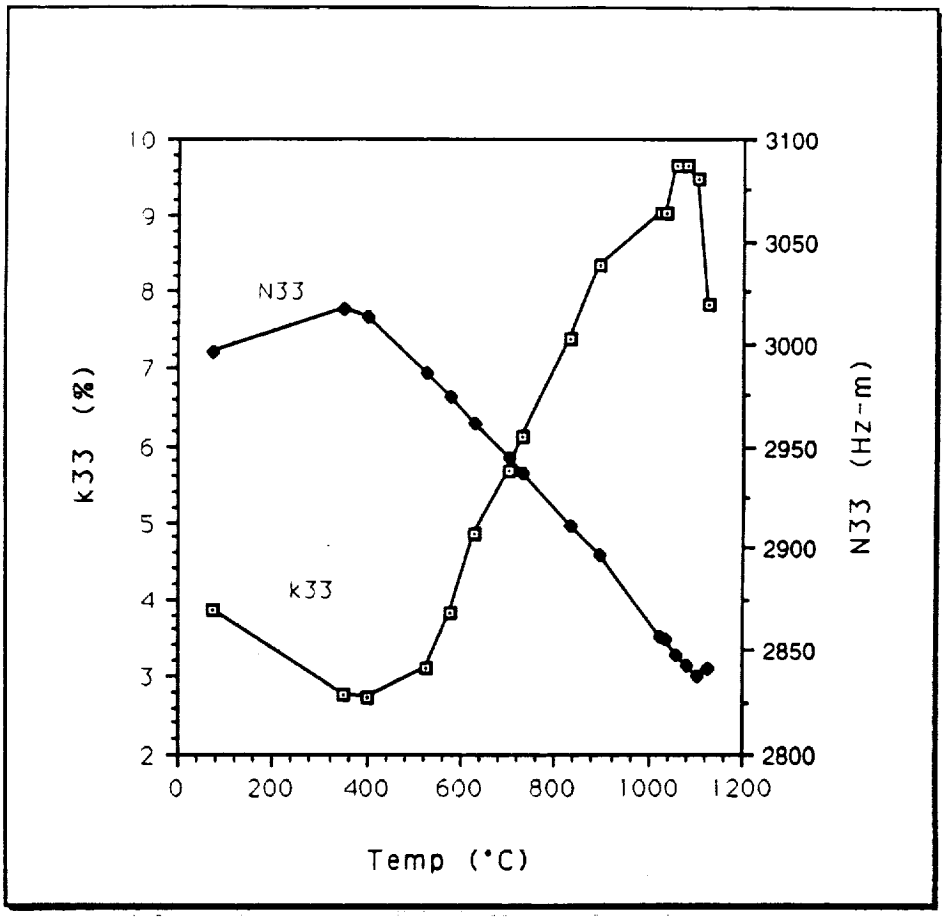

Figure 8.9 Coupling coefficient, k_{33}, and frequency constant, N_{33} for hot forged 8SN2STa ceramics, as a function of temperature. Changes in slopes of both parameters indicate phase transitions.

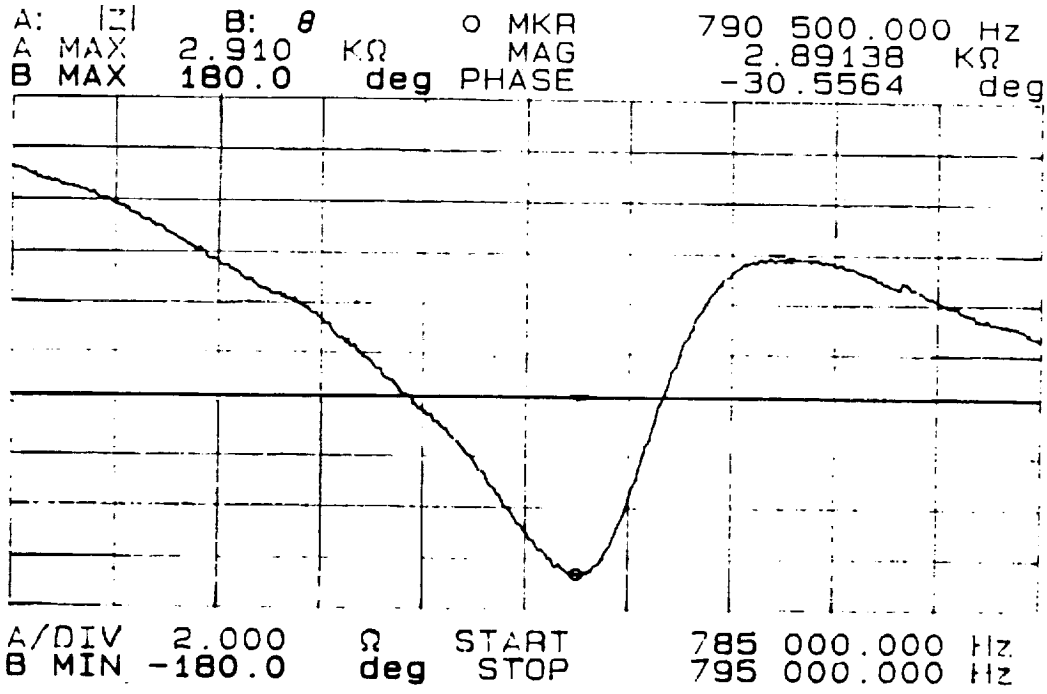

Figure 8.10 The (33) mode resonance of 8SN2STa ceramic at ll25°C.

With increased temperature, the series capacitance, C_s, increased while the resonance and antiresonance impedances (Z_r and Z_a of the equivalent circuit) decreased as did the DC resistance, R (Table 8.5).

Table 8.5

Values of capacitance, impedance and resistance for (33) mode sample at 25° and 1000 C

Parameter	25°C	1000°C
C_s (pf)	2.4	25
Z_r (kΩ)	74.8	14.7
Z_a (kΩ)	82.8	15.0
R (MΩ)	>100	0.1

Changes in capacitance and resistance of the resonator play a role in the frequency range at which it can operate as was discussed earlier. Using equation 4.12,

$$f_{LL} = \frac{1}{2\pi RC} \qquad \text{(eq. 4.12)}$$

the lower operating limit, at 1000°C, was calculated to be approximately 66 *kHz*

The sample, as a resonator, became progressively lossy as the temperature increased, but appeared to worsen considerably in the area of 600°C. As the difference between Z_r and Z_a narrows, it becomes increasingly difficult to sort the resonant peaks from the noise and requires the use of rather sophisticated electronic processing.

Upon cooling after the high temperature test, the coupling coefficient had decreased to 2.1 % from its pre-test value of ~4%, the result of partial depoling. Since depoling occurs as a function of both time and temperature, it is not known how long the

sample could have sustained the 1125°C before a total loss of measurable piezoelectric activity would have occurred. It is believed, however, that the 8SN2STA material could withstand 1000°C for several hours.

8.5 Chapter Summary and Conclusions

Samples of 8SN2STa were successfully hot forged at a temperature of 1340°C, about 85°C below the conventional sintering temperature. Two techniques of hot forging were used: one in which the sample was allowed to spread radially, unconstrained; the other in which the flow of material was directed along the walls of a rectangular shaped die. The latter technique was explored in an effort reduce cracking and to control the geometry of the finished piece to increase the material yield from the sample.

Examination of the microstructure of the free flow HF samples by SEM showed them to possess plate-like grains, highly oriented in directions perpendicular to the hot forging axis; however, the grain orientation was not complete. The outer perimeter of the discs contained small regions in which the grains were oriented at oblique angles to the direction of the grains in the bulk of the disc. This condition resulted in cracking at the interface between these two regions.

The die assisted hot forged samples also exhibited regions of grains in parallel alignment; but unfortunately, the orientations did not show a common direction, leading to more extensive cracking because stresses set up at the numerous sites of oblique grain orientation.

An interesting observation was made of samples, hot forged by the die assisted method, on which an applied field of ~2 V/cm and a current flow of 40 mA was applied (section 7.6.2). The sample contained a large dark region in the center (believed to be the current path—see the section on high temperature poling), separated by fracturing from

surrounding normal colored light regions. Examination of both regions by SEM showed the dark region contained platelets nearly twice as long as the ~4-5μ m long platelets found in the light region and in samples not subjected to current flow during die assisted hot forging. The thickness dimensions of the platelets were about the same (~1μm) in both regions. No explanation for this observation is offered at this time.

Room temperature evaluations of piezoactivity showed the HF samples to be superior to the OF samples. The (24) mode samples exhibited coupling coefficients more than twice that of the (33) mode samples. High temperature tests were another matter. The relatively large piezoelectric constant of the (24) mode, the result of shear motion between perovskite slabs (Fuierer 1991), became weaker with increasing temperature as the relative position of the slabs shifted due to anisotropic thermal expansion. At ~600°C the shear modes could no longer be seen.

The (33) mode samples exhibited strong resonance peaks up to 1125°C. The observation of piezoelectric activity at 1125°C is believed that this is the highest reported temperature measurement of piezoelectric activity in a ferroelectric ceramic. The only report found for piezoelectric activity in a ceramic at a higher temperature (1150°C) was for AlN film, a non-ferroelectric (Patel and Nicholson 1990).

Increased temperature also brought an increase in dielectric loss and decreased resistivity. By applying the formula for the lower limit frequency of operation f_{LL}, it was determined that the minimum frequency at which the sample could be operated at 1000°C is ~66 kHz, well above the audio frequencies associated with microphones.

CHAPTER 9

DEVELOPMENT OF A HIGH TEMPERATURE MICROPHONE

Chapter 3 discussed several "high" temperature vibration sensors which are currently available. An obvious omission to the list of sensors was the variety of commercial microphones, because microphones are not generally associated with high temperature applications owing to numerous technical difficulties in their design and application. Current practices of monitoring noise and acoustic emissions at high temperatures largely require the use of accelerometers and buffer pipe systems. It would, however, be useful to monitor noise in the atmosphere with a microphone.

In recent years the development of *active noise control* technology has become an important application for microphones. Once detected by the microphone, the acoustic signals (noise) are processed to broadcast in the form of acoustic "anti-noise" signals, which are 180° out of phase with the detected noise, thus, causing a cancellation effect. Methods of noise cancellation have shown considerable success in numerous commercial and military applications (McCloy 1987), and are the subjects of ongoing research at Penn State and other research centers. Special compressed air loudspeakers have been developed for installation in the exhaust systems of internal combustion engines and gas turbines to generate counter sound waves to dampen exhaust noises (Chapman and Glendinning 1990). Pickups for noise cancellation techniques are, however, restricted to fairly low temperatures because of the unavailability of suitable, economical, high temperature microphones for noise detection. At present, higher temperature applications must use buffer tubes to isolate the microphones from the high temperature areas (Tichy 1993).

The ultimate goal of this work was to investigate and design microphone which

can be installed in a jet engine (with temperatures approaching 1000°C) to detect sounds originating from combustion sources and air turbulence. Before attempting to design such a microphone, using the new high temperature piezoelectric materials described earlier, it was deemed instructive to first design, construct and test a prototype microphone using commercially available lithium niobate, which has a use temperature approaching 700°C. By constructing such a prototype, it was possible to address some of the technical issues, *i.e.*, structural materials, electrical connections, and sound and electromagnetic isolation, which are likely to be encountered in a higher temperature environment. It was also necessary to devise some method of evaluating the SNSTa material, discussed earlier, in a simulated microphone setting. This chapter will discuss the development of the prototype microphone thus far outlined.

9.1 Commercially Available High Temperature Microphones

A search of the catalogs of prominent manufacturers of high temperature acoustic sensors revealed that only one (Endevco 1989) lists microphones designed for use at elevated temperatures. The microphones, models 2510/2510M4A and 8550M1 are rated for a maximum use temperature of 260°C, with an approximately flat frequency response curve from 10 to 10,000 Hz. The transducers used in their designs are composed of stacks of DOD Type II PZT plates connected in parallel. The high piezoelectric (d_{33}) and high dielectric (K) constant of the PZT, along with the relative large surface area of the stack arrangement provides a high output and high capacitance; factors which would maximize the sensitivity and facilitate electrical impedance matching to cables and amplifiers. Unfortunately, at temperatures above that rated for these microphones, PZT has a tendency to depole thus rendering the device ineffective.

9.2 Microphone Operation

The accelerometers discussed earlier are designed to detect acoustic signals transmitted through the solid structure on which they are mounted, and employ a seismic mass to actuate the transducer. On the other hand, microphones detect sound waves transmitted through the air, and use diaphragms with very small inertial masses and relatively large surface areas, to enhance the detection of minute pressure changes arising from the impingement of sound waves. Special precautions are taken to prevent vibrations from entering through the body of the microphone.

In air sounds propagate exclusively by wave motions which are longitudinal in character. Air molecules within the wave have an oscillatory displacement along the axis of propagation and kinetic energy is transmitted by the displacement of molecules of air. Figure 9.1 graphically displays this motion, along with the sinusoidal displacements in the direction of wave propagation, plotted as distances above a zero axis, and by the backward displacements as distances below the axis.

Molecule density increases in the region of compression, and decreases in the region of rarefaction. Because of the relatively large spacing between the individual molecules, energy losses occur resulting in an exponential decrease in sound intensity with distance. The molecular spacing in air is greater than that of solids; consequently, air is a less efficient carrier for acoustic energy (Robertson 1963). The differences in efficiency between acoustic transmission media accounts for the practice of using a diaphragm in a microphone and a seismic mass in an accelerometer.

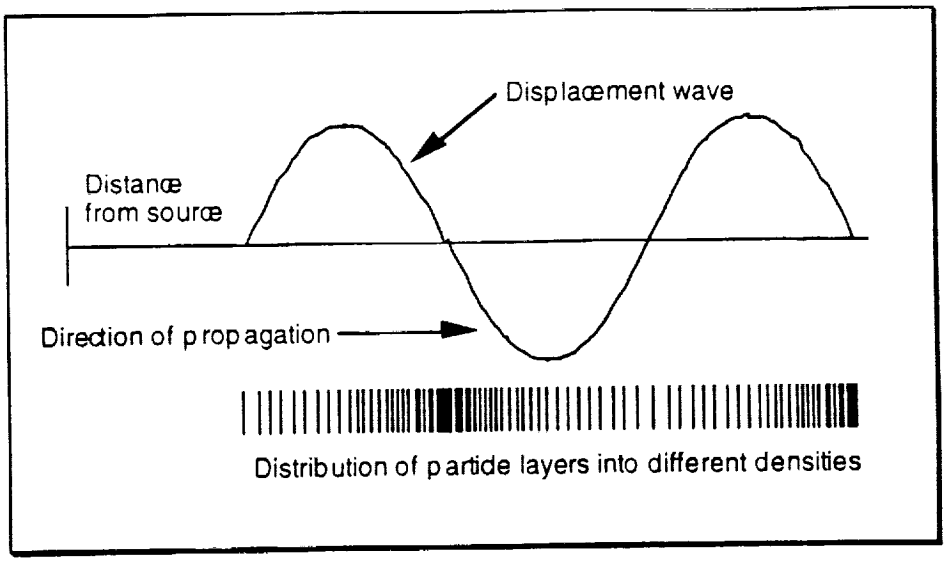

Figure 9.1 Schematic representation of the propagation of sound through air.

9.3 Measurement of sound

In his early studies of speech, hearing and sound, Alexander Graham Bell encountered a tremendous range of acoustic power, e.g.,

1.22×10^{-11} J/sec for threshold of hearing at 1 meter
12.2 J/sec for the threshold of pain at 1 meter

Thus, it can be said that human hearing covers the tremendous dynamic range of twelve orders of magnitude. Because the sensitivity of the range is logarithmic, it is convenient to describe sounds in terms of the exponent in units called the BEL; and, subsequently the BEL was subdivided by10 into the decibel (dB). The acoustic field then coined the term *Sound Power Level* (PWL) and equated it to the logarithmic ratio:

$$\text{Sound Power Level (in dB)} = 10 \log \frac{\text{measured sound power}}{\text{reference sound power}} \qquad \text{(eq. 9.1)}$$

It, however, is more convenient to measure sound pressure than sound power, which is defined as:

$$\text{Sound Pressure Level (in dB)} = 10 \log \frac{(\text{measured sound pressure})^2}{(\text{reference sound pressure})^2} \qquad \text{(eq. 9.2)}$$

since the sound power is proportional to the square of the sound pressure. At a given point source,

$$\text{Sound Pressure} = \frac{\pi(2rp)^2}{\rho c} \qquad \text{(eq. 9.3)}$$

where: r is the distance from the source in *cm*
p is rms pressure in Pa
ρ is density of the medium in g/cm^3
c is the velocity of sound in that medium in cm/sec.

The Sound Pressure Level (SPL) can be rewritten

$$\text{dB SPL} = 20 \log \frac{\text{measured sound pressure}}{\text{threshold of hearing}} \qquad \text{(eq. 9.4)}$$

The threshold of hearing is a statistical value derived from measurements performed on healthy teenage subjects, and is referenced at zero. For other acoustic applications, such as NDT and sonar, other specific reference levels are used. For comparison, Table 9.1. lists the levels of sound pressures in different environments ranging from the threshold of hearing to the noise from jet engines.

Table 9.1

Sound pressure levels in various environments (Endevco 1989)

SOURCE	SOUND PRESSURE (in Pa)	SPL (in dB)
Threshold of human hearing	0.00002	0
Electric clock	0.0002	20
Conversation at 1 meter	0.002	40
Normal office environment	0.2	80
Threshold of pain = acid rock	20	120
Jet Engine at 15 meters	200	140

The sensitivity of acoustic transducers is commonly expressed in dB re 1 volt at 1 Pa (*i.e.*, at 94 dB SPL).

$$\text{Transducer Sensitivity} = 20 \log \frac{\text{output (V rms) at 1 Pa}}{\text{1 V rms at 1 Pa}} \qquad \text{(eq. 9.5)}$$

If a microphone has an output of 1 mV at 1 Pa its sensitivity is expressed as –60 dB re 1 V per Pa. Sensitivity of piezoelectric microphones is given in dB re 1pC at 1 Pa; whereas, accelerometers are described in terms of acceleration and are expressed in terms of V/g (Endevco 1989).

9.4 Types of Microphones

For each of the different types of accelerometers, described in Chapter 3, there are microphone analogs; and a few of the basic types are presented in this section.

9.4.1 Carbon Piezoresistive Microphone

Earliest microphones were piezorestive devices composed of carbon granules contained in a canister which was covered with a diaphragm (Figure 9.2). The carbon acts as a resistor, but when sound waves impinge upon the diaphragm, the bulk mass of carbon granules is compressed briefly, causing a reduction in resistance proportional to the duration and intensity of the sound wave. When a voltage is applied across the microphone, the flow of current is modulated by the sound.

Although carbon microphones are found in the handsets of older telephones, they have a narrow frequency response, low sensitivity and self-generated noise; thus, they have been largely replaced by newer designs (Borwick 1990).

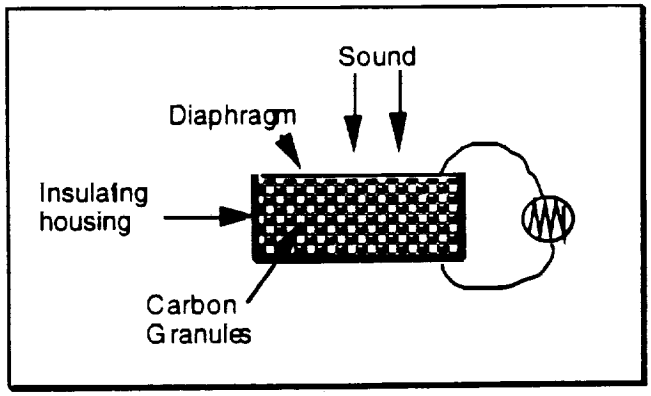

Figure 9.2 Illustration of a piezoresistive carbon granule-type microphone.

9.4.2 Electrostatic (condenser) Microphone

The transducer in an electrostatic microphone is a simple air capacitor whose two electrodes or plates are formed by thin conductive diaphragm and a fixed back plate separated by a narrow air gap (Figure 9.3). A polarizing DC voltage is applied across the two electrodes via a very high resistance R, establishing a nearly constant charge (Q) on the capacitor. The capacitance is given earlier by equation 3.3. The voltage across the capacitor is given by:

$$V=\frac{Q}{C} \quad \text{or} \quad V=\frac{Qd}{KA} \qquad \text{(eq. 9.6, 9.7)}$$

An electric field resulting from the applied voltage (V) is inversely proportional to the spacing (d) between the plates. When the diaphragm vibrates in response to the incident sound pressure wave, d is changed, and the applied DC polarizing voltage is modulated into an AC signal. This AC component is taken through the DC blocking capacitor (C) to provide the microphone's output signal, which is then amplified.

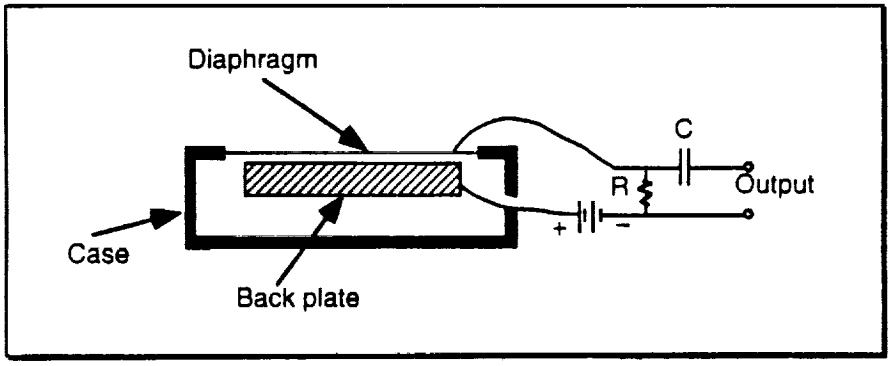

Figure 9.3 Schematic diagram of an electrostatic (condenser) microphone.

9.4.3 Piezoelectric (crystal) Microphone

Microphones found in many low cost consumer products today use piezoelectric transducers as elements. Typical construction is composed of a sandwich or "bimorph" of oppositely poled plates or discs bonded together with cement to form a single unit. Each plate is metallized on both flat surfaces, but termination is made only with the outer electrodes while the inner electrodes serve as an internal connection only (Figure 9.4).

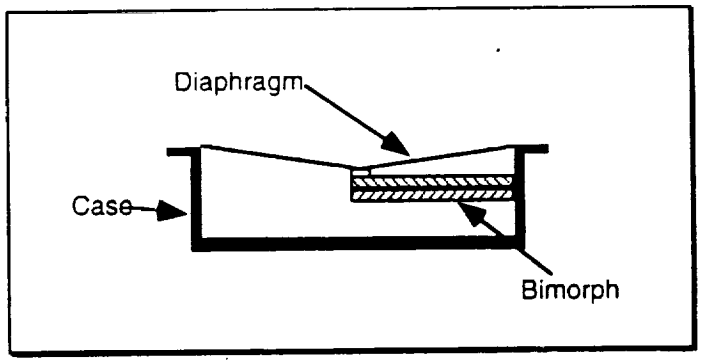

Figure 9.4 Schematic drawing of a typical piezoelectric microphone.

The sound is received by a conventional diaphragm which is connected to a single point on the bimorph. The alternating stress applied to the bimorph results in an alternating electrical output at the terminals, proportional to the displacement. The charge generated by the two plates is additive, because the sandwich construction effectively enhances the compressive stress on one plate simultaneously with a tensional stress on the other; thus, the output voltage is optimized. For this reason, the bimorph configuration is particularly attractive for microphone applications (Borwick 1990).

The first piezoelectric microphones used thin plates of Rochelle salt, and later

ammonium dihydrogen phosphate (ADP) single crystals, as the active element; thus, giving rise to the term crystal microphone. Most current applications use a soft PZT with a large d_{33} (Herbert 1982).

Other types of microphones such, as the cardioid and ribbon microphones, are in common use, but most use permanent magnets in their construction (Borwick 1990). Since this work is concerned with high temperature applications, or at least designs which have potential for high temperature work, magnetic types, because of their tendency to demagnetize at high temperatures, will not be discussed.

9.5 Design of a Prototype High Temperature Microphone

Before attempting to design a microphone capable of operating at 1000°C with an experimental piezoelectric ceramic, it was thought that it would be instructive to first construct a prototype microphone using the commercially available materials. This effort would aid in addressing issues, such as, construction material, element termination and high temperature test methods. If the prototype meets its objective, the design could then be adapted to take advantage of new, higher temperature piezoelectric materials.

In the course of designing the prototype microphone, efforts were made to keep its construction simple with the fewest number of components. Lithium niobate (LN) was chosen for the piezoelectric element because of its high temperature operating capability (~650°) and its availability from a commercial source*. The element, an "X-cut" ring machined from a single crystal, was polarized in the z direction. The dimensions of the ring were 11.11 mm outside diameter x 6.35 mm inside diameter x 3.00 mm thick (Figure 9.5).

* Kappler Crystal Optics Inc., Holliston, MA.

Gold electrodes were sputtered on the outside and inside perimeter surfaces of the element. (Sputtered Pt electrodes were not used because it did not adhere well and had excessively high sheet resistance.) In this configuration, the element operates in the shear mode, to take advantage the highest piezoelectric and dielectric constants (for LN), and to avoid possible problems that can arising from pyroelectric voltage build-up.

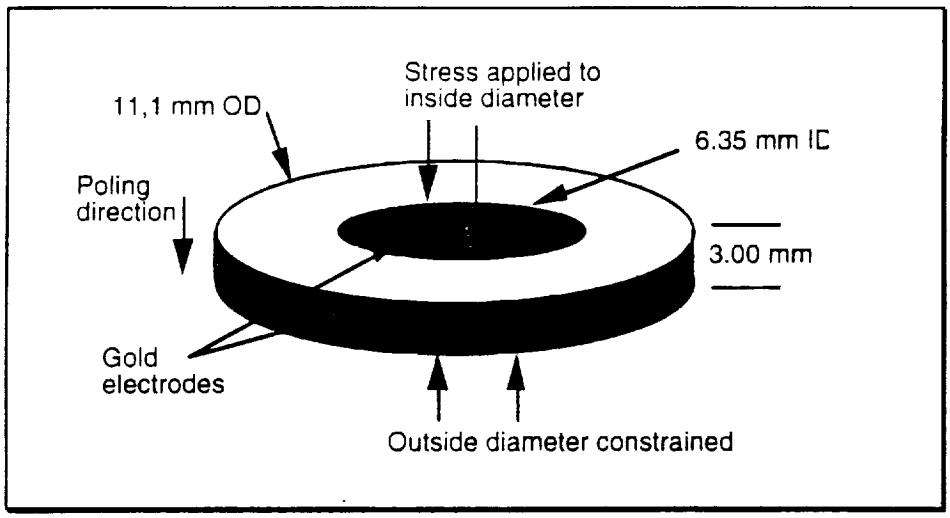

Figure 9.5 LN element used in the prototype microphone.

Figure 9.7 is an illustration of its internal components, which are as follows:

1. Element
2. Housing and diaphragm assembly
3. Element support
4. Plunger assembly
6. Leads

Figure 9.6 shows a photograph of the completed prototype microphone.

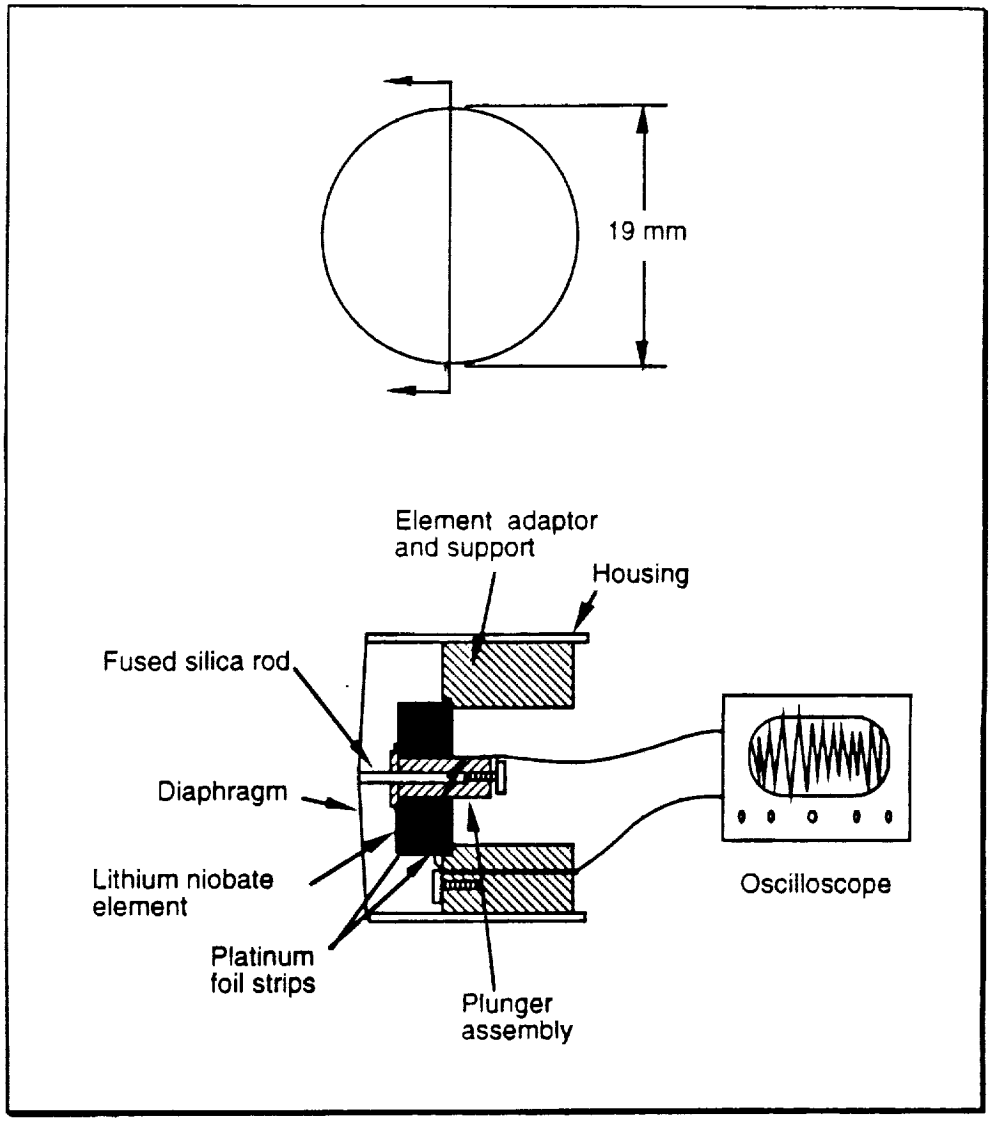

Figure 9.6 An illustration of the prototype high temperature microphone developed for this work.

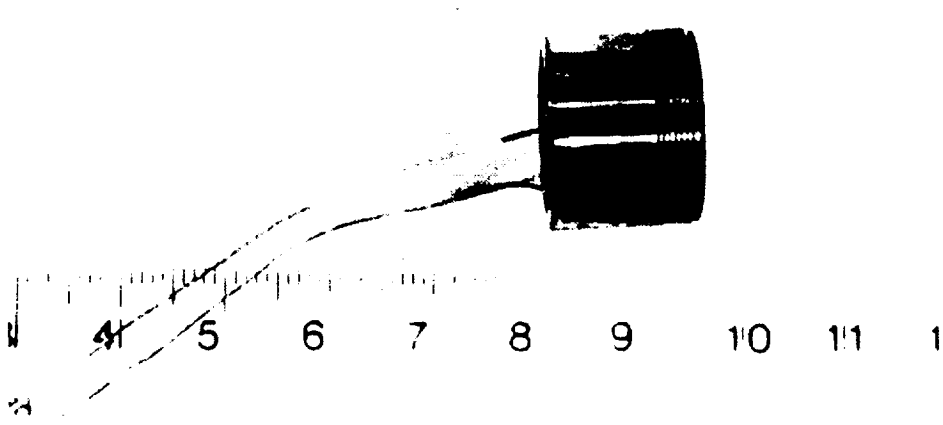

Figure 9.7 Photograph of the assembled prototype high-temperature microphone

The housing and diaphragm assembly was purchased from Endevco* and is the same as that used in their model 2510 microphone. The assembly consisted of a stainless steel tube 19 mm in diameter, 14 mm long, with a wall thickness of 1.5 mm. The internal bore was threaded throughout to facilitate the installation and adjustment of the internal components. The diaphragm, fabricated of 0.13 mm thick stainless steel, was welded along its edge over one end of the housing tube. The element support, fabricated in-house from stainless steel, was a plug 9.5 mm long threaded on the outside diameter to match the threads in the housing assembly. In one end of the adapter, a recess was machined to a depth of 1.0 mm to accommodate the element. The inside diameter was bored out so that only the outside 0.7 mm of the element was supported. A small hole was drilled lengthwise through the element to accommodate a platinum wire lead. Platinum was used wherever possible because of its temperature resistance.

The plunger shaft was machined from stainless steel to allow it to be inserted into the hole in the element with enough clearance to allow for the greater thermal expansion of the plunger body. The plunger body was formed with a 1.0 mm thick "nail head" configuration whose outer perimeter contacted only 0.7 mm of the inner perimeter face of the element. With the small contact lip on the inner part of the element, and a small support lip on the element adapter, shear stresses are generated whenever a force is applied to the plunger. Contact of the plunger to the center of the diaphragm is made through a short length of 2.0 mm diameter fused silica rod inserted into a hole drilled into the element end of the shaft. The fused silica rod serves as both a mechanical coupling and an insulator between the diaphragm the plunger and the diaphragm. Upon assembly, a small, pre-loaded force provided by the plunger against the diaphragm is sufficient to hold the element and plunger assembly in place.

---

* Endevco Div. Allied Signal Corp. San Juan Capistrano, CA.

Lead attachment to the element's electrodes was accomplished by inserting strips of platinum foil between the element and the support (and plunger). Tabs on the foil strips provide connection to the platinum lead wires. One lead is secured to the plunger assembly, and the other lead is secured to the element support with small machine screws.

The plunger assembly, as described, presents a seismic mass to the element and causes the microphone to respond, to some degree, as an accelerometer. Although this arrangement was not ideal, it was a necessary compromise needed to make the lead attachment to the center electrodes of the element. To help isolate the microphone from vibrations picked up through the housing during testing, it was mounted in an alumina tube, packed with sound absorbing refractory fiber and installed in the test furnace shown in Figure 9.8*a*.

The stainless steel was used for the structural components because of the ready availability of the housing/diaphragm assembly. In order to minimized potential damage to the stainless steel by oxidation during high temperature testing, a nitrogen atmosphere was maintained inside the test furnace. Had a refractory alloy such as Inconel® 600 been used a nitrogen atmosphere might not have been necessary.

9.6 Experimental Procedures

The frequency response of the prototype microphone was measured at room temperature in an anechoic chamber. However, high temperature frequency response could not be determined because high temperature acoustic testing facilities were unavailable. Therefore it was necessary to devise a special set-up using an available horizontal tube furnace.

9.6.1 Resonance Measurements

Resonances of the element and microphone assembly were analyzed with a Hewlett Packard 4194A Impedance Analyzer using the standard extension lead fixture. The spectrum from 1 kHz to 2 MHz was examined and important frequency-impedance events were recorded.

9.6.2 Frequency Response

The frequency response evaluations were performed at room temperature in the Acoustics Laboratory at Penn State University. Tests were conducted with the microphone placed in an anechoic chamber alongside a commercial condenser microphone used for comparison and calibration. A Hewlett Packard 35665A Dynamic Signal Analyzer provided the signal source of random noise of 100 Hz – 25 kHz, and the analyses of the microphone's output.

9.6.3 High Temperature Evaluations

In order to perform high temperature tests, a small tube furnace was modified so that the microphone could be placed in the center of the hot zone, and a loud speaker could be mounted on one end (Figure 9.8*a*). The 32 mm diameter alumina furnace tube was cut into two sections to facilitate mounting the microphone in the center of the furnace; the halves of the tube were then butted together. Ceramic fiber was packed in the space between the tube and microphone to provide sound isolation. A reference thermocouple was mounted alongside the microphone to monitor the temperature. Nitrogen was fed to the back side of the microphone through a ceramic tube.

Acoustic signals to the speaker originated from a HP 3562A Dynamic Signal Analyzer and were amplified by a 100 watt audio amplifier. The output from the microphone was amplified by a charge amplifier with a gain of about 10,000, then analyzed by the same dynamic signal analyzer. Unfortunately, this arrangement didn't work well because of difficulties encountered in projecting enough sound energy from the speaker to the microphone, and because the charge amplifier proved incapable of tracking the microphone's output over a broad range of impedances that occurred with changing temperatures.

An alternative arrangement (Figure 9.8*b*) proved to be more successful. By directly stimulating the diaphragm at 60 Hz with a commercial electromagnetic vibrating engraver (via an intermediate alumina rod 300 mm long *x* 6.0 mm diameter), a pronounced signal could be observed on an oscilloscope. At chosen temperature intervals, the controller for the furnace was unplugged (to eliminated radiated electronic signals) and the diaphragm was stimulated. Because it was not possible to attach a recorder to the oscilloscope, only comparative readings were taken.

9.7 Experimental Results

The prototype microphone was evaluated for resonance and frequency response at room temperature, and for voltage output at temperatures up to 800°C. The results of these evaluations are described below:

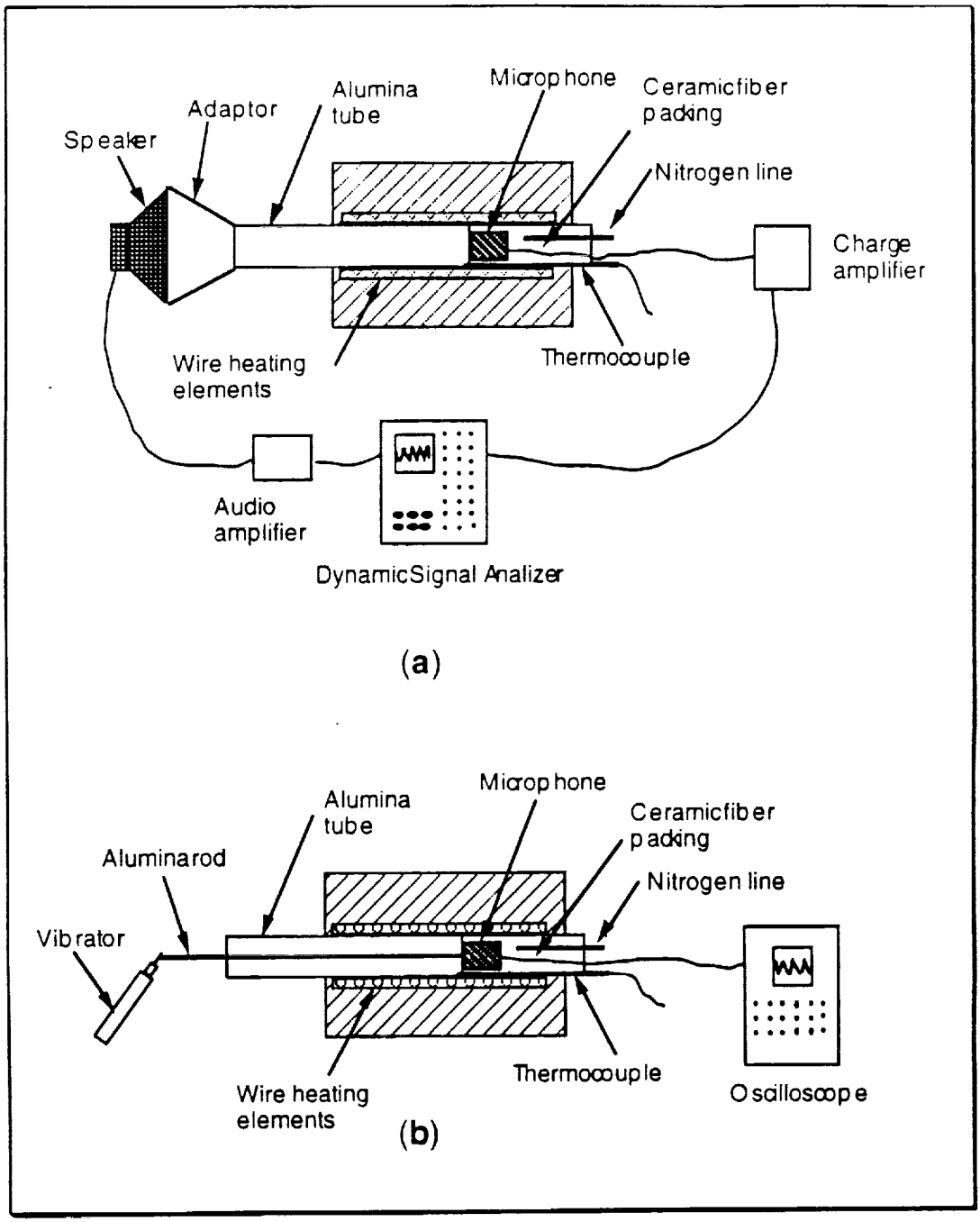

Figure 9.8 Test set-ups for determining the high temperature response of the prototype microphone using (a) a loud speaker (b) mechanical vibrator, for diaphragm stimulation.

9.7.1 Room Temperature Evaluation

The performance of the prototype was first characterized at room temperature. With the impedance analyzer, it was found that the strongest resonance of the element occurred at 984 kHz, while the resonance of the diaphragm assembly occurred at 25 kHz, well above audio frequencies. The capacitance of the assembled microphone was 28 pf, compared with a capacitance of 23 pf for the element alone; the difference resulting from the added capacitance arising from proximity of the internal components within the assembly. During the frequency response and output tests in the anechoic chamber, the prototype microphone, with the charge amplifier installed, performed well, having a reasonably flat frequency response from 1 kHz to 25 kHz. Figure 9.9*a* shows the comparison of the prototype with the standard microphone; and it can be seen that the prototype outperformed the standard microphone, especially above 13 kHz. Without the charge amplifier, the frequency response was essentially the same except that the output level was down by about 80 dB indicating a low fairly low sensitivity (Figure 9.9b). In a jet engine where the noise levels are very high, lower sensitivity may be an asset.

9.7.2 High Temperature Results

The first series of high temperature tests used the arrangement shown Figure 9.8*a* with a loud speaker providing the acoustic signal. Attempts were made to transmit sound from a 100 mm diameter speaker through a 32 mm tube; but that, proved to be impractical. The acoustic pressure reaching the microphone could drive it only to a level slightly above the detection limit of the dynamic signal analyzer. As the microphone was heated, the signal weakened steadily; and at ~300 °C the signal was below the detection limit of the instrument (Figure 9.10).

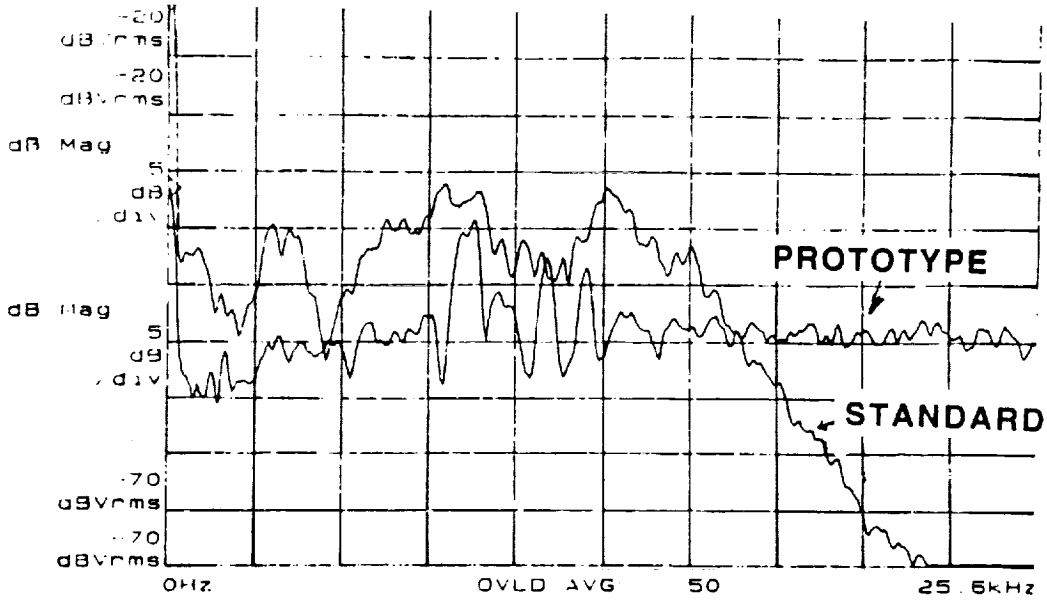

a

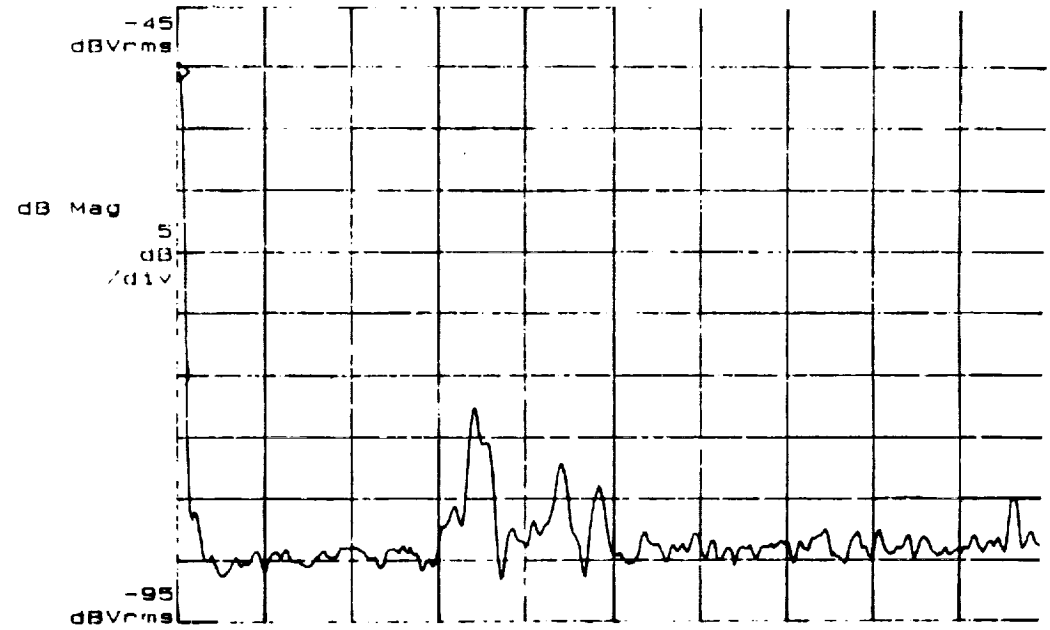

b

Figure 9.9 The frequency response-output curves for the prototype microphone (*a*) with the charge amplifier installed, and compared with a standard commercial microphone and (*b*) without the charge amplifier installed.

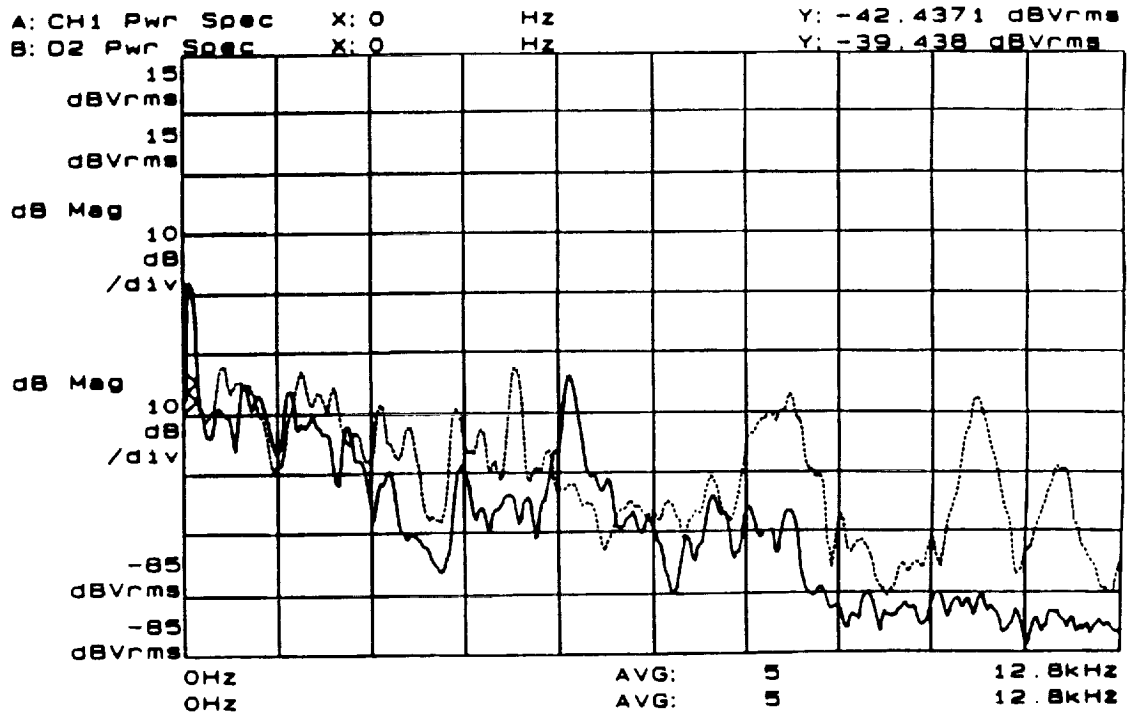

Figure 9.10 The output of the prototype microphone—using the test set-up shown in Figure 9.8*a*—measured at 300°C. The solid line represents the microphone's output, and the dashed line represents background "noise".

By applying direct stimulation to the diaphragm (Figure 9.8*b*), the microphone generated a signal that could be readily detected on the screen of an oscilloscope. As shown in Figure 9.11, the room temperature the output was approximately 10 volts peak to peak and remained so until about 450°C (which corresponds to a force applied to the element of ~0.25 Pa). With increased temperature, the signal decreased gradually to about 4 V at 600°C, above which the signal strength decreased at a more rapid rate until 700°C, where it became nearly imperceptible. Resonance tests performed after cooling, showed the performance of the microphone to be unchanged by the high temperature tests.

The DC resistance of the microphone was measured during the course of the high temperature tests. The resistance decreased to 10 kΩ ($\rho \approx 12 \times 10^4$ Ω-cm) at 650°C and 3.5 kΩ ($\rho \approx 4 \times 10^4$ Ω-cm) at 700°C. This rapid decrease in resistance (accounting, in part for the decreased resistance) with increased temperature is consistent the resistivity graph shown earlier, in Figure 5.1.

The stainless steel case suffered only moderate discoloration from the high temperature exposure; but the diaphragm was softened somewhat and lost much of its resilience. It is likely that at 700°C, the compliance of the diaphragm was increased enough to adversely affect the sensitivity of the microphone. However, electrical termination, using the wrap-around Pt electrodes, worked well at the evaluation temperature.

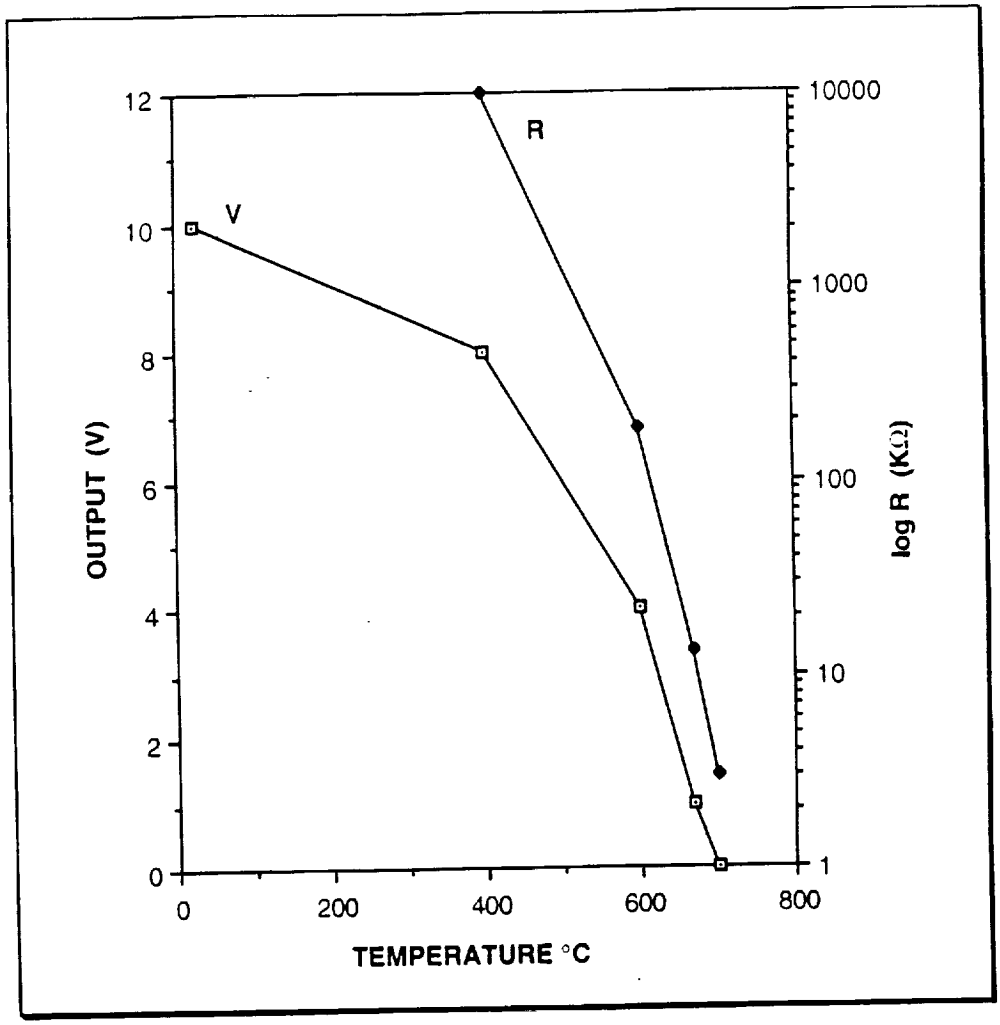

Figure 9.11 The voltage out put and resistance of the prototype microphone measured from 25°C - 700C.

9.7.3 SNSTa Evaluation by Direct Stimulation

The direct stimulation method, albeit crude, was an instructive way to evaluate the SNSTa material for the possible use as elements in high temperature microphones. In the first test, the sample was held between two lead wires while it was stimulated directly with the vibrator at 60 Hz. Because of its relatively small voltage constant (~5.6 x 10^{-3} Vm/N, compared with 91 x 10^{-3} Vm/N for LN), and its smaller size, the sample generated only a few mV and its wave form was difficult to discern from the background electronic radiation picked up by the lead wires. It is possible, however, that, if incorporated in a microphone with a large ratio of diaphragm area to element area, the voltage output, with the same applied stress could be increased.

In order to evaluate the high temperature performance of the material, a fixture was fabricated to hold the sample in place while it was being stimulated. The fixture was fashioned by cutting a slot, the width of the sample, in one end of 6 mm diameter alumina thermocouple insulator rod. The holder held both the sample and the lead wires. Although this arrangement required some dexterity to hold and manipulate, the sample could be stimulated by the extension rod from the vibrator.

At temperatures up to 850°C, the upper limit of the test furnace (Figure 9.8*b*), the sample showed only a slight increase in output, estimated to be about three times in magnitude over the room temperature output, but even so, its magnitude was small. Extraneous electrical noise was a problem because the holding fixture could not be shielded.

9.8 Chapter Summary and Conclusions

Microphones differ from accelerometers in that they are used to detect sound waves in air rather than in solid media. Some accelerometers, using lithium niobate elements, are designed to operate at temperatures up to 700°C, but there are no commercially available microphones capable of withstanding temperatures in excess of 260°C. This leaves an important application for high temperature microphones, active noise control, unsatisfied.

This chapter reviewed briefly a few of the different types of (low temperature) microphones in use today. The focus, however, was to address the issues related to the total design and performance of a microphone capable of use in the range of 600-700°C leading to an ultimate design for use at 1000°C.

A prototype microphone, using a lithium niobate element, was fabricated and tested. By in large, the prototype microphone met its design objective by exhibiting excellent frequency response characteristics at room temperatures, in an anechoic chamber.

On the test furnace set-up, white noise source using a commercial loud speaker was installed, but proved inadequate to provide a noise level at the microphone's diaphragm sufficiently high to be detected at elevated temperatures. It was, therefore, necessary to apply direct stimulation to the diaphragm with a ceramic rod attached to an electromagnetic vibrator, and by doing so, the microphone showed responses to the acoustic signals by generating discernible voltage outputs at temperatures up to 670°C. The temperature of 670°C is believed to be the highest temperature for microphone operation. The direct stimulation method was also used to test the SNSTa sample bars described in Chapter 6.

Although the samples were observed to generate a perceptible signal at 850°C

(the upper limit of the test furnace), its level was very small compared with that generated by the LN element in the prototype microphone.

During the course of this work, a number of issues concerning the design and testing of a high temperature microphone were raised, leading to the following conclusions:

- The stainless steel components required an N2 atmosphere They discolored, but were otherwise mechanically sound even after exposure at 800°C.
- The stainless steel diaphragm appeared to have lost much of its spring (temper).
- The platinum foil element contacts worked well as did the Pt leads.
- Isolation of the microphone element from sound picked up through the case is a problem which must be addressed.
- Electromagnetic shielding is essential for the microphone and lead wires.

CHAPTER 10

SUMMARY

10.1 Existing Needs

High temperature technology is of major importance for chemical and material processing, automotive, aerospace, and power generating industries to name just a few (Meetham 1991). For many, the primary benefit of operating at higher temperatures is the direct cost savings associated with increased efficiency in fuel conversion. In a related matter, the development of advanced structural materials such as silicon nitride and carbon-carbon composites promotes a need for high temperature electronic materials to monitor these systems. This is exemplified by the organization of the First International High Temperature Electronics Conference by Sandia National Laboratory and Wright Laboratory with other similar conferences forth coming (King and Thome 1991). Along with semiconductor, capacitor, magnetic, and packaging materials, electromechanical transducing materials, required to sense strains, vibrations, and noise under severe thermal conditions, are of considerable interest. Of the several different types of acoustic or strain sensors investigated, including accelerometers, strain gauge, air gap, eddy current, and fiber optic, piezoelectric based devices are probably the best candidates when one considers sensitivity, cost and simplicity of design.

Of the piezoelectric materials on the market available for acoustic sensor use, only one, lithium niobate, can be operated at temperatures above 500°C. If the use requirement be greater than 700°C, then there are no commercial materials, and very few "new" materials which are suitable. In a careful search of scientific literature, it was found that the most promising of the new materials are: the family of PLS ferroelectrics,

with the highest known Curie temperatures (some in excess of 1500°C), and AlN thin film, which has shown piezoelectric responses at 1150°C.

10.2 High Temperature Piezoelectric Ceramic

This work expanded research reported earlier by Fuierer (1991) on the strontium niobate-strontium titanate solid solutions of the PLS family of materials. The composition, hot forged 8SN2STa (with a projected T_c of 1160°C) was found to exhibit piezoactivity at a temperature of 1125°C, the highest temperature measurement reported for a ferroelectric ceramic. At 1000°C, the effective coupling factor (k_{33}) was ~ 9.7% compared with the room temperature value of ~4 %, and showed only minimal loss of piezoactivity, *i.e.*, aging; but at that temperature, the lower frequency limit f_{LL} was ~66 kHz, well above audio frequencies. The room temperature piezoelectric strain and voltage constants were found to be ($d_{33} < 3 \times 10^{-12}$ C/N) and ($g_{33} < 6 \times 10^{-3}$ Vm/N) respectively.

10.3 Hot Forging

Attempts to improve the hot forging process, over that in other reports, met with only limited success. Greater control of the rate of high temperature loading reduced the amount of cracking in the samples to some extent, but fracturing remained a problem. Owing to the high degree of anisotropy of the platelets, along with localized variations in the degree of texturing, the generation of internal tensile stresses in the structure (and subsequent cracking) was inevitable.

Attempts, to use a die to direct the flow of material during hot forging failed because the material not flow in a laminar fashion; but rather, it took a turbulent flow

path along the die walls. The inability to obtain well-textured samples frustrated attempts to simultaneously hot forge and pole the samples with the application of an electric field applied through electrodes installed on the die walls.

10.4 High Temperature Microphone

Although there exists a real need for the capability to measure noise in air at high temperatures, there are no commercially available microphones to fill the requirement. An important objective of this work was to design, construct and test a microphone that could operate at high temperatures — up to 1000°C — in an effort to determine issues and problems which may be encountered, including:

- Sensitivity appropriate for the application
- Structural components—including diaphragm
- Electrodes on the element
- Termination and interconnection
- Wiring—special shielded cable
- Long term effects at high temperature (aging)
- Thermal cycling effects

The design of the prototype incorporated lithium niobate as the piezoelectric element. High temperature evaluations were largely successful with the microphone responding to acoustic signals up to 670°C — also the maximum operation temperature of LN based accelerometers (Endevco 1991). Using direct contact acoustic stimulation, SNSTa samples were evaluated as possible voltage generating elements in a microphone. The signal to noise ration of these elements were very low, making it difficult to discern from ambient electronic noise in the test set-up.

CHAPTER 11

FUTURE WORK

Further work is needed to improve the properties of piezoelectric materials to make them useful at high temperatures. Piezoelectric sensitivity must be maximized to overcome sources of noise such as pyroelectric, thermocouple and galvanic voltages. Insulation resistance must be maximized by using "cleaner" processing techniques. Apart from the sensor material itself, there are numerous problems associated with the auxiliary materials and their integration that need to be addressed. These include electrode metals and their interactions, electrical connections, bonding, thermal expansion, and impedance matching. In order to develop new high temperature sensor and electronic materials, researchers need to broaden the scope of understanding from room temperature transport processes to less familiar high temperature phenomena. Applications are already numerous today, and more are certain to come in the future.

11.1 PLS Compounds

In this work, hot forging techniques were used to maximize the piezoelectric properties of the SNSTa material. Considering the difficulties encountered in hot forging, efforts might be well spent exploring other methods to optimize the unique properties found in these materials. The ordinary fired samples exhibited only about half the coupling value of the HF samples, but that might be high enough for use as a high temperature resonator. They, too, seemed to exhibit high sensitivity to small changes in stress. Piezoelectric properties would surely benefit from process enhancements including, low temperature texturing method including: extrusion or tape casting grain

oriented particles (Watanabe *et al.* 1989) in order to achieve a relatively high degree of grain alignment without the cracking associated with hot forging.

Untextured and partially textured samples could be further densified by hot pressing, and perhaps poled at the same time by installing electrodes on the punch faces.

Conduct a study of single crystal SNSTa compounds (with SN < 80%) to determine if their piezoelectric modulii and resistivity are high enough to be used in a high temperature microphone.

Continuous field poling of the SNSTa samples at the high E-fields and temperatures used (30-50 kV/cm @ 225°C) was difficult because of frequent dielectric breakdown resulting from electrostatic attraction of impurities to the surfaces of the samples. This difficulty may be alleviated by intermittent "pulse poling" techniques resulting in more thoroughly poled material with greater piezoelectric modulii.

It was observed that a sample, subjected to current flow (~40 ma), during hot forging, possessed platelets nearly twice the length (but the same thickness) compared with samples not so exposed (see summary section in Chapter 8). Little information could be found in the literature about this phenomenon, suggesting that studies of field applied during hot forging, and conventional sintering could be a fruitful.

11.2 Other Ferroelectric Compounds

New ferroelectric compounds possessing very high transition temperatures, a few of which are shown in Table 10.1, have been predicted based on the Abrahams-Kurtz-Jameson relationship and an extensive inorganic crystal structure database (Abrahams 1990). This study, and other computer assisted studies of materials, may well identify the next generation of high temperature vibration sensor materials.

Table 11.1

Examples of ferroelectric materials with very high transition temperatures proposed by Abrahams (1990).

Material	Projected T_c °C
$Na_3TmSi_2O_7$	1017
$RbTiI_3$	1427
$Co_2Mo_3O_8$	1547
$LiFeSnO_4$	1827
$Al_7C_3N_3$	2327

11.3 Non-Ferroelectric Piezoelectric Material — AlN

SAW devices using thin films of aluminum nitride (AlN) were reported to have operated at 1150°C (Patel and Nicholson 1990). Another report (Kanda and Gross 1976) describes a technique used to measure small pressure variations by means of a SAW device. The spacing of the electrodes is such that slight amounts of flexing of the substrate can be detected as a change in phase of the waveform of the device. It seems reasonable that this technique could be used in the development of a high temperature vibration sensor incorporating AlN thin films.

AlN thin films have been incorporated in small loud speakers (Shiosaki *et al.* 1982). Since speakers and microphones are, in principle, converse devices, high temperature microphones could be fabricated of AlN films deposited on a thin refractory substrate.

11.4 High Temperature Microphone Design

The bar shaped resonators, used in this study, seemed to be rather sensitive to relatively small changes in applied stresses resulting in measurable shifts in frequencies a phenomenon which also occurs in other piezoelectric materials. It seems possible that this response could be exploited in the design of a high temperature microphone using SNSTa as a pressure sensitive resonant element, rather than a voltage generating element.

$$\text{Sensitivity} \sim \frac{f_m}{\sigma}$$

Designs could incorporate two elements: one stressed by the diaphragm, and the other unstressed to compensate of the temperature-induced frequency changes. The resonance of each element could be mixed and the difference in the beat frequency could be used to detect the acoustic signal. Considering the material's low piezoelectric and voltage constants, perhaps, this might be a practical use of its high temperature capabilities. Efforts could be coordinated among materials and electronic design specialists.

The issue of structural materials (housing, diaphragm, internal, connections, *etc.*) must be addressed. High temperature operation mandates that the microphone assembly be constructed of temperature resistant materials such as ceramic (BeO, MgO, AlN), refractory metal (Cr-NI-Fe-Co alloys such as those produced by Hastings Metals Corp. and others), or a combination of both.

The issues of high temperature wiring and shielding are also serious considerations which must be addressed. Interesting results with high temperature resistant metallization, using PdCr alloys, reported by Lei, et al. (1990) might be applicable.

11.5 Air Gap Capacitors

The air gap capacitors discussed in Chapter 3 and condenser microphones (see Figure 9.3) could be constructed of metallized ceramic or from refractory metals, thus greatly extending their use into high temperature ranges.

11.6 Piezoresistive Microphone

A piezoresistive microphone, similar to the carbon microphone shown in Figure 9.2, could be fabricated using granules of a ceramic that is conductive at high temperatures such as $LaCrO_3$ (Schafer and Schmidbarger 1987), β-alumina (Tuller 1986) or C (or coated C granules). Along with materials, optimum particle size and distribution are important considerations.

In the case of materials which exhibit large temperature coefficients of resistivity, microphones of this design could be tailored to operate within specific temperature ranges. Temperature related resistance changes within the range could be compensated for by including, in the microphone, a fixed reference resistor with the same temperature-resistance characteristics as that of the granules.

REFERENCES

Abrahams, S. C., "Systematic Prediction of New Ferroelectrics on the Basis of Structure", *Ferroelectrics*, **104**, 37 (1990).

Akishige, Y., T. Kubota, and K. Ohi, "ESR Study of Orthorhombic Fe^{3+} Centers in $Sr_2Ta_2O_7$ and $Sr_2Nb_2O_7$", *J. Phys. Soc. Japan* **51** [12] 3929 (1982).

Angleton, P.A. and J. R. Hayer, "Ceramic Transducer Elements and Accelerometers Using Same", U. S. Pat. #3,487,238 (1967)..

ASA, *American Standard Method of Measurement of Piezoelectric Ceramics*, American Standards Association, New York (1961).

Bissonnette, M. and. M. Cloutier, "Air Gap Measuring System", 1st International Machinery Monitoring and Diagnostic Conference", Las Vegas, Nevada (1989).

Bollman, W. and M. Gernand, "On the Disorder of $LiNbO_3$ Crystals", *Phys. Stat. Sol.* A **9** [1] 301 (1972).

Borwick, J., *Microphones: Technology and Technique*, Focal Press London (1990).

Buchanan, R. C., "Properties of Ceramic Insulators", p. 1 in *Ceramic Materials for Electronics* edited by R. C. Buchanan, Marcel Dekker, Inc. New York (1986).

Cady, W. G., *Piezoelectricity*, McGraw Hill, New York (1946).

Car, W., "Eddy Current Proximity Sensors", *Sensors*, Nov. p. 21 (1987).

CEC Instruments Division of IMO Industries, Inc., San Dimas, CA, Product Literature (1991).

Chapman, C. J. and A. G. Glendinning, "A Theoretical Analysis of a Compressed Air Loudspeaker", *J. of Sound and Vibration*, **138** [3] 493 (1990).

Crystal Technology, Inc., Palo Alto, CA, Product Catalog.

Davis, R. F., "Diamond and Silicon Carbide Thin Films: Present Status and Potential as Wide Band Gap Semiconducting Materials", *Int. J. of Materials and Product Technology* **4** [2] 81 (1989).

Dayton, G. O., "Processing and Mechanical Property Relations in Tungsten-carbide-cobalt Alloys", Ph.D Thesis, The Pennsylvania University, University Park PA (1980).

Droney, B. E. and T. J. Pfeiffer, "Ultrasonic Inspection of Hot Steel Blooms to Detect Internal Pipe", *Materials Evaluation* **36** [6] 31 (1980).

Endevco Div. Allied Signal, San Juan Capistrano, CA General Catalog, 92675 (1989).

Fowler, T. J., "Acoustic Emission Testing of Vessels", *Chemical Engineering Progress* Sept., p. 59 (1988).

Francombe, M. H. and S. V. Krishnaswamy, "Growth and Properties of Piezoelectric and Ferroelectric Films", *J. Vac. Sci. Technol.*, **A8** [3] 1382 (1988).

Fraser, M., "Poling Crystals of Lithium Niobate", *Properties of Lithium Niobate*, INSPEC, The Institute of Electrical Engineers, London (1989).

Fuierer, P.A. and R. E. Newnham, "$La_2Ti_2O_7$ Ceramics", *J. Am. Ceram. Soc.* **75** [11] 2876 (1991).

Fuierer, P.A., Grain-Oriented Perovskite Layer Ceramics for High Temperature Applications", Ph.D. Thesis, The Pennsylvania State University (1991).

Gildenblat, G. S., Grot, S. A., and Badzian, A., "The Electrical Properties and Device Applications of Homoepitaxial and Polycrystalline Diamond Films", *Proceedings of the IEEE*, 79 [5] 647 (1991).

Guess, J. F., "Analysis of Piezoelectric Benders Used as Knock Sensors", p. 79 in *Sensors and Actuators 1983*, Society of Automotive Engineers, Inc., Warrendale, PA (1983).

Gurevich, V. M., and I. S. Rez, "Possibility of Controlling the Conductivity of Lead Metaniobate by Doping", *Isv. AN SSSR, Ser. Fiz.*, ***24***, *Noll* (Trans. Bulletin) p. 1258 (1960).

Gurevich, V. M., *Electronic Conductivity of Ferroelectrics*, English trans. from Russian (Israel Program for Scientific Translators, Jerusalem 1971).

Haertling, G. H. "Piezoelectric and Electrooptic Ceramics", p. 139 in *Ceramic Materials for Electronics* edited by R. C. Buchanan, Marcel Dekker, Inc. New York (1986).

Helmshaw, R., *Non-Destructive Testing*, 2nd Edition, Edward Arnold Publishing, London (1991).

Herbert, J. M., *Ferroelectric Transducers and Sensors*, Gordon and Breach Science Publishers, NY (1982).

IEEE Standard on Piezoelectricity, ANSI/IEEE Std. 176-1978, IEEE, New York (1978).

Ikegami, K. and I. Ueda, "Piezoelectricity in Ceramics of Ferroelectric Bismuth Compound with Layer Structure", *Jpn J. of Appl. Phys.*, **13** [10] 1572 (1974).

Ishizawa, N., F. Marumo and S. Iwai, "Compounds with Perovskite Type Slabs", *Acta Cryst* **B37**, 26 (1981).

Ishizawa, N., F. Marumo, T, Kawamura and M. Kimura, "The Crystal Structure of $Sr_2Nb_2O_7$, a Compound with Perovskite Type Slabs", *Acta Cryst* **B31**, 26 (1975).

Jaffe, B.,. W. R Cook, Jr., and H. Jaffe, *Piezoelectric Ceramics*, Academic Press Ltd., London (1971).

Kamo, R. *et al.*, NTID Conference 790747 (1979).

Kanda, Y. and C. Gross, "A New Type of Pressure Sensor Utilizing Surface Acoustic Waves", *Ferroelectrics* **10**, 71 (1976).

Keramos, Inc., Indianapolis, IN, General Catalog (1991).

King, D. B., and F. V. Thome, editors, *Transactions of the First International High Temperature Electronics Conference*, Sandia Nat. Lab., Albuquerque, N. M., June (1991).

Kingery, W. D., H. K. Bowen, and D. R. Uhlman, *Introduction to Ceramics*, Wiley and Sons. New York (1976).

Kistler Instruments, AG, Winterthur, Switzerland, General Catalog (1989).

Korzunova, L. V., "Piezoelectric Ceramics for High Temperature Transducers", *Ferroelectrics* 134, 175 (1992).

Kusakabe, H., T. Okauchi, and M. Takigawa, "A Cylinder Pressure Sensor for Internal Combustion Engine", SAE (Society of Automotive Engineers) paper 920701 Warrendale. PA (1992).

Lei, J. F., J. Mentor, and H. J. Van Horn, "Influence of Rare Earth Oxide Addition on the Oxidation Behavior of PdCr Strain Gauge Material", *1990 Meeting of the Electrochemical Society, Montreal, Canada* (1990).

Managan, W., "Needs for High Temperature Electronics in Fossil Energy Plants, " *Conference on High Temperature Electronics*, Tucson, AZ (1981).

Matsushita Electric Industrial Co., LTD, Osaka, Japan.

McCloy, J. J., Chairman, Noise Cancellation Technologies, Inc., Great Neck, NY, "Letter to Shareholders", May 19 (1987).

McCormick, B. J., "Preface", in *High Temperature Electronics*, IEEE, Tucson, AZ (1981).

Measurements Group, Inc., Tech-Note TN-513, "Measurement of Thermal Expansion Coefficient Using Strain Gages", Raleigh NC (1986).

Meetham, G. W., "High Temperature Materials: a General Review", *J. Matl. Sci.* **26** [4] 853 (1991).

Ménard, P., and J. M. Bourgeois, "Using Capacitive Sensors for AC Generator Monitoring", International Conference on Large High Voltage Electric Systems, Paris (1990).

Mujasaka, Y., S. Hashino, S. Takahashi, "Advances in Structure and Fabrication Process for thin Film Acoustic Resonators", *1987 Ultrasonics Symposium*, IEEE, New York p. 385 (1987).

Naito, M. "Recent Sensors for Automotive Applications", *Ceram. Eng. Sci. Proc.* **8** [9-10] 1106 (1987).

Nanamatsu, S., M. Kimura, and T. Kawamura, "Crystallographic and Dielectric Properties of Ferroelectric $A_2B_2O_7$ (A=Sr, B=Ta, Nb) Crystals and Their Solid Solutions", *J. Phys Soc. Japan* **38** [3] 81 (1975).

Nanamatsu, S., M. Kimura, K. Doi., S. Matsushita, and N. Yamada, "A New Ferroelectric, $LaTiO_3$", *Ferroelectrics* **8**, 511 (1974).

Nanamatsu, S., M. Kimura, K. Doi, and M. Takahashi, "Ferroelectric Properties of $Sr_2Nb_2O_7$ Single Crystals", *J. Phys. Soc. Japan* **30**, 300 (1971).

Neto, A. S., "Ferroelectrics with High Curie Temperature for Piezoelectric Applications", Ph.D. Thesis, The Pennsylvania University, University Park, PA (1978).

Newnham, R. E. and W. Huebner, "Electroceramics", Science of Advanced Materials, ed. H. Weidesch and M. Meshii, ASM International, Ohio p. 267 (1990).

Omega Engineering, Inc., Stamford, CT, "*Pressure, Strain, and Force Measurement Handbook and Encyclopedia*", (1987).

Onoe, M. and H. Jumonji, "Useful Formulas for Piezoelectric Ceramic Resonators and Their Application to Measurement of Parameters", *J. Acoust. Soc. Am.* **41** [4] Part 2 p. 974 (1967).

Patel, N. D. and P. S. Nicholson, "High Frequency, High Temperature Ultrasonic Transducers", *NDT International* **23** [5] 262 (1990).

Richards, V. L., T. Y. Tien, and R. D. Pehlke, "High-Temperature Electrical Conductivity of Aluminum Nitride", *J. Mat. Sci* **22**, 3385 (1987).

Robertson, A. E. *Microphones*, Hayden Book Co. Inc., New York (1963).

Schafer, W. and R. Schmidbarger, "Ca and Sr Doped $LaCrO_3$: Preparation and High Temperature Applications", in *High Tech Ceramics*, edited by P. Vincenzini, Elsevier Science Publishers, Amsterdam (1987).

Scheunemann, K. and H. K. Muller-Buschbaum, "Zur Kristallstruktur von $La_2Ti_2O_7$", *J. Inorg. Nucl. Chem.*, **37**, 1878 (1975).

Shannon, R. D., "Revised Effective Ionic Radii and Systematic Studies of Interatomic Distances in Halides and Chalcogenides," *Acta Cryst*, **A32** 751 (1976).

Sheppard, L.. M. "Automotive Sensors Improve Driving Performance", *Ceram. Bull.* **71** [6] 905 (1992).

Shiosaki, T., M. Hayoshi, and A. Kawabata, "Audio-Frequency Characteristics of a Piezoelectric Speaker Using an AlN Film Deposited on a Polymer or Metal Membrane", *1982 Ultrasonics Symposium, Proc.* IEEE New York, p. 529 (1982).

Shrout, T., R., A. Safari and W. A. Schulze, "Low Field Poling of Soft PZTs", *Ferroelectrics Letters*, **44**, 227 (1983).

Swartz, S. L., "Topics in Electronic Ceramics", *IEEE Transactions on Electrical Insulation*, **25** [5] 935 (1990).

Swartz, S. L., W. A. Schulze and J. V. Biggers, "Fabrication and Electrical Properties of Grain Oriented $Bi_4Ti_3O_{12}$ Ceramics" *Ferroelectrics* **38**, 765 (1981).

Takahashi, M., "Electrical Resistivity of Lead Zirconate Titanate Ceramics Containing Impurities", *Jpn. J. of Appl. Phys.* **10** [5] 643 (1971).

Takenaka, T. and K. Sakata, "Grain Orientation and Electrical Properties of Hot-Forged $Bi_4Ti_3O_{12}$ Ceramics", *Jpn. J. of Appl. Phys.* **19**[1] 32 (1980).

Takenaka, T. and K. Sakata, "Grain Oriented and Mn-Doped $(NaBi)_{(1-x)/2}Ca_xBi_4Ti_4O_{15}$ Ceramics for Piezo and Pyrosensor Materials", *Sensors and Materials* **1**, 35 (1988).

Tichy, J., Chairman, Graduate Program for Acoustics, Penn State U., private communication (1993).

Token Corp. Tokyo, Japan, Piezoelectric Ceramic Catalog.

Tsubouchi, K. and N. Mikoshiba, "Zero Temperature Coefficient Saw Delay Line on AlN Epitaxial Films", *1983 Ultrasonic Symposium Proc.*, IEEE New York, p. 299 (1980).

Tuller, H. L., "Highly Conductive Ceramics", p. 425 in *Ceramic Materials for Electronics* edited by R. C. Buchanan, Marcel Dekker, Inc. New York (1986).

Ueda, I., "Effects of Additives on Piezoelectric and Related Properties of $PbTiO_3$ Ceramics", *Jpn. J Appl. Phys* **11** [4] 450 (1972).

Vibrometer, Inc., Longueuil, Quebec, Canada, Product Catalog (1988).

Watanabe, H., T. Kimura and T. Yamaguchi, "Particle Orientation During Tape Casting in the Fabrication Of Grain-Oriented Bismuth Titanate", *J. Am. Ceram. Soc.*, **72** [2] 289 (1989).

Xue, W. R. , J. N. Kim, S. J. Jang, L. E. Cross and R. E. Newnham, "Temperature Behavior of Dielectric and Electromechanical Coupling Properties of Samarium Modified Lead Titanate Ceramics", *Jpn. J. Appl. Phys.*, **24** [24 Suppl. 24-2] 718 (1985).

Applied Acoustics **41** (1994) 299–324

Materials for High Temperature Acoustic and Vibration Sensors: A Review

R. C. Turner, P. A. Fuierer, R. E. Newnham & T. R. Shrout

The Materials Research Laboratory, The Pennsylvania State University, University Park, Pennsylvania 16802, USA

ABSTRACT

The industrial and scientific communities have expressed a real need for the capability of pressure, acoustic, and vibration sensing at elevated temperatures. This review compares the various commercial methods and materials for acoustic transduction, identifying their advantages and limitations. Techniques and devices include simple piezoelectric sensors, accelerometers, strain gauges, proximity sensors, fiber optics and buffer rods. Sensors with operating temperatures in excess of 650°C are readily available from commercial sources. Of the mechanisms investigated, the piezoelectric approach offers several advantages, including design cost and simplicity. Therefore, the bulk of this review concentrates on piezoelectric materials, both those that are already available commercially, and those that are presently under development. The new materials include perovskite layer structure ferroelectric ceramics, which possess the highest known Curie temperatures, and thin film AlN, which has been reported to be piezoactive at 1150°C.

1 INTRODUCTION

High-temperature electronics is an area of research offering interesting materials and design challenges and one of significant industrial importance. The major impetus for the development of high-temperature electronic materials, devices, circuits, and systems can be credited to the energy crisis of 1974, when a commitment was made to the development of national energy resources by geothermal exploration.[1] At that time, geothermal and oil-well logging industries voiced their need for sensors and electronic

Applied Acoustics 0003-682X/94/$07.00

systems with higher operational temperatures for deep drilling in the earth's crust. The economic importance of world energy independence and reduced waste provided additional incentive for their development.

The aerospace and aircraft industries have especially difficult high-temperature requirements. With space and weight at a premium, engine designers and builders find it difficult to protect sensitive electronic systems in a cool, remote place. Electronic controls are to be placed directly inside jet engines because of reliability and noise requirements, so sensors need to be built that can withstand temperatures of 500–1000°C while allowing mission lifetimes up to 100 000 h.

In automotive electronics, the number of sensors and actuators continues to increase each year. Ceramic and semiconductor sensors which record temperature, oxygen pressure, and preignition knock are used in conjunction with microprocessor-based controls to improve the efficiency and reliability of internal combustion engines.[2] Further efficiency can be realized by operating combustion engines at higher temperatures. Research on the use of ceramic components in a diesel engine has led to higher operating temperatures, resulting in a potential increase in fuel efficiency up to 65%, along with a notable reduction in exhaust pollution.[3] Higher operating temperatures do, however, place additional requirements on the sensors. Environments of 150°C with repeated temperature cycles are at present considered the automotive norm, and higher temperatures are expected in the future.

Until the present, there has not been a review of the types of sensors commercially available for high-temperature acoustic sensing applications. The purpose of this paper is to provide such a review. Included in the discussion are the commercially available high-temperature piezoelectric materials used in many of the sensors described. In addition, new advances in materials that may permit the design of sensors which can operate at temperatures well above those currently available will be presented.

2 ACOUSTIC MEASUREMENT TECHNIQUES AND APPLICATIONS

Critical parameters for acoustic and vibration sensors involve the measurement of dynamic pressure pulses, vibrations (relative and absolute), acoustic emissions, strains, and the dynamic proximity of machine components. An example of a dynamic pulse is the rapid increase in pressure upon ignition of the air–fuel mixture in the cylinders of an internal combustion engine. The timing and the shape of the pulse have a large effect upon

engine efficiency. Transducers fitted into the cylinder head have been used for monitoring combustion pressure to optimize ignition timing.[4]

Dynamic monitoring is also employed in such machines as aircraft engines, gas turbines, and power generators, all of which have high speed rotors. Sensors strategically mounted on the machine detect destructive conditions of imbalance, or unequal loading of the rotor, enabling the possibility of corrective measures to be implemented. The sensors convert the associated mechanical energy of the vibration to electrical energy which can then be amplified and monitored. Computer coupling, allows real-time status reports of the condition of the machine while providing a comparison with an operating norm.

Non-destructive testing (NDT) is another widely used application of acoustic sensors that involves either passive sensing of 'acoustic emissions', or active 'ultrasonic testing' techniques. An application of the first method involves affixing a number of acoustic sensors in strategic locations on the wall of a vessel, such as a chemical storage tank, pressurizing the vessel to create strains, and examining the acoustic emissions which result from the Kaiser effect.[5] Cracks and poor joints can then be detected and logged so that repairs can be made. This method has also been successfully applied in the inspection of the fuselage of large aircraft to detect cracks resulting from fatigue. The ultrasonic method of NDT incorporates a transducer to generate an acoustic signal at ultrasonic frequencies that is transmitted through the test specimen. When the acoustic wave reaches an interface of the sample it is reflected back to the transmitter/sensor which, therefore, acts as a transceiver. If, however, the wave impinges upon a flaw, a portion of the wave is reflected and thus reaches the sensor ahead of the original wave. This, then, becomes a valuable tool for locating defects within a structure.[6] Figure 1 is a simple illustration of the technique. Acoustic sensors also find use in the hostile environments of deep oil wells for seismic data logging, and in nuclear power plants to monitor the condition of heat exchange pumps and pipes.[7]

An indirect way of sensing vibration is by measuring capacitive changes in an air gap. An air gap sensor placed in close proximity to a

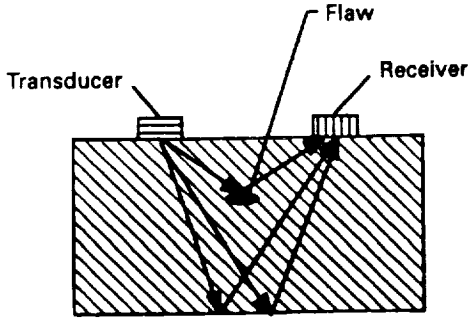

Fig. 1. Detection of a flaw in a solid by ultrasonic testing (NDT).

TABLE 1
Acoustic and Vibration Measurement: Industrial Applications

Aerospace	Measure rotational speed of jet turbine rotors
	Space vehicle acceleration
	Trajectory monitor
	In-flight vibration monitor
	Nozzle pressure
	NDT test of air frames
Automotive	Knock sensor
	Fluid level sensor
	Crash test
	Vibration control
Industrial	Dynamic pressure monitors
	Vibration detectors
	Flow detectors
	NDT testing
	Proximity detectors
	Noise 'fingerprinting'
Medical	Diagnostic imaging
	Impact sensors
Military	Hydrophones
	Range finders
	Noise detection in vehicles
	Security systems
Power generation	Leak detector
	Liquid sodium coolant pump monitor
	Nuclear reactor monitor
	Air gap monitoring between stator and rotor
	Fuel rod monitor
	Coal feeder monitor
	NDT of pressure vessels
Commercial	Fish finders
	Phonographs pick-up
	Microphones

high-speed rotor will detect dynamic changes in the spacing between the two which, in effect, is an indicator of an imbalance condition or some other malfunction. This type of sensor has found wide acceptance in hydroelectric power plants.[8]

Examples of pressure, acoustic and vibration measurement techniques described above serve to illustrate the wide variety of possible applications. Additional applications are listed by industry in Table 1. These are routinely employed in the range of −55°C to 125°C, however, several devices are needed to operate in much harsher thermal conditions. Sensor designs and their respective temperature limitations are described in the following section.

3 SENSOR DESIGNS

Listed in Table 2 are current commercial sensor designs. They include piezoelectric discs or plates, accelerometers, strain gauges, proximity sensors, fiber-optic sensors, and systems incorporating buffer rod extensions. Brief descriptions of these devices are as follows.

3.1 Simple disc

The most basic sensor incorporates a simple disc, or other simple shape, composed of a piezoelectric ceramic, which is attached directly to the wall or frame of an engineering structure, embedded in a recess, or mounted in a replaceable fixture. Figure 2 is a schematic construction of a piezoelectric knock sensor using a bending mode resonance to detect vibrations. The piezoelectric element 'generates' a voltage in response to stresses caused by the acoustic energy impinging upon it.[9] The magnitude of the voltage generated is directly related to the product of the applied stress and the piezoelectric voltage or 'g' constant of the material. The electrical signal is then amplified and fed to a microprocessor in the control system. This arrangement is capable of extremely high sensitivity on the order of pico (10^{-12}) strains. It is also self-generating, rugged, low-cost, and simple. The temperature limitations of these sensors arise from the loss of piezoelectric properties that occur as the material approaches its transition (Curie) temperature T_c, a topic which will be discussed later. For lead zirconate–titanate, (commonly called PZT), the most widely used piezoelectric ceramic material, the maximum use temperature is ~200°C. Other temperature limitations result from the failure of the adhesives used to mount the disk, and melting of the solder used to attach the leads.

3.2 Buffer rod extensions

For many high-temperature applications, buffer rod extensions are utilized to transmit and receive acoustic signals from very hot areas, effectively

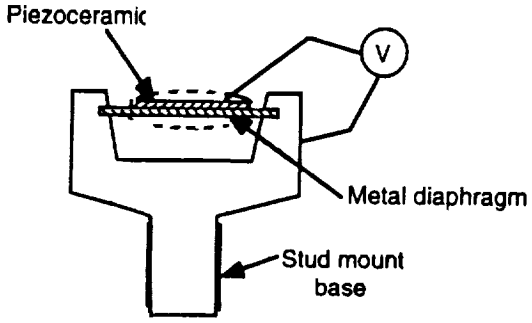

Fig. 2. Two methods of mounting a piezobender used in automotive knock sensors (after Ref. 9).

TABLE 2
Comparison of Commercial Strain, Vibration, and Acoustic Senors

Operation principle	*Piezoelectric disc or plate*	*Accelerometer*		*Strain gauge*	*Proximity sensor*		*Buffer rod*	*Fiber-optic sensor*
	Piezoelectric	*Piezoelectric*	*Magnetic induction*	*Resistive metal*	*Capacitive*	*Eddy current*	*Piezoelectric*	*Laser/optic*
Measured parameter	Acoustic waves vibration	Acceleration absolute dynamic	Vibration pressure	Load, force vibration absolute	Relative air gap displacement	Vibration	Acoustic waves	Strain vibration
Present maximum temperature (°C)	400	650	480	850	150	450	1100	300
Temperature stability	Good	Good	Good	Fair	Good	Fair	Good	Poor
Temperature sensitivity	Good	Good	Good	Fair	Good	Fair	Good	Poor
Resolution/ sensitivity	High	High	Fair	Low	Low	Low	Fair	High
Frequency range	0·05–1 MHz	0·05– MHz	0·015–2 kHz	DC–kHz	DC–kHz	DC–10 kHz	0·05 kHz–MHz	DC–10 kHz
Power consumption	Low	Low	Low	Medium	Medium	Medium	Low	High
Cost and complexity	Low	Medium	Medium	Low	Low	High	High	High
Durability	Good	Good	Good	Fair	Good	Fair	Good	Poor

isolating temperature-sensitive transducers from hostile environments. The rod serves as an acoustic wave guide to couple the hot test specimen with the sensitive piezoelectric transducer. The rods are generally constructed of stainless-steel and are cooled with water or air to prevent damage to the transducers. This arrangement permits the use of a conventional piezoelectric material, which would otherwise lose its piezoelectric properties at high temperatures. This technique is widely used on NDT probes in the metals industry to detect cracks and other defect in hot steel blooms and pipes at temperatures in the neighborhood of 1100°C.[10] A similar application employs hollow 'buffer pipes' to couple dynamic pressure sensors with jet and rocket engines.

3.3 Accelerometers

Accelerometers most often use a piezoelectric as the internal sensing element. The various designs exploit different mechanisms to translate mechanical energy to a measurable response, but all operate based on Newton's second law:

$$F = ma$$

The accelerometer shown in Fig. 3 differs from the simple disk piezoelectric sensor in that a seismic mass (m) is attached to the piezoelectric element and the assembly is hermetically sealed in a protective case.[11] As a response to acceleration (a), the mass imparts a force (F) on the element, which in turn generates a voltage in proportion to the magnitude of the stress. Depending upon the sensitivity and temperature range required for the application, transducer manufacturers utilize several different piezoelectric materials. Commercial accelerometers using lithium niobate ($LiNbO_3$) single crystal elements are rated for continuous use up to 650°C.[12,13]

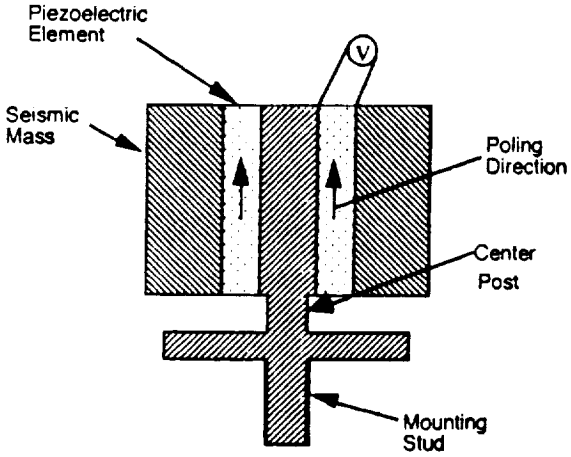

Fig. 3. Cross-section of a tubular accelerometer element (after Ref. 11).

Accelerometers based on magnetic induction, employ a permanent magnet as the seismic mass and a field coil for the active element. The mass is partially restrained by a spring, but when the mass is accelerated, it moves relative to the coil, thus inducing an electromotive force. As with the case of piezoelectric types, the resulting electric signal must be amplified and filtered before it is fed to the instrumentation. The upper temperature limit of this type of device is determined by the Curie temperature of the permanent magnet. Commercial units are rated for temperatures as high as 480°C.[14]

3.4 Strain gauges

Figure 4(a) is an illustration of a bonded metallic foil strain gauge.[15] Resistive strain gauges involve a change in electrical resistance (ΔR) resulting from the mechanical strain ($\Delta L/L$) of the sample to which the gauge is bonded. The sensitivity is determined by the gauge factor (GF):

$$\mathrm{GF} = \frac{\Delta R/R}{\Delta L/L}$$

With a typical gauge factor of 2, and a nominal resistance $R = 100\ \Omega$, these gauges require an ohmmeter with very high sensitivity to measure the ΔR accompanying a strain of 1×10^{-6}. A more accurate way of measuring small changes in resistance incorporates a Wheatstone bridge as shown in Fig. 4(b).

To compensate for the nonlinear character of the thermal coefficients of expansion of the alloys used, an unstrained reference gauge is installed in an adjacent bridge arm. This second gauge is subjected to the same temperature as the first, thereby effecting electrical cancellation of the apparent strain. Commercial metal gauges are typically limited in temperature range to about 300°C; however PtW wire gauges are available for

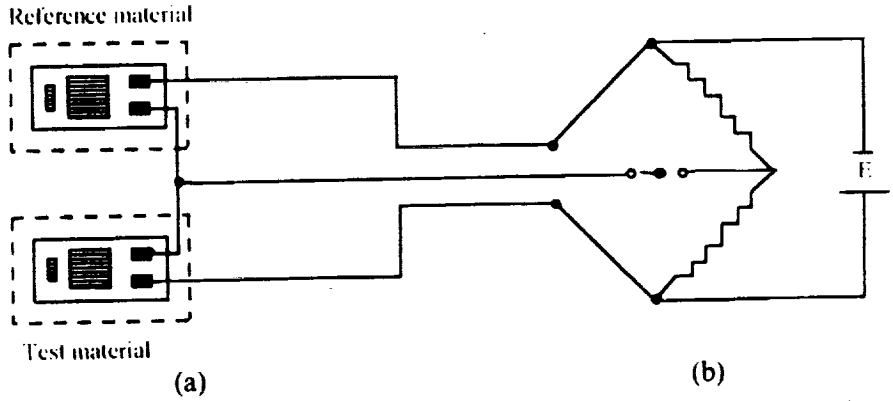

Fig. 4. Bonded grid resistance gauges including (a) the measurement and reference components, and (b) Wheatstone bridge circuit for measuring strain (after Ref. 15).

use up to 850°C,[16] and other exotic metals such as PdCr are being studied for use up to 1000°C.[17]

Metal strain gauges are simple in design, low-cost, and can detect static strains. Even using the Wheatstone bridge configuration, however, strain sensitivity is low compared with piezoelectric transducers.

3.5 Proximity sensors

Proximity sensors are often used to monitor the degree of rotation of the armatures of electric generators as well as the clearance between the armature and the stator. This serves as an indirect method of measuring vibration if an unbalanced condition exists. The two types of proximity sensors available commercially are (i) air gap capacitors, and (ii) eddy current detectors. Both types require electronic conditioners to supply an input signal, and processors to analyze the signals modified by the sensors.

(i) An example of an air gap capacitor is illustrated in Fig. 5.[18] In this application on an electric power generator, the armature serves as one plate of the capacitor while the other plate is an integral part of the sensor and air is the dielectric. The plates are maintained at a close proximity with one another so that a small change in spacing results in significant changes in capacitance. The change in capacitance can then be detected by the control circuitry and acted upon accordingly. The detection of variations in air gap as small as one micron are possible in installations on hydroelectric power generators. At present, commercial units are constructed of fibreglass composites for use at temperatures up to 150°C,[12] but it seems reasonable that units could be constructed from more refractory materials for higher temperature applications.

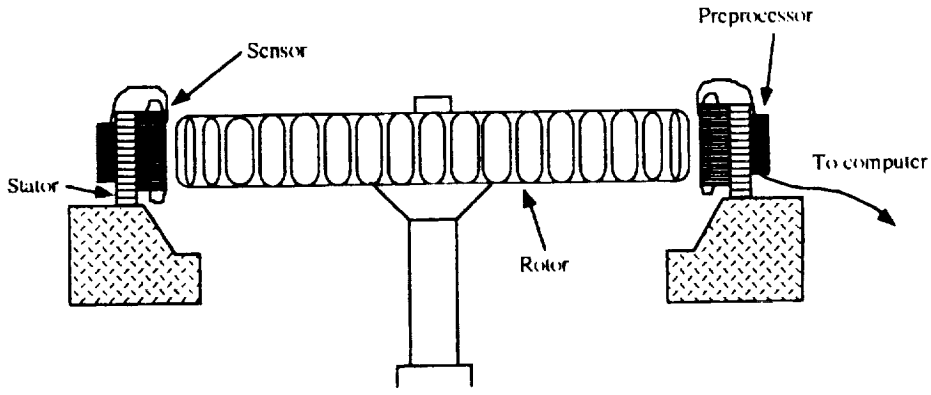

Fig. 5. Air gap sensors mounted on an AC generator (after Ref. 18).

(ii) The second kind of proximity sensor is the eddy current type. It determines the relative position of a rotating shaft by detecting changes in magnetic field between the sensor and the target shaft. The eddy current sensor operates in a manner similar to that of an electrical transformer. The sensing coil resembles the primary winding, and the small eddy current loops induced in the target by the variable magnetic field of the sensing coil act like the secondary windings. The small eddy currents cause a change in phase and amplitude of the sensing coil signal. The target material must therefore be metallic. The sensing coil is mounted near the rotating shaft or moving component of a machine with lead cables attached to the exterior end. Commercial models are currently rated for use up to 450°C.[14] The temperature limitation is primarily due to the temperature coefficient of resistance of the wire used to wind the probe coil.[19]

3.6 Fiber optic sensor interferometers

Fiber optic sensor (FOS) interferometers or phase sensors are used to detect small strains, (in the order of 10^{-7}) or vibrations in a sample without making physical contact. This capability allows measurements to be made inside a hostile environment, such as a furnace. A simplified schematic of a system is shown in Fig. 6. There are several different designs, but all are based on measuring a phase change in the transmitted light signal resulting from a change in length of the optical fiber. Optical fibers are typically SiO_2 glass; however, fibers of more heat-resistant materials such as sapphire (Al_2O_3) are commercially available. Along with the fiber, a large number of additional components, such as a laser source, phase demodulator, filters, and microprocessors, etc., are needed for these systems. High cost, complexity and sensitivity to variations in temperature are disadvantages of this approach.

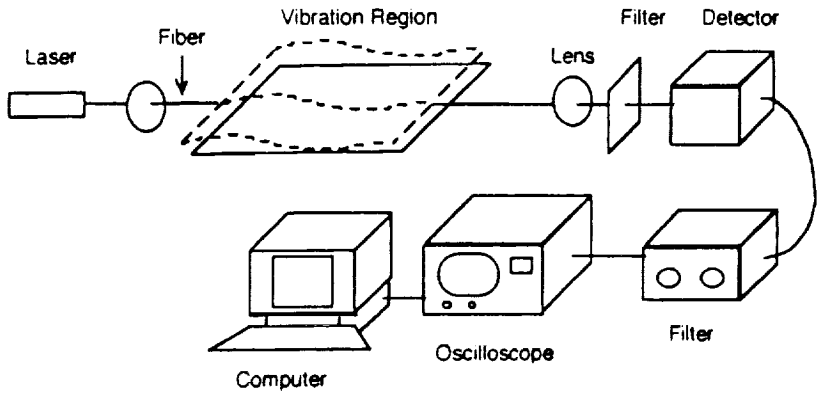

Fig. 6. Fiber-optic vibration sensor and associated electronics.

In summary, with respect to the operational parameters listed in Table 2, piezoelectric trandusers offer many advantages over the other types of acoustic sensors. Specifically, their compliment of sensitivity, stability over a wide temperature range, and simple design offers the lowest cost approach. Polycrystalline ceramics are often the material of choice because they can be readily manufactured into a variety of configurations. Therefore, the remainder of this paper concentrates on high-temperature piezoelectric materials, with a review of those currently available, and a discussion of future prospects.

4 PIEZOELECTRIC CERAMICS

4.1 Piezoelectricity

The phenomenon of piezoelectricity was first reported in 1880 by Pierre and Jacques Curie. Since that time, a number of crystalline materials have been found to exhibit piezoelectric activity, although only a few are of practical concern. The common feature of all piezoelectric crystals is that they have no center of symmetry along the piezoelectric axes. Ferroelectric ceramics possess a multitude of individual dipole domains which are distributed throughout the body in various crystallographic orientations, resulting, in a net dipole moment of zero. In a process, called poling, a relatively large electric field is applied through the body causing a common alignment of a large portion of the dipoles, thus rendering the material piezoelectric. These crystals develop an electric field when subjected to an applied stress (sensor), or conversely, exhibit a mechanical deformation with the application of an electric field (actuator). Since the details of piezoelectricity are covered in a number of excellent texts and review articles, the reader is advised to consult them for further information.[11,20–22]

4.2 Electromechanical properties

In order to describe the electromechanical properties of piezoelectric materials, a large number of interrelated coefficients are used, many of which have been standardized by the IEEE.[23] However, with regards to high-temperature materials, only the most important coefficients and properties will be presented in this section, (Note: where subscripts are used with coefficients, the first number refers to the axis of polarization, and the second refers to the axis of applied stress, or applied field.)

4.2.1 Ferroelectric Curie temperature

Most of the piezoelectric materials described in this paper are ferroelectric and capable of being polarized, with the polarization resulting from the asymmetry of its crystal structure. When the crystal is heated, its internal kinetic energy increases. At a certain temperature, called the Curie temperature (T_c), the crystal changes to a structure of a higher symmetry, the alignment of the dipoles is lost and all piezoelectric activity disappears. Upon cooling, the dipoles do not realign unless they are subjected to a strong electric field. Other consequences of increasing temperature are changes in the values of electromechanical coefficients, which become more pronounced as the T_c is neared. This can be particularly important in applications where the electrical properties of the sensor are closely matched to the instrumentation. In addition, dipoles that were polar oriented have a tendency to reverse back to their original position thus degrading the piezoelectric effect in a process known as 'thermally activated aging'. Generally, a maximum operating temperature of one-half the T_c is considered safe.

4.2.2 Resistivity and the RC *time constant*

High electrical resistivity is necessary so that a large field can be applied during poling without breakdown or excessive charge leakage. High insulation resistance 'R' is also required during operation of the device. The transducer must not only develop a charge for an applied stress or strain, but must also maintain the charge for a time long enough to be detected by the electronic system. The length of time the charge is maintained is proportional to the RC time constant (resistance × capacitance). The minimum useful frequency of a sensor, known as the lower limiting frequency (f_{LL}), is inversely proportional to the time constant:

$$f_{LL} = \frac{1}{2\pi RC}$$

where C is the device capacitance.

Below f_{LL}, the charge will drain off before it is detected because of conduction in the sensor. With low f_{LL} the dynamic bandwidth can be extended to sonic frequencies, and thus, a large RC constant is desirable for many applications.

4.2.3 Piezoelectric constants

The piezo strain 'd' constant gives the ratio of the strain developed in the specimen to the electric field applied at the electrodes, and conversely, the ratio of short circuit charge, per electrode area, to the applied stress. The stress can be applied to the body in different modes as illustrated in

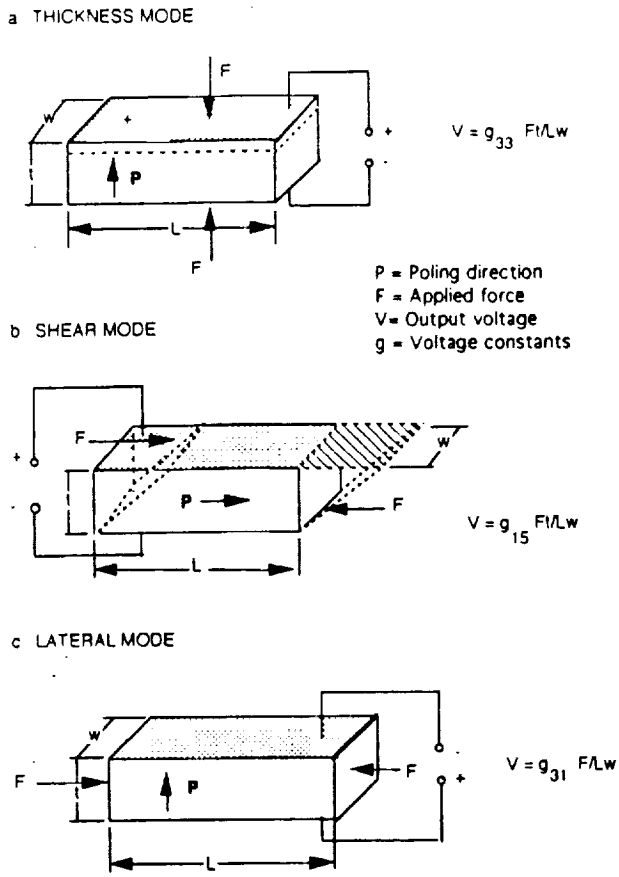

Fig. 7. (a) Thickness, (b) shear, and (c) lateral mode piezoelectric sensors. P indicates the poling direction. The output voltage (V) is proportional to the applied force (F) and piezoelectric voltage coefficient (g_{ij}) of the material.

Fig. 7. The piezoelectric voltage 'g' constant gives the ratio of the field developed to the stress applied, and conversely, the ratio of strain to the applied charge to the electrode area. The 'g' constant is related to the 'd' constant by the permittivity, $K\varepsilon_0$.

$$g = \frac{d}{K\varepsilon_0}$$

In comparing the properties of high-temperature piezoelectric materials, the 'g' constant tends to be the more meaningful coefficient.

4.2.4 Mechanical Q

The mechanical Q expresses the ratio of strain in phase with stress to strain out of phase with stress in the vibrating element, or in other words, the relative amount of input electrical energy that is converted to mechanical energy as opposed to that which is lost as heat. Piezoelectric materials with high 'Q_m' factors are characterized by having narrow

resonant peaks, whereas, those with low 'Q_m' factors have broader bandwidths.

4.2.5 Sensitivity

For a given stress applied to the device, the output voltage generated by the piezoelectric 'generator' should be sufficiently high to be detected above background noise. The most sensitive devices produce the greatest output per unit of stress. Unfortunately, for high-temperature sensors, ferroelectric materials exhibit a considerable increase in permittivity, with increasing temperature, a condition which effectively reduces the voltage constant 'g'. Every piezoelectric material reaches some temperature at which its voltage constant 'g' and resistivity are diminished to the point where the output becomes undetectable. In practice, the relatively small output signals generated by high temperature accelerometers necessitate the use of electronic charge amplifiers for enhancement, but there is a practical limit to how small a signal that can be accurately detected.

5 COMMERCIAL PIEZOELECTRIC CERAMICS

Table 3 lists typical piezoelectric ceramic materials found in commercial accelerometers and vibration sensors, along with reported room temperature properties.[21,24–28] Owing to the lack of reliable published high-temperature data available for this work, samples were obtained, their electrical properties were measured at elevated temperatures, and the data reported in Table 4.[25–29] In addition, the resistivity of each material was measured over a wide range of temperatures as shown in Fig. 8.[25–28,30–34] Good agreement was found with values reported in the literature (as shown in Fig. 8).

A brief description of each of these piezoelectric materials, or related compositional families, is presented in this section. With the exception of quartz, all are ferroelectric.

5.1 Quartz

Quartz (SiO_2) is one of the earliest piezoelectric materials used in electronic devices. Originally, natural quartz crystals were used, but now have been widely replaced by hydrothermally-grown synthetic quartz. Because of its low mechanical loss (high Q_m), narrow bandwidth, and highly temperature-stable resonant frequency, quartz is the material of choice for timing standards and monolithic filters in communication equipment. However, as seen in Table 3, the piezo 'd' coefficient is relatively small and thus

TABLE 3
Reported Room Temperature Electrical Properties of Commercial High Temperature Piezoelectric Materials

Material	*Structure*	*Curie point* T_c *(°C)*	*Dielectric constant* K *(10^{-12} C/N)*	*Piezoelectric strain constant (10^{-3} Vm/N)*		*Piezoelectric voltage constant*		*Electromechanical coupling (10^{12} Ω-cm)*		*Mechanical quality* Q_m	*Resistivity 20°C* ρ	*Ref.*
				d_{33}	d_{15}	g_{33}	g_{15}	k_{33}	k_{15}			
$Pb(Zr, Ti)O_3$ (Soft PZT)	Perovskite	330	1800	417	710	25	41	0·73	0·77	75	100	N-21[26]
$(BaPb)Nb_2O_6$ (BPN)	Tungsten bronze	400	300	85	100	32	46	0·30		15	1	K-81[25]
$PbTiO_3$ (PT)	Perovskite	470	190	56	68	33	32	0·45		1300	10	LTT-3[28]
$Na_{0·5}Bi_{4·5}Ti_4O_{15}$ (NBT)	Bismuth	~600	140	18		15		0·15		100	1000	K-15[25]
$LiNbO_3$ (LN)	Corundum	1150	25	6	69	23	91	0·23	0·60	NR	1	[27]
SiO_2	α-Quartz	573	4·5	$2(d_{11})$		50		NR		10^5	1000	[21,24]

TABLE 4
Selected High Temperature Properties of Piezoelectrics

Material[a]	T_c (°C)	*Vibration mode (ij)*	*g (RT)*[b] ($\times 10^{-3}$ Vm/N)	*TCF* (ppm/°C)	ρ (Ω-cm)	ε_r (10 kHz)	*tan δ* (10 kHz)	*RC* (s)	*Ref.*
PZT (DOD II) (200°C)	360	[33]	15 (25)	+200	10^{12}	3000		250	N-21[26]
$(BaPb)Nb_2O_6$ (300°C)	400	[33]	24 (30)	−135	10^7	530	0·036	0·0005	K-81[25]
$PbTiO_3$ (400°C)	450	[15]	21 (29)	−97	2×10^5	1000	0·35	0·00002	LTT-3[28]
$Na_{0·5}Bi_{4·5}Ti_4O_{15}$ (400°C)	600	[33]	10 (18)	−118	3×10^8	262	0·10	0·007	K-15[25]
$LiNbO_3$ (400°C)	1150	[15]	93 (99)	−76	3×10^7	100	0·001	0·0003	[27]
Sr_2NbTaO_7 (400°C)	823	[24]	5 (6)	−74	4×10^9	40	0·10	0·01	[29]

[a] PZT and BPN were evaluated at approximate maximum use temperatures, the others at 400°C.
[b] Room temperature values (RT) also shown for the voltage constant (*g*).

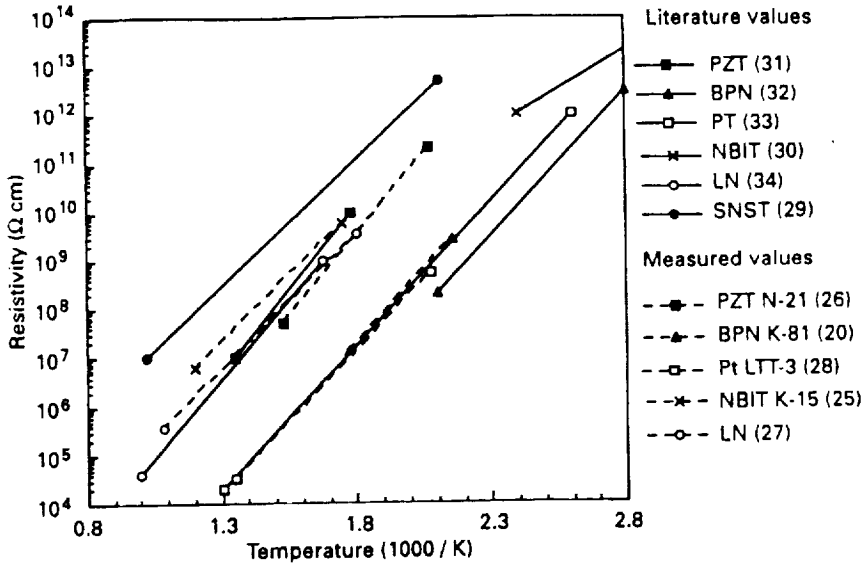

Fig. 8. Temperature dependence of resistivity for piezoelectric ceramics: 'soft' lead zirconate titanate (PZT), barium-doped lead metaniobate (BPN), sodium bismuth titanate (NBIT), lead titanate (PT), lithium niobate (LN), and perovskite layer structure strontium niobate tantalate (SNST). Solid lines represent data taken from literature, while dashed lines represent data measured from commercial materials for this work. All are polycrystalline ceramics except single crystal LN.

the amount of electric charge that can be generated is low. Although piezoelectric α-quartz has a transition temperature of 573°C, its use temperature is normally limited to 350°C. Above that temperature the crystal structure is subject to twinning, destroying its piezoelectric properties.[24]

5.2 Lead zirconate titanate

Lead zirconate titanate ($Pb(ZrTi)O_3$)(PZT) has the perovskite structure and is a solid solution of tetragonal $PbTiO_3$(PT) and orthorhombic $PbZrO_3$(PZ). Because of the large number of polarization directions available, compositions near the morphotropic phase boundary at approximately 53:47 PZ to PT are easily poled to high remanent polarization and exhibit extremely high values of electromechanical coupling coefficients and electrical permittivity. Because of its superior piezoelectric properties and higher operating temperature, PZT has largely replaced barium titanate (BT)—T_c ~ 130°C, the first widely used ferroelectric, in all but the lowest cost commercial products. Useful variations in properties of PZT can be obtained by compositional additives. Niobium-doped PZT (DOD Type II) is used extensively in accelerometers, hydrophones (underwater microphones), and acoustic emission instruments. Although its electrical resistivity and RC time constant remain quite high

up to a T_c of 360°C (Table 4 and Fig. 8), its use is kept well under 200°C because of its tendency to age very rapidly, leading to depoling.[11]

5.3 Lead titanate

Lead titanate ($PbTiO_3$)(PT) the solid solution end member of PZT family, has a T_c of about 490°C. As in the case of PZT, a large number of modifications have been developed to optimize specific electrical and mechanical characteristics. Many commercial compositions of PT are doped with samarium or calcium for use in hydrophones, but this has the effect of lowering the T_c to around 240°C. Compositions, doped with other elements, have T_c values near 490°C and have found applications in knock sensors for automobile engines. The higher operating temperature of PT allows it to be mounted closer to the combustion chamber, thus giving a faster response time as compared to PZT.[6] The data presented in Tables 3 and 4 and Fig. 8 reflects the latter composition. Evaluation at 400°C has shown it to have a resistivity of only about 10^5 Ω-cm. Such a low value would adversely affect the *RC* time constant.

5.4 Lead metaniobate

Lead metaniobate ($PbNb_2O_6$)(PN) belongs to the tungsten-bronze family. Because of its low Q_m (wide bandwidth) and relatively high d_{33} to d_{31} ratio (high degree of anisotropy), PN finds its greatest use in transducers in NDT and medical diagnostic imaging. Commercial PN compositions are modified to enhance specific electrical characteristics but at the expense of the T_c. A commonly used composition contains about 10% Ba(BPN) and has a T_c of about 400°C. Although BPN is reported to resist depoling up to its T_c, limitations are imposed by its high conductivity above 300°C.[35] Figure 8 reveals that BPN exhibits the lowest resistivity of the materials tested. Other problems associated with this material are its high level of porosity and relatively low mechanical strength.[21]

5.5 Bismuth titanate

Bismuth titanate ($Bi_4Ti_3O_{12}$) is the titular compound of bismuth layer structure ferroelectrics (BLSF). Modification by one or more of a large number of other elements, to enhance dielectric and piezoelectric properties, is also common. A member of the family, reported to have favorable piezoelectric properties, high resistivity and high T_c (>600°C), is $Na_{0.5}Bi_{4.5}Ti_4O_{15}$, (NBT). Commercially available,[25] it is used in accelerometers operated at temperatures up to 400°C.[36] The strongest mode of vibration in NBT is the [33] mode but d_{33} and g_{33} are somewhat lower

than many of the perovskite ferroelectrics previously discussed (see Table 3). Nevertheless, the high T_c and high resistivity make NBT an attractive, moderately high-temperature piezoelectric.

Although not commercially available, other complex variations of BLSF compounds have been reported to have Curie temperatures of over 800°C. Representative of this group is Bi_3TiNbO_9 for which room temperature values of d_{33}, and g_{33} were reported to be near those of NBT.[37] To date, little else has been reported about other properties, particularly at high temperature.

Unlike previously mentioned ferroelectric ceramics, BLSF materials can be made with grains having a plate-like structure. In ceramics formed and fired by conventional processes, these grains are oriented in a more or less random fashion, which leaves only a limited number of crystallographic orientation directions available for polarization due to the low symmetry of the structure. The achievement of an optimum degree of remnant polarization in polycrystalline ceramics necessitates the use of some mechanism to provide grain orientation. By employing hot forging techniques, researchers have prepared samples of several BLSF family members which display a high degree of texturing. The textured samples exhibited a twofold increase in coupling coefficient k_{33} and piezoelectric constant d_{33} over those from conventional sintering.[37]

5.6 Lithium niobate

Lithium niobate ($LiNbO_3$)(LN) has the corundum structure and a reported Curie point near 1150°C. Single crystals are grown from a melt using the Czochralski technique. Single crystals are preferred because of the higher piezoactivity, as well as difficulties encountered in conventional sintering of the polycrystalline form. As with polycrystalline ferroelectrics, single crystals of $LiNbO_3$ exhibit a multidomain structure, and must be polarized. This is accomplished by applying relatively small electric field (1 V/cm DC) at a temperature just below the T_c, thus converting the structure to single domain. The polarized crystal is then sliced along the desired axis indicated for the application, and the faces polished.[38] For accelerometers, electrodes are usually applied parallel to the poling axis to take advantage of the greater value of the d_{15} piezoelectric constant and to eliminate pyroelectric effects The voltage output of LN ($g_{15} = 91 \times 10^{-3}$ Vm/N) is significantly larger than those of the other piezoelectric materials listed in Table 3 due to the inherently low dielectric constant. Sensitivity remains high up to 400°C (Table 4) but resistivity is the limiting factor for use above 650°C (Fig. 8).

The tantalum analog, $LiTaO_3$, exhibits many of the same characteristics

of $LiNbO_3$; however, the T_c (720°C) and piezoelectric constants are somewhat lower, thus offers no apparent advantage for high-temperature acoustic sensors.

6 NEW HIGH-TEMPERATURE PIEZOELECTRIC MATERIALS

In general, the ferroelectric ceramics discussed thus far are limited to temperatures of approximately $T_c/2$. Therefore, applications requiring yet higher temperatures than those just presented, require other materials such as ferroelectrics with higher Curie temperatures, oriented polar non-ferroelectric materials, non-polar piezoelectric single crystals, or piezoelectric thin films. Several novel materials currently under investigation are presented below.

6.1 Perovskite layer structure (PLS) ferroelectrics

PLS ferroelectrics have the general formula $A_2B_2O_7$ and possess an anisotropic layered structure similar to the BLSF family. Single crystals of the two most recognized compounds, $Sr_2Nb_2O_7$ and $La_2Ti_2O_7$, possess the highest known ferroelectric Curie temperatures, 1342°C and 1500°C respectively.[39,40] Thus, PLS ferroelectrics have been proposed for use in transducers with high operating temperatures and good thermal stability. Unfortunately, the cost of growing good-quality single crystals is high due to the high melting points of these compounds (which is considerably higher than that of $LiNbO_3$).

In a manner similar to that used for BLSF compounds, previously described, hot-forging was used to synthesize PLS compounds. The resulting samples, shown in Fig. 9, were found to exhibit near theoretical density and high degree of orientation, and polarizability.[29,41] The use of solid solutions with $Sr_2Ta_2O_7$(T_c = −107°C), to adjust T_c of the parent compound to <900°C, aided poling and the subsequent piezoactivity. One compound, $Sr_2(Nb_{0.5}Ta_{0.5})_2O_7$, had a T_c of 820°C and demonstrated the ability to resist depoling at temperatures as high as 650°C. The electromechanical properties for $Sr_2(Nb_{0.5}Ta_{0.5})_2O_7$ are listed in Table 4. Although the room temperature d-coefficient is low (d_{24} = 2·6 × 10^{-12} C/N), a value similar to that of quartz, the piezoelectric voltage constant at 400°C is significant (g_{24} = 6·3 × 10^{-3} Vm/N). From Fig. 8 is is also seen that the hot-forged PLS ceramics have the highest resistivity at elevated temperatures of any of the materials tested. By using compositions of $Sr_2(Nb_{1-x}Ta_x)_2O_7$ with a higher Nb content, the T_c can be increased to 1200°C with no loss of resistivity. Efforts to optimize the composition and processing variables are currently under way and may lead to improved properties.[42]

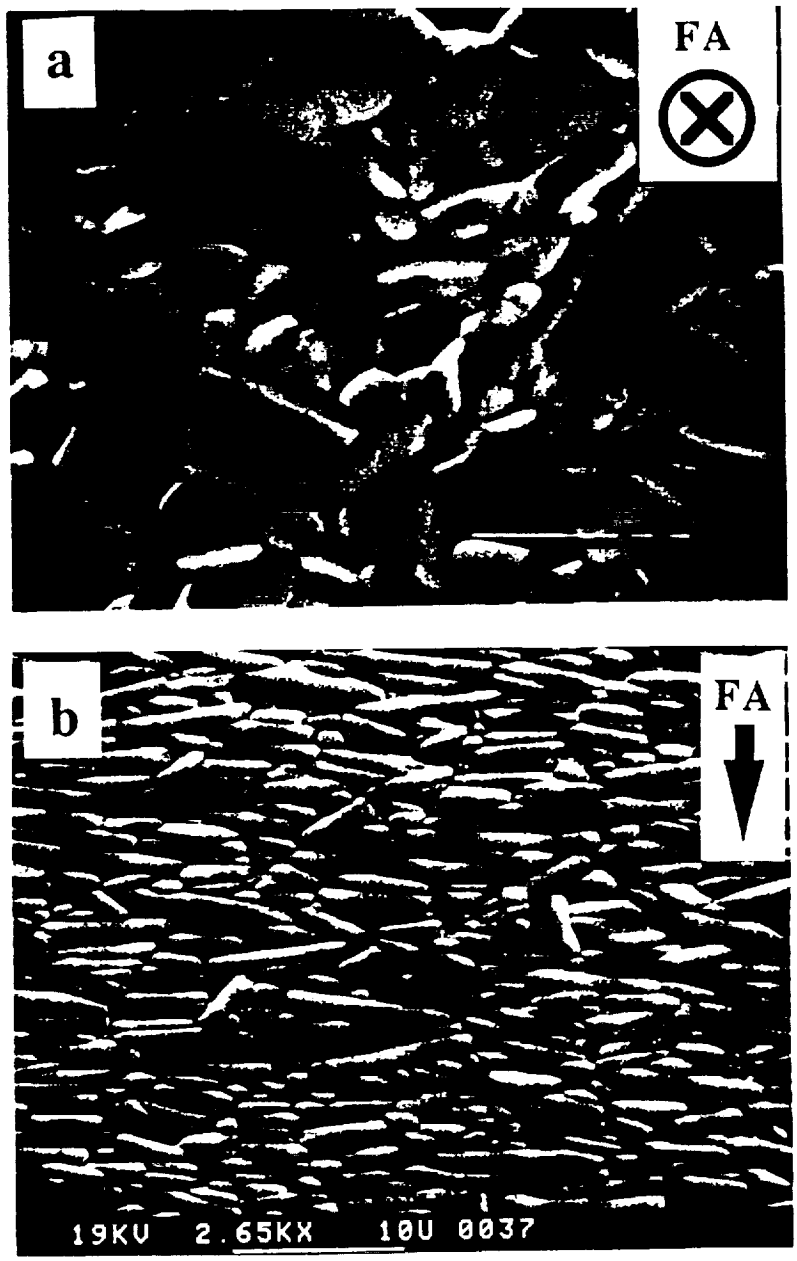

Fig. 9. Micrographs of hot forged $La_2Ti_2O_7$ ceramic. The plane perpendicular to the forging axis (FA) is shown in (a). The plane parallel to FA is shown in (b).

6.2 Polar glass ceramics

A classification of piezoelectric materials, totally diffrent from any previously discussed, exists in the form of polar glass ceramics. These non-ferroelectric compounds require single crystal growth or polar texturing for piezoactivity. One successful technique for obtaining oriented grains is the texturing of microscopic recrystallized polar crystals in an amorphous

glassy matrix. Using a controlled thermal gradient technique, the polar material $Ba_2TiSi_2O_8$ (fresonite) was recrystallized from a glass of the composition $2BaO3SiO_2TiO_2$ resulting microstructure that contained polar oriented grains. With room temperature values of d_{33} and g_{33} were 7×10^{-12} C/N and 88×10^{-3} Vm/N respectively, and relatively low density (4·01 g/cm^3), these composite materials may be of interest for hydrophone applications.[43]

It has been suggested that polar glass ceramics may also be useful for high temperature piezoelectric devices. Since they are polar, but not ferroelectric, poling is unnecessary and, consequently, there is no problem with depoling or aging effects. Foreseen problems do exist, though, including softening of the glassy phase and possible ferroelastic phase transitions that would restrict the high-temperature capabilities. Further evaluation of the electrical properties, including resistivity at high temperatures, is needed before these materials can be commercialized.

6.3 AlN thin films

In recent years, numerous studies have been made of the piezoelectric properties of thin films of several materials, including the ferroelectrics previously discussed.[21] Thin films of non-ferroelectric materials are also of great interest, including aluminium nitride (AlN). Because of its exceptionally high thermal conductivity and dielectric breakdown strength, polycrystalline (AlN) is an important ceramic material used in substrates for hybrid microelectronics, but in the bulk form exhibits no piezoelectric activity. However, when properly oriented on a compatible substrate, AlN thin films exhibit piezoelectric properties which have been studied for their potential use as pressure transducers, speakers, and SAW devices.[44]

Of most interest for this report are the high-temperature piezoelectric properties of AlN thin films. A recent paper[45] reported that an AlN SAW device deposited on a fused quartz substrate, operating at 60–100 MHz, exhibited piezoelectric responses at temperatures up to 1150°C. Other reports on chemical vapor deposited (MOCVD) AlN thin films have shown room temperature d_{33} values of $5{\cdot}5 \times 10^{-12}$ Vm/N (about the same as $LiNbO_3$) and a dielectric constant K_{33} of 12.[46] Tsubouchi and Mikosheba[47] reported room temperature resistivity values of 10^{16} Ω-cm, a value higher than any other piezoelectric material discussed in this paper. With this combination of very high temperature operation, high resistivity, and reasonable piezoelectric coefficients, it seems that AlN thin films warrant further investigation.

7 SUMMARY

High-temperature technology is of major importance for chemical and material processing, automotive, aerospace, and power generating industries to name just a few. For many, the primary benefit of operating at higher temperatures is the direct cost savings associated with increased efficiency in fuel conversion. In a related matter, the development of advanced structural materials such as silicon nitride and carbon–carbon composites promotes a need for high-temperature electronic materials to monitor processing of these systems. This is exemplified by the recent organization of the First International High Temperature Electronics Conference by Sandia National Laboratory and Wright Laboratory.[48] Along with semiconductor, capacitor, magnetic, and packaging materials, electromechanical transducing materials are required to sense strains, vibrations, and noise under severe thermal conditions. Of the several different types of acoustic and strain sensors investigated, including accelerometers, strain gauge, air gap, eddy current, buffer rod, and fiber optic, piezoelectric types offer the best candidates when one considers sensitivity, cost, and design.

Figure 10 summarizes the maximum use temperature of widely commercial piezoelectric materials and the projected values of two experimental ones. If an operating temperature of 400°C or greater is required, the number of available sensor materials is clearly limited. If an operating

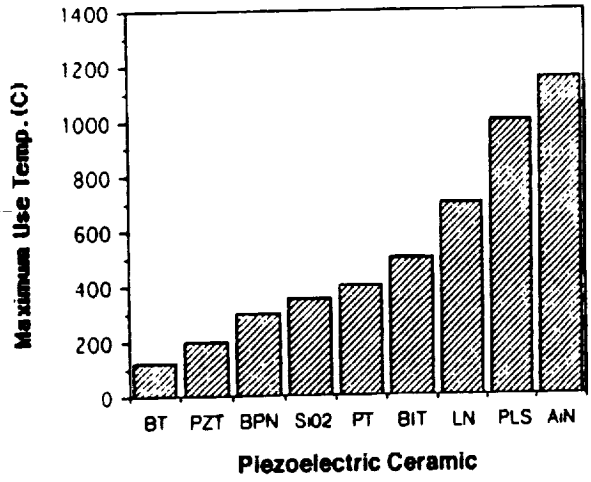

Fig. 10. Approximate maximum temperature of operation for piezoelectric ceramics. Most are estimated by combined consideration of the ferroelectric Curie temperature, sensitivity, and measured electrical resistivity. Others are known with a higher degree of certainty such as barium titanate (BT) limited by its T_c of 125°C, lead zirconate titanate (PZT) known to experience accelerated depoling at 200°C and quartz (SiO_2) with a maximum use temperature of 350°C.

temperature 750°C is chosen, there is no commercial material available. It is reasonable to assume that there now exists a need for vibration sensors that can function at 750°C, or even at 1000°C, and that the need will be even more pressing in the future. The design of such sensors presents a great challenge and will require the development of new materials and novel processing techniques.

This paper has discussed two options for very high temperature piezoelectric materials. The first was the family of PLS ferroelectrics, with the highest known T_c (some greater than 1500°C), The second was non-ferroelectric AlN thin film with a reported operating temperature of 1150°C. New ferroelectric compounds, also with very high T_c, have been predicted based on the Abrahams–Kurtz–Jameson relationship and an extensive inorganic crystal structure database.[49] This study, and other computer assisted studies of materials, may well identify the next generation of high-temperature vibration sensor materials.

ACKNOWLEDGMENT

The authors wish to thank NASA-Lewis for their support under grant number NA63-125.

REFERENCES

1. McCormick, B. J., Preface. In *High Temperature Electronics*. IEEE, Tucson, AZ, USA, 1981.
2. Naito, M., Recent sensors for automotive applications. *Ceram. Eng. Sci. Proc.*, **8**(9–10) (1987) 1106–19.
3. Meetham, G. W., High temperature materials—a general review. *J. Mat. Sci.*, **26**(4) (1991) 853–60.
4. Kusakabe, H., Okauchi, T. & Takigawa, M., *A Cylinder Pressure Sensor for Internal Combustion Engine*. SAE (Society of Automotive Engineers) paper 920701. SAE International, Warrendale, PA, USA, 1992.
5. Fowler, T. J., Acoustic emission testing of vessels. *Chem. Engng Prog.*, **Sept.** (1988) 59–70.
6. Helmshaw, R., *Non-Destructive Testing*, (2nd edn). Edward Arnold Publishing, London, UK, 1991.
7. Managan, W., Needs for high temperature electronics in fossil energy plants. In *Conference on High Temperature Electronics*. Tucson, AZ, USA, 1981.
8. Bissonnette, M. & Cloutier, M., Air gap measuring system. 1st International Machinery Monitoring and Diagnostic Conference. Las Vegas, NV, USA, 1989.
9. Guess, J. F., Analysis of piezoelectric benders used as knock sensors. In *Sensors and Actuators 1983*. Society of Automotive Engineers, Inc., Warrendale, PA, USA, 1983, p. 79.

10. Droney, B. E. & Pfeiffer, T. J., Ultrasonic inspection of hot steel blooms to detect internal pipe. *Mater. Evaluat.*, **36**(6) (1980) 31–6.
11. Jaffe, B., Cook, Jr, W. R. & Jaffe, H., *Piezoelectric Ceramics*. Academic Press Ltd, London, 1971.
12. Endevco Div. Allied Signal, San Juan Capistrano, CA, USA, General Catalog (1989) 92675.
13. Vibrometer, Inc., Longveuil, Quebec, Canada, Product Catalog (1988).
14. CEC Instruments Division of IMO Industries, Inc., San Dimas, CA, USA, Product Literature.
15. Measurements Group, Inc., Tech-Note TN-513, Measurement of Thermal Expansion Coefficient Using Strain Gages. Measurements Group Inc., Raleigh, NC, USA, 1986.
16. Omega Engineering, Inc., *Pressure, Strain, and Force Measurement Handbook and Encyclopedia*. Omega Engineering, Inc., Stamford, CT, USA, 1987.
17. Lei, J. F., Mentor, J. & Van Horn, H. J., Influence of rare earth oxide addition on the oxidation behavior of PdCr strain gauge material. *1990 Meeting of the Electrochemical Society*, Montreal, Canada.
18. Ménard, P. & Bourgeois, J. M., Using capacitive sensors for AC generator monitoring. International Conference on Large High Voltage Electric Systems, Paris, France, 1990.
19. Car, W., Eddy current proximity sensors. *Sensors*, **Nov.** (1987) 21–5.
20. Cady, W. G., *Piezoelectricity*. McGraw Hill, New York, USA, 1946.
21. Herbert, J. M., *Ferroelectric Transducers and Sensors*. Gordon and Breach Science Publishers, New York, USA, 1982.
22. Swartz, S. L., Topics in electronic ceramics. *IEEE Trans. on Electrical Insulation*, **25**(5) (1990) 935–87.
23. IEEE Standard on Piezoelectricity, *ANSI/IEEE Std. 176-1978*. IEEE, New York, USA, 1978.
24. Kistler Instruments AG Winterthur, Switzerland, 1989, General Catalog.
25. Keramos, Inc., Indianapolis, IN, USA, General Catalog, 1991.
26. Token Corp. Tokyo, Japan, Piezoelectric Ceramic Catalog.
27. Crystal Technology, Inc., Palo Alto, CA, USA, Product Catalog.
28. Matsushita Electric Industrial Co., LTD, Osaka, Japan.
29. Fuierer, P. A., Grain-oriented perovskite layer ceramics for high temperature applications. PhD thesis, The Pennsylvania State University, Pennsylvania, USA, 1991.
30. Korzunova, L. V., Piezoelectric ceramics for high temperature transducers. *Ferroelectrics*, **134** (1992) 175–80.
31. Takahashi, M., Electrical resistivity of lead zirconate titanate ceramics containing impurities. *Jpn J. of Appl. Phys.*, **10**(5) (1971) 643–51.
32. Gurevich, V. M., *Electronic Conductivity of Ferroelectrics*. English trans. from Russian (Israel Program for Scientific Translators, Jerusalem, 1971).
33. Ueda, I., Effects of additives on piezoelectric and related properties of $PbTiO_3$ ceramics. *Jpn J. Appl. Phys.*, **11**(4) (1972) 450–61.
34. Bollman, W. & Gernand, M., In the disorder of $LiNbO_3$ crystals. *Phys. Stat. Sol.*, **A9**(1) (1972) 301–23.
35. Gurevich, V. M. & Rez, I. S., Possibility of controlling the conductivity of lead metaniobate by doping. *Isv. AN SSSR. Ser. Fiz., 24, Noll* (Trans. Bulletin) (1960) p. 1258.

36. Angleton, P. A. & Hayer, J. R., Ceramic transducer elements and accelerometers using same. US Pat. No. 3,487,238 (1967).
37. Takenaka, T. & Sakata, K., Grain oriented and Mn-doped $(NaBi)_{(1+x)/2}$-$Ca_xBi_4Ti_4O_{15}$ ceramics for piezo- and pyrosensor materials. *Sensors and Materials*, **1** (1988) 35–46.
38. Fraser, M., Poling crystals of lithium niobate. *Properties of Lithium Niobate*. INSPEC, The Institute of Electrical Engineers, London, UK, 1989.
39. Nanamatsu, S., Kimura, M., Doi, K. & Takahashi, M., Ferroelectric properties of $Sr_2Nb_2O_7$ single crystals. *J. Phys. Soc. Japan*, **30** (1971) 300–4.
40. Nanamatsu, S., Kimura, M., Doi, K., Matsushita, S. and Yamada, N., A new ferroelectric, $LaTiO_3$. *Ferroelectrics*, **8** (1974) 511–13.
41. Fuierer, P. A. & Newnham, R. E., $La_2Ti_2O_7$ ceramics. *J. Am. Ceram. Soc.*, 75(11) (1991) 2876–81.
42. Turner, R. C., Work in progress.
43. Halliyal, A., Study of the piezoelectric and pyroelectric properties of polar glass ceramics. PhD thesis, The Pennsylvania State University, Pennsylvania, USA, 1991.
44. Mujasaka, Y., Hashino, S. & Takahashi, S., Advances in structure and fabrication process for thin film acoustic resonators. *1987 Ultrasonics Symposium*. IEEE, New York, USA, 1987, pp. 385–93.
45. Patel, N. D. & Nicholson, P. S., High frequency, high temperature ultrasonic transducers. *NDT International*, **23**(5) (1990) 262–6.
46. Shiosaki, T., Hayoshi, M. & Kawabata, A., Audio-frequency characteristics of a piezoelectric speaker using an AlN film deposited on a polymer or metal membrane. *1982 Ultrasonics Symposium, Proc.* IEEE, New York, USA, 1982, pp. 529–32.
47. Tsubouchi, K. & Mikoshiba, N., Zero temperature coefficient saw delay line on AlN epitaxial films. *1983 Ultrasonics Symposium, Proc.* IEEE, New York, USA, 1980, pp. 299–310.
48. King, D. B. & Thome, F. V., *Transactions of the First International High Temperature Electronics Conference*. Sandia National Laboratory, Albuquerque, NM, USA, 1991.
49. Abrahams, S. C., Systematic prediction of new ferroelectrics on the basis of structure. *Ferroelectrics*, **104** (1990) 37–48.